The electrophysiology of the atrioventricular node in normal and failing rabbit hearts

A thesis submitted in fulfilment of the degree of Doctor of Philosophy to the

University of Glasgow

Faculties of Medicine and Biomedical and Life Sciences

by

Ashley Muir Nisbet

BSc (Hons), MB ChB, MRCP (UK)

Glasgow Cardiovascular Research Centre

&

Institute of Biomedical and Life Sciences

University of Glasgow

2008

Abstract

Conduction abnormalities affect prognosis in chronic heart failure (CHF). Previous investigators have observed abnormal delay in atrioventricular (AV) conduction in a rabbit model of left ventricular dysfunction (LVD) due to apical myocardial infarction. In this model, AV conduction time increased with increasing pacing rates, suggesting the most likely site of delay is the AV node. The mechanisms by which this occurs are not fully understood. The purpose of this thesis was to confirm that the abnormal prolongation of AV conduction time originates at the AV node in a rabbit model of LVD due to apical myocardial infarction, and explore possible mechanisms underlying the observation.

Using surface electrogram recording and standardised pacing techniques in an isolated AV node tissue preparation I confirmed that there is abnormal prolongation of AV nodal conduction in this rabbit model of LVD, as evidenced by prolongation of atrio-hisian (AH) interval and Wenckebach cycle length (WCL) in LVD compared to control. Furthermore, using optical mapping of electrical activation using voltage sensitive dye I observed that the prolongation of the AH interval is predominantly a consequence of conduction delay between the inputs of the AV node and the compact nodal region.

Neuro-hormonal derangement in chronic heart failure has a central role in the pathogenesis of the disease, with evidence of downregulation of beta (?)-adrenoceptors in the left ventricular myocardium. I therefore explored the possibility of ß-adrenoceptor downregulation in the AV node as a mechanism underlying the abnormal AH interval prolongation in LVD. There was no evidence of ß-adrenoceptor downregulation in the AV node in LVD compared to control to account for the observed abnormal conduction delay.

Adenosine is known to have profound effects on AV nodal conduction and the possibility of tonic excess of adenosine in LVD was explored as a possible mechanism for the prolonged conduction delay. Using an exogenously applied adenosine A_1 receptor antagonist there was no evidence of excess endogenous adenosine in LVD compared to control. There was, however, an increase in the sensitivity of the LVD samples compared to control to exogenous adenosine, with a significant increase in AH interval and WCL with increasing concentrations.

This thesis also investigates the effect of acidosis on AV nodal conduction. There was significant prolongation of the spontaneous sinus cycle length, AH interval and WCL, as well as the AV nodal functional and effective refractory periods, proportional to the degree of acidosis. These effects were reversible with return to normal pH. Optical mapping studies showed that the spatiotemporal pattern of AV nodal delay during acidosis was similar to that observed in LVD, with the predominant delay in conduction between the AV nodal inputs and the compact AV node.

In summary this thesis has confirmed that even in the absence of a direct ischaemic insult to the AV junction, conduction abnormalities in the AV node may still occur as a pathophysiological response to a myocardial infarction resulting in LVD. The mechanisms underlying this response are likely to be complex and multiple, and are not yet clear. Establishing the electrophysiological basis and the effects of neuro-hormonal modulators of atrioventricular nodal function may lead to development of targeted therapeutic strategies to improve overall survival and improve symptom control for patients with CHF.

Table Of Contents

List of tables

List of figures

Table of abbreviations

4AP	4-Aminopyridine
ACh	Acetyl choline
Ado	Adenosine
ADP	Adenosine di-phosphate
AI	Aortic incompetence
ANOVA	Analysis of variance
AP	Action potential
APD	Action potential duration
APD50	APD at 50% repolarisation
ATP	Adenosine Triphosphate
AV	Atrioventricular
AVN	Atrioventricular Node
cAMP	Cyclic adenosine monophosphate
CCD	Charged coupled device
CHF	Chronic heart failure
CO_2	Carbon dioxide
CPX	8-cyclopentyl-1,3-dipropylxanthine
CRT	Cardiac resynchronisation therapy

CrT	Crista terminalis
CS	Coronary sinus
Cx	Connexin
DC	Direct current
EC_{50}	The molar concentration of an agonist, which produces 50% of the maximum possible response for that agonist.
ECG	Electrocardiogram
ERP	Effective refractory period
FO	Fossa ovalis
FRP	Functional refractory period
IAS	Inter-atrial septum
$I_{Ca,L}$	L-type calcium current
I_f	Funny current (pacemaker current)
I_{kr}	Delayed rectifier potassium current
I_{Na}	Sodium current
I_{to}	Transient outward current
IVC	Inferior vena cava
LAD	Left atrial dimension
LV	Left ventricle
LVD	Left ventricular dysfunction

LVEDD	Left ventricular end diastolic dimension
LVEDP	Left ventricular end diastolic pressure
LVEF	Left ventricular ejection fraction
M	Molar
MAP	Monophasic action potential
MI	Myocardial infarction
ms	Milliseconds
NA	Numerical aperture
NE	Norepinephrine
NYHA	New York Heart Association
O_2	Oxygen
PCL	Pacing cycle length
pHi	Intra-cellular pH
pHo	Extra-cellular pH
Pi	Inorganic phosphate
RAM	Random access memory
RV	Right ventricle
RVEF	Right ventricular ejection fraction
SA	Sinoatrial

SAN	Sinoatrial Node
SEM	Standard error of the mean
SSCL	Spontaneous sinus cycle length
SVT	Supra-ventricular tachycardia
TCA	Tricarboxylic acid
TrV	Tricupsid valve
tT	Tendon of Todaro
WCL	Wenckebach cycle length

Acknowledgements

This PhD was funded by a British Heart Foundation clinical PhD studentship. Coronary ligation procedures, surface electrocardiogram recordings and echocardiography were carried out by Dr Michael Dunne and the late Dr Martin Hicks. I would also like to acknowledge the staff of the animal house in the Glasgow Cardiovascular Research Centre for their animal husbandry skills and general helpfulness. Dr Patrizia Camelliti, University of Oxford, carried out histological and immunohistochemical analysis of AV nodal tissue for which I am very grateful. Dr Inada and colleagues at the University of Manchester have provided interesting mathematical modelling data (detailed in Appendix 2). Dr Francis Burton and his impressive programming skills provided much of the software used for analysis of data in this thesis. I am also grateful to him for his assistance in setting up and running the optical mapping experiments.

Professor Andrew Rankin has been an invaluable advisor throughout my research. I would like to thank Professor Stuart Cobbe for his professional support throughout my career, both in clinical and academic cardiology. I would also like to express thanks to Professor Godfrey Smith. He has been a mentor, motivator and friend over the last almost 4 years and I am grateful for his endless encouragement.

Thank you to Aileen Rankin for her assistance with all technical matters and general helpfulness, not to mention friendship. I extend a big thank you to all of my friends in the laboratory (you know who you are!) for making life as a scientist so enjoyable! In particular, thank you to Rachel and Gillian for being great office mates – even if we did end up eating too much tablet! And a big thank you goes to Sarah for her friendship and proof reading skills.

My family have always supported me in everything I do and I am eternally grateful to them, in particular to those who are no longer around to share pride in this achievement. My husband Michael has been my rock for many years, and I am eternally thankful to him for his patience with me during the years creating this thesis (especially the last few months!). Finally I must thank our daughter Lucy – your expected birth provided me with the ultimate deadline!

Declaration

The research reported in this thesis is original and my own work except where otherwise acknowledged. None of the work has been submitted for the fulfilment of any other degree.

Details of presentations and publications from this work:

Posters presented

Increased AH interval in isolated AV node from rabbits with LV dysfunction due to myocardial infarction. **A Muir**; GL Smith; FL Burton; A Rankin; SM Cobbe. 4th Mammalian Myocardium Symposium, University of Bristol, UK, July 2005

Functional remodelling of the atrioventricular node in a rabbit model of left ventricular dysfunction. **Dr AM Nisbet**, Dr FL Burton, Prof A Rankin, Prof GL Smith, Prof SM Cobbe. UK Heart Rhythm Congress, Birmingham, September 2006

Effect of isoproterenol on sinoatrial and atrioventricular nodal function in left ventricular dysfunction in rabbit. **Dr AM Nisbet**, Dr FL Burton, Prof A Rankin, Prof GL Smith, Prof SM Cobbe. Europace, Lisbon, Portugal, June 2007

Oral presentations

Delay of AV nodal conduction in rabbits with LV dysfunction following myocardial infarction. **A Muir**; GL Smith; FL Burton; A Rankin; SM Cobbe. Scottish Society for Experimental Medicine, University of Glasgow, UK, November 2005

Published abstracts

Increased AH interval in isolated AV node from rabbits with LV dysfunction due to myocardial infarction. **A Muir**; GL Smith; FL Burton; A Rankin; SM Cobbe Journal of Molecular and Cellular Cardiology (July 2005) 39:197

Delay of AV nodal conduction in rabbits with LV dysfunction following myocardial infarction. **A Muir**; GL Smith; FL Burton; A Rankin; SM Cobbe. Scottish Medical Journal (in press).

Functional remodelling of the atrioventricular node in a rabbit model of left ventricular dysfunction**. AM Nisbet**, FL Burton, A Rankin, GL Smith, SM Cobbe. Europace (June 2007) 9 (Suppl.2): ii5.

Effect of isoproterenol on sinoatrial and atrioventricular nodal function in left ventricular dysfunction in rabbit. **AM Nisbet**, FL Burton, A Rankin, GL Smith, SM Cobbe. Europace (June 2007) 9 (Suppl. 3): iii180.

Chapter 1 - Introduction

1 Introduction

1.1 Clinical Context

1.1.1 Conduction system abnormalities in chronic heart failure

1.1.1.1 Survival and prognosis in chronic heart failure

Chronic heart failure (CHF) is a significant cause of morbidity and mortality, with a 10% annual mortality rate in newly diagnosed patients, and in established heart failure, 5-year survival rates of only 25% in men and 38% in women (1-3). A number of variables have been found to be predictors of prognosis, including New York Heart association (NYHA) class, peak oxygen consumption and total exercise time, left ventricular ejection fraction (LVEF), right ventricular ejection fraction (RVEF), pulmonary capillary wedge pressure, ventricular arrhythmias, levels of catecholamines, atrial peptides, plasma sodium, the presence of cachexia and conduction abnormalities (1;4).

1.1.1.2 Electrocardiographic predictors of outcome in chronic heart failure

ECG parameters are also associated with an adverse outcome in CHF. Figure 1-1 illustrates how the various components of the surface ECG arise from the spread of activation and repolarisation throughout the heart. First or second-degree atrioventricular (AV) block has been shown to be an independent risk factor in idiopathic dilated cardiomyopathy, particularly in combination with either reduced LVEF or frequent ventricular couplets (5). Shamim *et al* (6) showed an increase in all cause mortality with progressive increase in the duration of the QRS complex. QRS duration was an independent variable on multivariate analysis, as were LVEF and peak oxygen consumption. Furthermore in 2002 this group demonstrated that the relative change in QRS duration over time was a more sensitive prognostic indicator than absolute values of QRS duration (7). This correlated with echocardiographic markers of deterioration of ventricular systolic function and increased LV filling pressures. The PR interval was also significantly longer in non-survivors than in survivors. Therefore, there is a close relationship between electrical and haemodynamic components of cardiac function and clinical outcome.

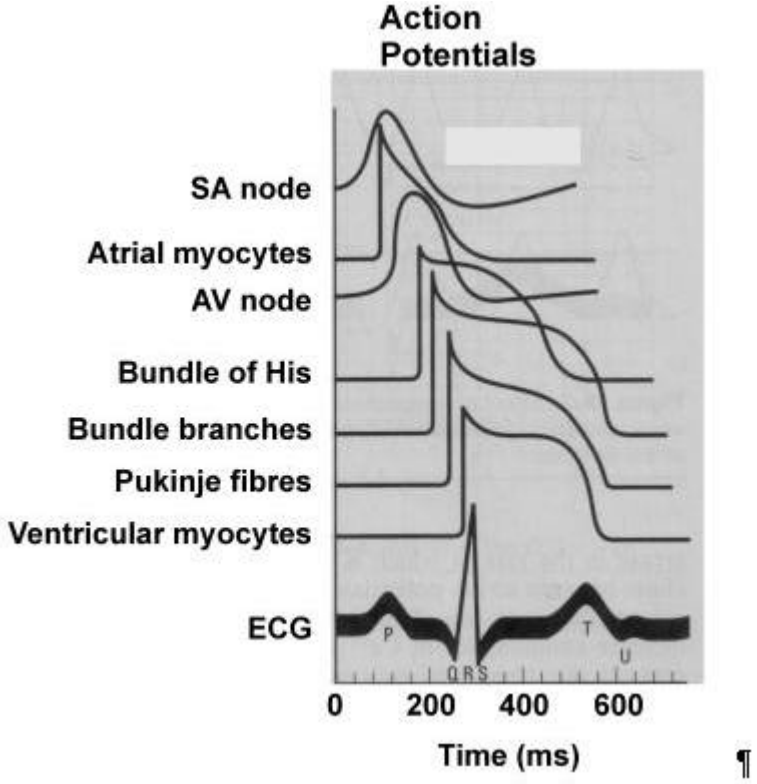

Figure 1-1- Origins of the ECG. The transmembrane AP for the SA node, the AV node, other parts of the heart's conducting system, atrial muscle and ventricular muscle are illustrated with reference to the surface ECG. The 'p' wave corresponds to the depolarisation of the atrial myocytes. The QRS complex corresponds to the spread of activation across the ventricles. The ST segment occurs due to the electronegative summation of the ventricular AP plateaux, and the T wave results from the sequential repolarisation of the ventricular myocytes. (Adapted from (8)).

1.1.2 Clinical significance of prolonged atrioventricular nodal delay

Conduction delays are present in approximately 50% of patients with CHF (9). Atrioventricular and intraventricular conduction delay produce adverse haemodynamic effects by their impact on AV synchrony and left ventricular contraction/relaxation respectively. A long PR interval predisposes to pre-systolic mitral regurgitation (10). Multisite biventricular pacing techniques (also known as cardiac resynchronisation therapy (CRT)) improve cardiac function by synchronising ventricular contraction and relaxation (11-16). Further improvements in systolic function can be achieved by optimisation of preload by correct timing of AV delay (17-22). Breithardt *et al* (23) demonstrated that optimum cardiac index and Doppler indices of LV filling occurred at AV delays between 80 and 120ms in patients with NYHA Class III-IV CHF. Thus maximum improvement in LV performance requires both resynchronisation of AV conduction and optimisation of AV delay.

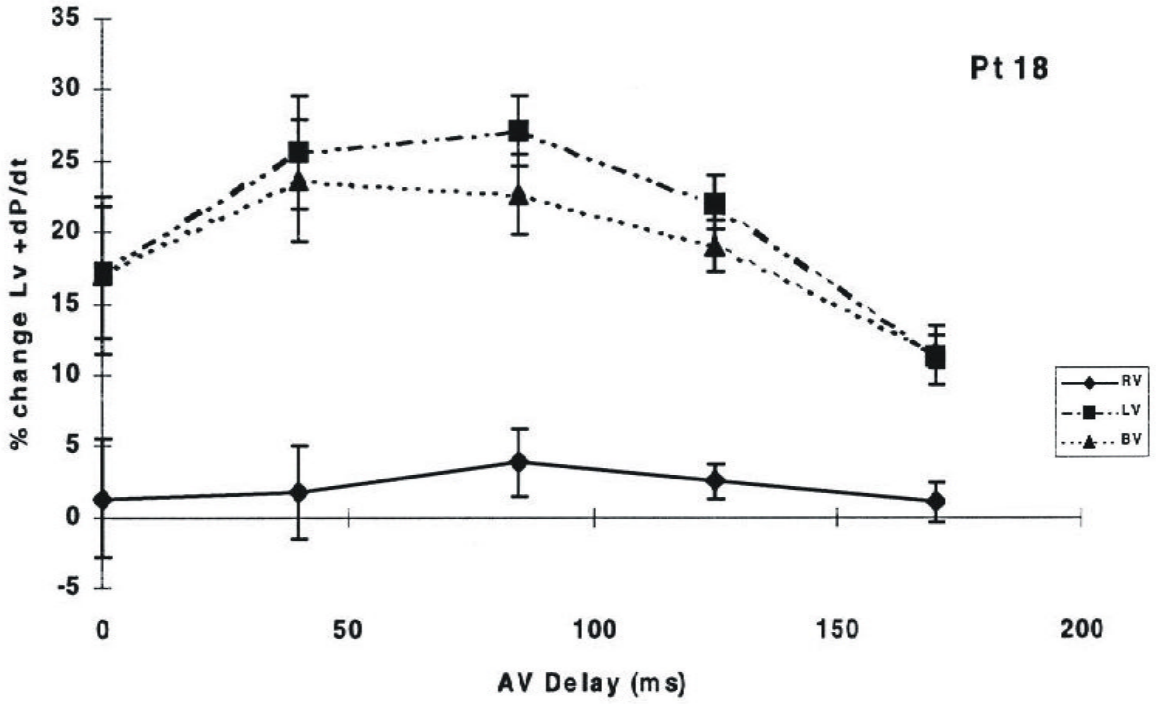

Figure 1-2– Percentage change in LV +dP/dt as a function 5 AV delays. Values shown for each pacing chamber (RV – right ventricle; LV – left ventricle; BV – biventricular). (Adapted from (24)).

In a normal heart, atrial and ventricular systole are temporally coordinated allowing the efficient transfer of blood between the chambers and optimisation of cardiac output. Prolonged atrioventricular conduction in heart failure patients compromises ventricular filling, by reducing the atrial contribution to LV preload and due to pre-systolic mitral regurgitation, resulting in a drop in the LV end diastolic pressure (LVEDP). In the Pacing Therapies for Congestive Heart Failure study (PATH-CHF), Auricchio *et al* (24) established that in addition to the improvement of contractile function due to the resynchronisation of inter/intraventricular contraction by biventricular pacing, AV delay is a significant determinant of changes in parameters of LV systolic function, as measured by LVEDP and LV dP/dt_{max} (Figure 1-2). A further subgroup analysis published in 2002 (25) confirmed that in the group of patients who responded to CRT, the maximum increases in pulse pressure were obtained at an AV delay that preserved the baseline values of LVEDP. This supports the hypothesis that preload is a significant determinant of the optimum acute haemodynamic impact of CRT. Overall, in comparison to standard medical therapy, CRT has been shown to reduce the combined end point of all cause mortality or first hospitalisation in patients with advanced heart failure (NYHA class III-IV) (Figure 1-3) (12;26). Furthermore, a recent systematic review of trials of CRT in patients with

symptomatic heart failure has shown that when added to optimal medical therapy, CRT reduces both all cause mortality and heart failure hospitalisations by approximately 25% (27).

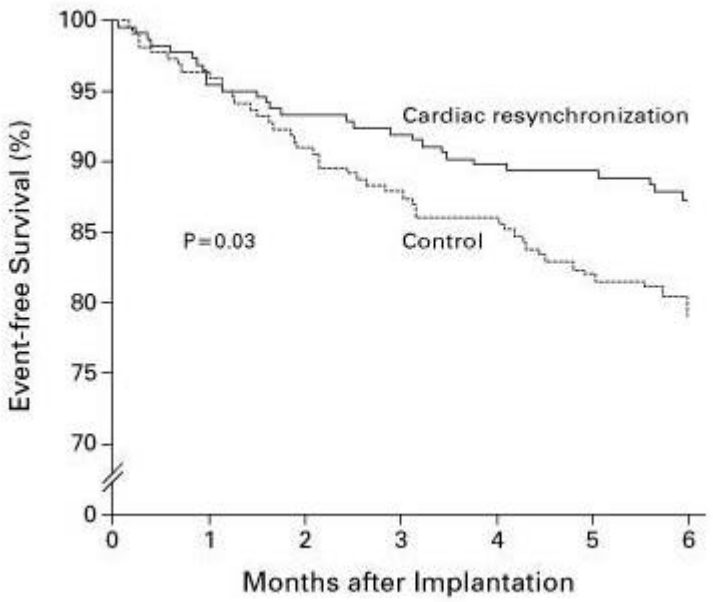

Figure 1-3 – Kaplan-Meier estimates of the time to death or hospitalisation from worsening heart failure in control versus cardiac resynchronisation groups. The risk of an event was 40% lower in the resynchronisation group. (Adapted from (12)).

1.2 The atrioventricular node

"A riddle wrapped in a mystery inside an enigma"

Winston Churchill, 1939

Douglas P Zipes, 2000

1.2.1 Historical perspective

On a radio broadcast in 1939, Winston Churchill characterised Russia as "a riddle wrapped in a mystery inside an enigma". This conclusion was also drawn by Douglas P Zipes in reference to our present understanding of the electrophysiology of the atrioventricular node (28). From the 19th to the early 20th century, the question "Why does the heart beat?" dominated cardiac research. The "myogenic versus neurogenic" debate had been ongoing for many years previously. In the second century, Claudius Galen observed "The heart, removed from the thorax, can be

seen to move for a considerable time, a definite indication that it does not need the nerves to perform its function" (29). The physiological debate over whether the heart beat was triggered by intrinsic excitation by the heart muscle itself or due to an external stimulus was ultimately decided by anatomists.

In 1839, Purkinje discovered a network of grey, flat gelatinous fibres in the ventricular sub-endocardium of the sheep heart. He initially believed these fibres to be cartilaginous but then decided they were muscular (30). The true function of these conducting fibres was not realised until many years later.

In 1893, Wilhelm His Jr, a Swiss born cardiologist and anatomist, discovered the bundle of specialised muscle fibres, which became known as the "Bundle of His". This bundle was noted to be the only direct connection to conduct impulses between the atria and the ventricular muscle. In years thereafter his experiments confirmed that when the bundle was severed it caused "asynchronie in the beat of the auricle and ventricle" (31).

In 1906, the monumental monograph of Sunao Tawara was published (32) . Through his work he described how he traced the Bundle of His back to find a compact node of fibres at the base of the inter-atrial septum, and forward where it connected with the fibres described by Purkinje years previously. He believed the conducting bundles were muscular tissue surrounded by connective tissue as opposed to nerve tissue, supporting the myogenic theory of the initiation and conduction of the heart beat (30;32).

Finally, in 1907, Martin Flack and Arthur Keith discovered a structure at the sino-auricular junction in the heart of a mole that histologically resembled the AV node. They recognised that this is where the dominating rhythm of the heart normally begins. It was named the sino-auricular (ultimately the sino-atrial) node (30).

Cardiac research has now reached the centenary of the discovery of the sino-atrial and atrioventricular nodes. Despite many years of progress, the complex function of these structures, in particular the atrioventricular node, remains largely enigmatic and mysterious.

1.2.2 Anatomy of the atrioventricular junction

1.2.2.1 Gross anatomy

The atrioventricular node is the only normal electrical connection between the atria and the ventricles. The node lies in the lower atrial septum within the Triangle of Koch, bound superiorly by the tendon of Todaro, laterally by the orifice of the coronary sinus and inferiorly by the attachment of the septal leaflet of the tricuspid valve (Figure 1-4). The AV node has a multilayered structure. The most superficial layer is the transitional zone between fast conducting atrial muscle (A zone) and the region of the compact AV node (N zone). Action potentials from the transitional zone (AN cells) are similar in character to atrial action potentials. The mid-nodal region describes the "compact node" or nodal (N) zone, an area of slow conduction and slow action potential upstrokes (N-cells). The deepest layer is a transitional zone between the N zone and the His bundle and exhibits so called "NH (nodal-His)" action potentials (18;33-36).

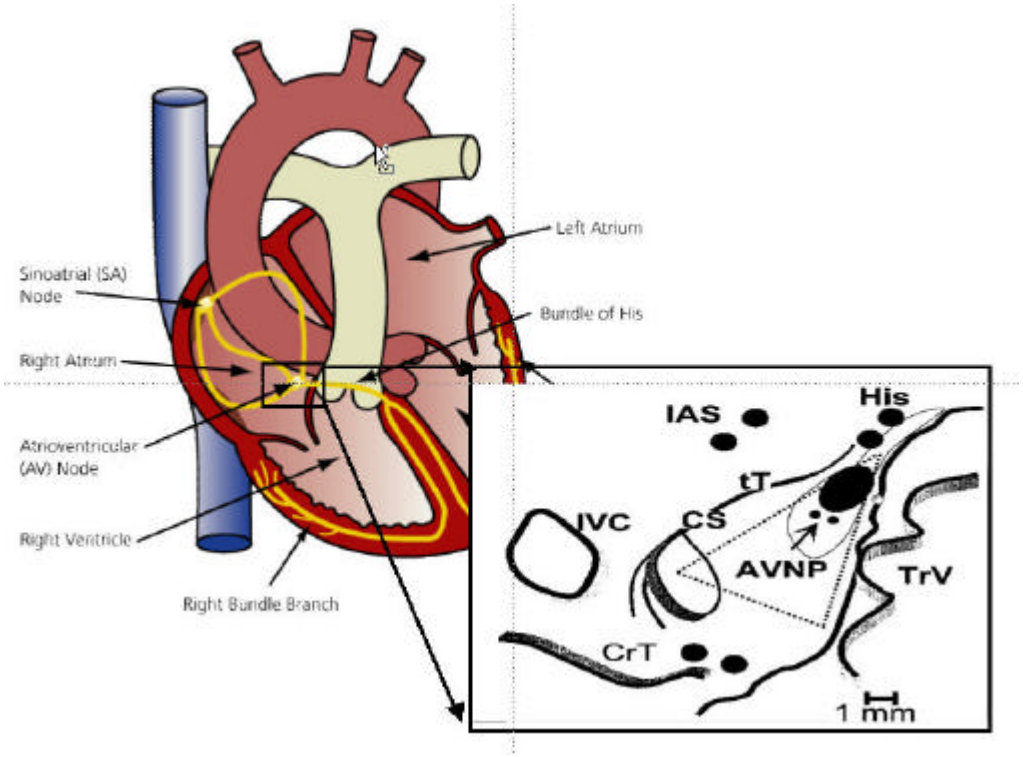

Figure 1-4 - The Triangle of Koch. IAS – inter-atrial septum; IVC – inferior vena cava; CrT – Crista terminalis; tT – tendon of Todaro; TrV – tricuspid valve; CS – coronary sinus; His – His bundle; AVNP – AV nodal input pathways.

1.2.2.2 Dual AV nodal pathways

Anatomical and functional studies of the AV node have demonstrated the presence of two distinct input pathways, providing the substrate for clinically important AV nodal re-entrant tachy-arrhythmias. This was first demonstrated in dog (37), where the authors observed an "echo" (non-stimulated) ventricular beat elicited when they delivered an appropriately timed ventricular premature beat to the heart. Further studies in human subjects some years later demonstrated similar findings (38;39). The findings in dog and human studies have been confirmed in studies of the rabbit AV node (40-44). However, anatomical studies of humans with AV nodal re-entrant tachycardia or dual AV nodal pathways have shown that the AV node is structurally normal (45). Therefore dual AV nodal pathways are a functional rather than an anatomical problem, as demonstrated by Figure 1-5.

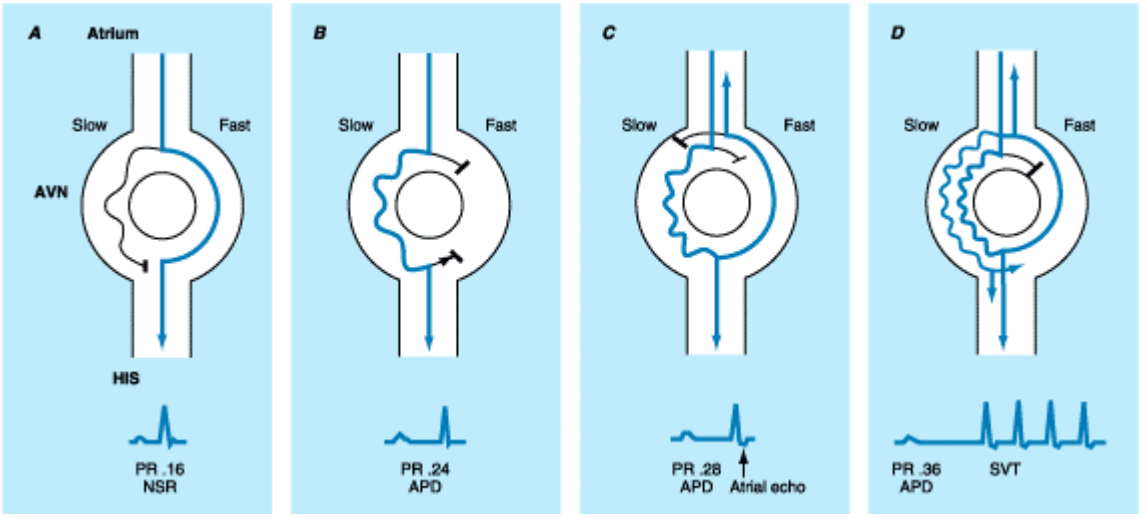

Figure 1-5 – Dual AV nodal physiology. The atrium, AV node (AVN), and His bundle are shown schematically. The AV node is longitudinally dissociated into two pathways, slow and fast, with different functional properties. In each panel of this diagram, blue lines denote excitation in the AV node, which is manifest on the surface electrocardiogram, while black lines denote conduction, which is concealed and not apparent on the surface electrocardiogram. *A*. During sinus rhythm (NSR) the impulse from the atrium conducts down both pathways. However, only conduction over the fast pathway is manifest on the surface ECG, producing a normal PR interval of 0.16 s. *B*. An atrial premature depolarization (APD) blocks in the fast pathway. The impulse conducts over the slow pathway to the His bundle and ventricles, producing a PR interval of 0.24 s. Because the impulse is premature, conduction over the slow pathway occurs more slowly than it would during sinus rhythm. *C*. A more premature atrial impulse blocks in the fast pathway, conducting with increased delay in the slow pathway, producing a PR interval of 0.28 s. The impulse conducts retrogradely up the fast pathway producing a single atrial echo. Sustained reentry is prevented by subsequent block in the slow pathway. *D*. A still more premature atrial impulse blocks initially in the fast pathway, conducting over the slow pathway with increasing delay producing a PR interval of 0.36 s. Retrograde conduction occurs over the fast pathway and reentry occurs, producing a sustained tachycardia (SVT). (Adapted from http://rezidentiat.3x.ro/)

1.2.3 Cellular electrophysiology of the AV node

Heterogeneity of ion channel and gap junction expression exists within the AV nodal architecture (46). Transitional cells of the AV node (AN and NH cells) have a relatively abundant sodium current (I_{Na}). There is a relative lack of expression of sodium channels in the ovoid type isolated cells (N cells), in which the main depolarising current is the L-type calcium current ($I_{Ca,L}$). This results in a relatively slow Phase 0 of the action potential and therefore a slow speed of conduction. In addition there is an inwardly directed Na-Ca exchanger current ($I_{Na,Ca}$). Also, at potentials relevant to the diastolic potential during spontaneous activity in the majority of cells a small time-independent inward current is present (I_f). Some N cells also exhibit the dihydropyridine sensitive sustained inward current (I_{st}). There is generally no Phase 1 in nodal cells, and there is usually a very brief plateau phase. The main repolarising currents of the AVN are the transient outward K^+ current (I_{to}) and the delayed rectifier K^+ current (I_{Kr}). Unlike atrial and ventricular myocytes, the cells of the sino-atrial and atrio-ventricular nodes do not have a stable resting potential. Following repolarisation, the membrane potential undergoes spontaneous depolarisation (phase 4 depolarisation or the pacemaker potential). The interactions between the background current (I_b) and the delayed rectifier current (I_{Kr}) plus the hyperpolarisation activated (or "pacemaker" current), contribute to the generation of the pacemaker potential, and consequently to the automaticity of the N cells (47;48).

1.2.4 Specialised conduction characteristics of the intact AV node in response to rapid and premature stimulation

AV nodal conduction delay is inversely proportional to the stimulating atrial prematurity. This fact has been determined by pacing protocols in which regular atrial pacing (S1) producing atrial activation (A1) are followed by a premature stimulus S2 producing a response (A2). AV nodal conduction delay is then measured as the interval between the atrial electrogram (A1 or A2) and the corresponding bundle of His spike (H1 or H2). Plotting A1A2 against A2H2 creates the AV nodal conduction curve. The specialised nature of conduction through the AV node is believed to be a consequence of the interaction of three factors, namely AV nodal recovery, fatigue and facilitation (49-52). Incomplete AV nodal recovery results in the generation of a longer A2H2 delay with a shorter A1A2 interval. The cellular response to a premature stimulus, S2, applied before full recovery, exhibits

decreased action potential amplitude and Vmax (dV/dt). This reduces the proximal conduction velocity and may explain the subsequent delay in the activation of the NH cells or the development of AV nodal block. AV nodal fatigue is the term used to describe the conduction delay when the atrium is paced continuously at a fast rate. Rate dependent activation failure (49) of the AV node is known as Wenckebach phenomenon (53). It may be related to the refractoriness of the least excitable element in the heterogeneous AV nodal conduction pathway. "Exhaustion" of the AV node has been postulated as a cause, and metabolic factors are thought to contribute (49;54;55). The clinical literature on AV nodal function uses the term 'decremental conduction' to describe the increase in AH interval either in response to shortening S1S2 intervals, or to shortening of the basic S1S1 pacing interval. AV nodal facilitation describes the phenomenon that occurs following the premature atrial beat. For the same H2S3 interval (i.e. the recovery interval) the conduction delay becomes shorter with a shorter S1S2 interval.

1.2.5 Rate dependency of the action potential duration and effective refractory periods in isolated AV nodal and atrial cells

Rate-dependent periodicity has been demonstrated in single N cells isolated from the AV node as well as in intact node preparations (56-58). Isolated AV nodal cells beat spontaneously at between 180 and 260 beats per minute (bpm) (59). Repetitive stimulation of AV nodal cells at 300bpm results in a 1:1 response, but at rates of 480bpm, a 2:1 response is observed. At 400bpm, a progressive reduction in the V_{max} of successive APs is observed, with subsequent increasing latency. This results in failure of response to the 4^{th} pulse and subsequent 3:2 response. This response is analogous to Wenckebach 2^{nd} degree AV block in the intact heart. Atrial cells differ from AV nodal cells in that they sustain 1:1 activation even at pacing rates of 600 bpm. The effective refractory period (ERP) of the intact AV node lengthens at higher rates. AV nodal cells show significant shortening of ERP at low rates, but Workman *et al* found no effect on the ERP at higher rates (58;59). However the exact region of the AV node from which the cells originated was not known and there is evidence of a differing contribution of different regions of the node to refractoriness.

1.2.6 Factors affecting conduction velocity through the AV node

Conduction through the AV node is relatively slow compared to conduction through the atria or ventricles, ensuring the sequential contraction of the atria followed by

the ventricles. The AV node serves a protective function during arrhythmias such as atrial fibrillation by limiting the number of impulses transmitted to the ventricles. In contrast, the AV node plays a key role in the maintenance of other arrhythmias; for example in supraventricular tachycardia the AV node is an integral part of the re-entrant conduction circuit.

1.2.6.1 Ion channel conductance and membrane excitability

There are a number of determinants of conduction velocity. At the cellular level, conduction velocity is affected by the excitability of the cell membrane, i.e. by a reduction in K^+ conductance or by an increase in the current density of the depolarising current (Na^+ or Ca^{2+}) and by the degree of intercellular resistance (60).

1.2.6.2 Gap junctional channels

Gap junctional channels (connexins) play a prominent role in AV conduction. The mammalian heart contains three main isoforms of gap junctional protein, namely connexins Cx43, 40 and 45. There is heterogeneous expression of all three isoforms within the tissue of the Triangle of Koch. Cx43 has a major role in cell-cell communication between ventricular and atrial myocytes. It has relatively low expression within the N region of the AV node, but is expressed more in the transitional zones (the AN and NH regions). The posterior nodal extension has been shown to have the lowest Cx43 mRNA and the most abundant HCN4 mRNA expression in keeping with its low conduction velocity and pacemaker activity (61). Cx45 has been shown to be abundant in the compact node and both Cx40 and 45 in the NH region (44;62;63).

1.2.6.3 Specific mutations in cardiac voltage gated ion channels

Recently mutations in the cardiac voltage gated Na^+ channel $Na_v1.5$ (SCN5A) have been associated with familial cases of AV conduction disorders (64-67). Yoo et al (68) studied the expression of Na^+ channel isoforms at the AV junction in rat and found that $Na_v1.5$ expression was abundant in atrial and ventricular myocardium and left bundle branch, reduced in the inferior nodal extension and transitional zone, but absent in the compact node and penetrating bundle. In contrast, Greener *et al* (61) studied the expression of $Na_v1.5$ mRNA in rabbit AV junction and found it to be abundant in the compact node and penetrating bundle, but absent in the posterior nodal extension and the transitional region immediately adjacent to this. Despite

these important species differences in the relative expression of $Na_v1.5$ at the AV junction, mutations in or loss of this channel result in clinically important AV conduction disturbances and further research in human subjects is required to clarify the link.

1.2.6.4 Tissue architecture

Macroscopically the architecture of the myocardial tissue may also determine conduction velocity. In 2001, Kucera *et al* (69) studied microscopic impulse propagation using multiple optical recordings of transmembrane voltage in conjunction with patterned growth cultures of neonatal rat ventricular myocytes. They observed a 70% reduction in conduction velocity by reducing excitability, but a 99% reduction by reducing electrical coupling (in the absence of structural discontinuities). Furthermore, they observed slowing of conduction velocities evoked by branching tissue geometries in the absence of electrical uncoupling. The conduction velocities observed in the latter were similar to those observed in the AV node. Histological sections of the AV node have demonstrated a highly complex tissue architecture consisting of numerous intermingled strands separated by connective tissue, and this may correlate with the prototype tissue structures used in the above cited study. Furthermore, in studies of aged hearts, microfibrosis was found to result in a reduction in transverse conduction velocity in atrial and AV nodal tissues (70).

1.2.7 Autonomic modulation of AV nodal conduction

The AVN is richly innervated by the sympathetic and parasympathetic branches of the autonomic nervous system. There is reciprocal action of the two divisions of the autonomic nervous system, having different effects on the chronotropic, dromotropic and inotropic responses of the heart.

1.2.7.1 Sympathetic innervation

Acetylcholine (ACh) is the predominant sympathetic preganglionic neurotransmitter; norepinephrine (NE) is the predominant post-ganglionic neurotransmitter. The arrival of an impulse at the nerve terminal in the AVN effects NE release, and this interacts with ?-adrenergic receptors on the cardiac effector cell membrane. Increases in sympathetic activity raise intracellular levels of cyclic adenosine mono-phosphate (cAMP). This sets off a cascade of intracellular events culminating in

changes in the conductivity of ion channels within AV nodal conduction fibres. At rest, cardiac sympathetic activity occurs in rhythmic bursts synchronous with respiration. However, changes in heart rate and AV nodal conduction velocity do not follow the same pattern. The responses are slow, as are the recoveries of the responses to their basal level as a result of the slow removal and re-uptake of NE from the cardiac effector cell receptor and into the presynaptic nerve terminals respectively. AV conduction time depends on the interaction between the prevailing heart rate and the level of sympathetic tone, both of which exert opposite effects on AV conduction. If the heart rate is held constant by artificial pacing, sympathetic stimulation decreases AV conduction time. However, an increase in heart rate by atrial pacing prolongs AV conduction time.

1.2.7.2 Parasympathetic innervation

The vagus nerve carries the efferent parasympathetic fibres to the heart. ACh is the predominant neurotransmitter released from both pre- and post-ganglionic vagus nerve terminals. The right vagus nerve has a much greater effect on AV conduction than the left. Vagal stimulation leads to reduction in the conduction velocity and prolongation of the refractory period of the AVN by hyperpolarisation of the AVN cell membrane and reduction of the amplitude and the upstroke velocity of the cardiac action potential (51;71). This results in prolongation of the AH interval by blocking conduction at the mid-nodal (N) and NH regions of the AVN. When the heart rate is held constant by atrial pacing vagal stimulation always prolongs the AV conduction time.

1.2.7.3 Other neural modulators of AV nodal function

Adenosine is ubiquitous as it is involved in the metabolism and catabolism of adenosine tri-phosphate (ATP). ATP is packaged and co-released with ACh and NE, and serves as a source of adenosine to bind to cell membrane receptors and affect intracellular processes. Adenosine may signal conditions that are detrimental to the organism such as hypoxia. In hypoxia, adenosine reduces the myocardial oxygen demand by reducing sinus node automaticity and AV node conduction velocity. Furthermore, adenosine reduces AV nodal excitability by inactivation of $I_{Ca,L}$ and activation of a time-dependent inwardly rectifying potassium current. The effects of adenosine may counteract the effects of ?-adrenergic stimulation by inhibiting the activation of adenylyl cyclase. The renin-angiotensin system, via angiotensin II, has been implicated in the control of heart rate. Angiotensin II has a positive

chronotropic effect when infused directly into the sinus node via the cannulated sinus node artery in the isolated canine heart (72). Moreover, Bastien *et al* (73) observed an abundance of angiotensin II receptors of subtype AT2 in the conducting system of the neonatal and adult rat heart. The role of angiotensin II in the regulation of AV nodal conduction remains to be elucidated.

1.2.7.4 The autonomic nervous system in chronic heart failure

In chronic heart failure, excess norepinephrine levels lead to downregulation and desensitisation of myocardial ?-adrenoceptors. ? -1-adrenoceptors (the site of action of NE) are preferentially down-regulated in heart failure. This occurs through a combination of inhibition of receptor signalling pathways, upregulation of inhibitory G-proteins, and a reduction in adenylate cyclase and cAMP levels. All of these effects result in a reduction in contractility in ventricle (74-76). The negative inotropic effect of chronic catecholamine excess and subsequent ?-adrenoceptor downregulation has been demonstrated in rabbit models using chronic isoprenaline infusion via the implantation of an osmotic minipump (77;78). Furthermore, previous work in our laboratory has demonstrated evidence of reduced ?-adrenoceptor sensitivity to the inotropic effects of isoprenaline in papillary muscles from rabbits with LVD compared with sham operated controls (79).

1.3 The rabbit model of myocardial infarction

1.3.1.1 Pathophysiology of myocardial infarction

Myocardial infarction is the result of prolonged regional myocardial hypoperfusion resulting in tissue necrosis. A trans-mural infarct is produced as a result of abrupt, complete cessation of perfusion of sufficient duration to cause irreversible cell death. The infarct related artery determines the region of infarction, and the extent of necrosis is influenced by the presence or absence of previous ischaemia in that territory. Prior ischaemia may protect the tissue from further ischaemic insult through the development of collaterals. The most obvious structural change that occurs following a myocardial infarction is development of a fibrous scar in the infarct territory. Non-infarcted tissue also undergoes a process of remodelling. There is gradual hypertrophy of the non-infarcted ventricular myocytes as they adapt to the increased workload. This effect may be pro-arrhythmic (1;80).

1.3.1.2 Choice of animal model for this study

A well-characterised model of myocardial infarction (MI) induced by coronary artery ligation was used in this study. The marginal branch of the left circumflex coronary artery, which supplies most of the left ventricular free wall, was ligated halfway between the atrioventricular groove and the cardiac apex to produce an ischaemic area of 30-40% of the left ventricle. As there is relatively little collateral circulation in the rabbit, a homogenous apical infarct was produced occupying on average 14% of the total endocardial and epicardial surfaces towards the apex of the left ventricle. Many studies have previously used a canine model of infarction but the canine coronary circulation is different from human in that the epicardium is protected by a better developed collateral circulation. Thus the canine model does not necessarily reflect the infarct process that occurs in human hearts. In rabbit, the ligation of the marginal branch of the left circumflex coronary artery results in a trans-mural antero-apical myocardial infarction with associated left ventricular systolic dysfunction and electrophysiological dysfunction (as demonstrated by the increase in frequency of ventricular fibrillation compared to sham operated hearts). This model is thought to be consistent with acute MI in humans without prior ischaemia in the infarct related territory.

1.3.1.3 Evidence of altered atrioventricular nodal conduction in the rabbit model of heart failure

The prognosis in chronic heart failure is affected by conduction abnormalities affecting both the AV node and the His-Purkinje system (5-7;9;17). The mechanisms by which this occurs are not fully understood. Previous work from this laboratory has demonstrated delay in AV conduction in this rabbit model of left ventricular dysfunction (LVD)/heart failure due to MI (81). In this model as described above the infarct is localised to the left ventricular apex and there is no direct ischaemic insult to the basal myocardium. Using optical mapping, a mean increase of 20ms (20%) was found in the interval between right atrial stimulation and left ventricular epicardial activation in LVD hearts compared with controls. There was no decrease in left ventricular transmural or epicardial conduction velocity. The AV conduction delay increased with increasing pacing rates, suggesting that the site of increased delay was most likely to be the atrio-ventricular node. Initial histological analysis failed to demonstrate any change in the tissue architecture of the AV node to account for this. This suggests that in addition to structural re-modelling of non-infarcted ventricular myocytes, there may be electrophysiological re-modelling

affecting the conducting system, in particular the AV node, in this rabbit model of LVD due to MI.

1.4 Aims and hypothesis

The aims of this thesis were:

1. To confirm that abnormal prolongation of atrioventricular conduction time originates at the atrioventricular node in the rabbit model of heart failure;

2. To investigate the spatiotemporal pattern of this electrical slowing using optical mapping;

3. To examine in-vivo markers of AV delay in rabbit and identify any changes consistent with prolonged AV nodal conduction time in the rabbit model of heart failure;

4. To explore the mechanisms underlying any observed prolongation of AV nodal delay, and

5. To study AV nodal conduction characteristics in other clinically relevant conditions, namely acidosis and aging.

The hypothesis at the outset of this thesis was that chronic heart failure in the rabbit results in an increase in AV conduction time at the level of the AVN, and that the increased AV conduction time is a consequence of ?-adrenoceptor downregulation

Chapter 2 – General Methods

2 General methods

2.1 Rabbit model of left ventricular dysfunction due to apical myocardial infarction

A well-characterised model of myocardial infarction (MI) induced by coronary artery ligation was used in this study (82-88). Procedures were undertaken in accordance with the United Kingdom Animals (Scientific Procedures) Act 1986 and conform to the Guide for the Care and Use of Laboratory Animals published by the US National Institutes of Health (NIH Publication No. 85-23, revised 1985). Adult male New Zealand White rabbits (2.5-3.0kg) were given premedication with 0.4ml/kg intramuscular Hypnorm [fentanyl citrate (0.315mg/ml): fluanisone (10mg/ml), Janssen Pharmaceuticals]. Anaesthesia was induced with 0.25-0.5mg/kg midazolam (Hypnovel, Roche) given via an indwelling cannula in the marginal ear vein. The rabbit was intubated and ventilated using a Harvard small animal ventilator with a 1:1 mixture of nitrous oxide and oxygen containing 1% halothane at a tidal volume of 50 ml and a frequency of 40 per minute. Preoperative antibiotic prophylaxis was given with 1 ml Amfipen (ampicillin 100 mg/ml, Mycofarm UK Ltd) intramuscularly. A left thoracotomy was performed through the 4th intercostal space. Quinidine hydrochloride 10mg/kg (Sigma Pharmaceuticals) was administered intravenously prior to coronary artery ligation to reduce the incidence of ventricular fibrillation. The marginal branch of the left circumflex coronary artery, which supplies most of the left ventricular free wall, was ligated halfway between the atrioventricular groove and the cardiac apex to produce an ischaemic area of 30-40% of the left ventricle. As there is relatively little collateral circulation in the rabbit, a homogenous apical infarct was produced occupying on average 14% of the total endocardial and epicardial surfaces towards the apex of the left ventricle (Figure 2-1A)(89).

Ventricular fibrillation occurred in approximately 30% of cases; usually 8 to 12 min following occlusion, and defibrillation was undertaken with a 5-10J epicardial DC shock. Once the animal was stable, the thoracotomy was closed. The animals were then given 20ml of isotonic saline intravenously to replace perioperative fluid losses and allowed to convalesce in a warm clean environment with adequate monitoring for any early signs of distress. Analgesia was given with 0.04mg/kg intramuscular Vetergesic (buprenorphine hydrochloride 0.3mg/ml, Reckitt & Colman Products Ltd) immediately after surgery and the next morning.

Sham-operated animals underwent thoracotomy with the heart manipulated in a similar fashion except that the artery was not tied.

2.2 Characteristics of the rabbit model of myocardial infarction

Echocardiography was performed 1 week prior to sacrifice to assess in-vivo cardiac function, using a 5 MHz paediatric probe with a Toshiba sonograph (Sonolayer 100). The rabbit was sedated with 0.3 mg/kg Hypnorm and a small area of the anterior chest wall was shaved to allow a satisfactory echo window. The coronary ligated animals (MI) showed significant haemodynamic dysfunction in terms of increased left ventricular end-diastolic dimension (LVEDD), left atrial dimension (LAD) and decreased ejection fraction (90). Evidence of congestion was manifest in significant increases in lung and liver wet weight present at post-mortem examination. Previous work has shown that this animal model shows significant cardiac hypertrophy, evident as a 20-30% increase in heart wet weight, left ventricular dry weight (see Table 2-1) (91;92) and increased cardiomyocyte length (93). In vivo haemodynamic measurements reveal a normal cardiac output but raised end diastolic pressure and reduced response to an increased pre-load in this model (92;93). Increased inducibility of arrhythmias and lowered fibrillation threshold observed in vitro (89;93) suggesting accompanying electrophysiological dysfunction. The infarct model is associated with a significant late mortality as demonstrated by the Kaplan-Meier graph in Figure 2-1B.

	INFARCT (n = 25)	SHAM (n= 21)	p value
Body weight (kg)	3.60 ± 0.05	3.56 ± 0.07	NS
Ejection fraction (%)	42.6 ± 1.3	71.2 ± 1.4	<0.001
LAD (mm)	15.8 ± 0.3	10.9 ± 0.3	<0.001
LVEDD (mm)	20.0 ± 0.3	16.8 ± 0.3	<0.001
Liver weight (g)	93.0 ± 2.4	81.0 ± 4.0	<0.02
Lung weight (g)	13.1 ± 0.8	10.9 ± 0.3	<0.01
Heart weight (g)	13.1 ± 0.4	11.3 ± 0.4	<0.005
LV dry weight (g)	1.40 ± 0.06	1.15 ± 0.04	<0.002
RV dry weight (g)	0.57 ± 0.05	0.39 ± 0.02	<0.005

Table 2-1- Characteristics of the rabbit model of LVD (From (90)). Results expressed as mean ± SEM.

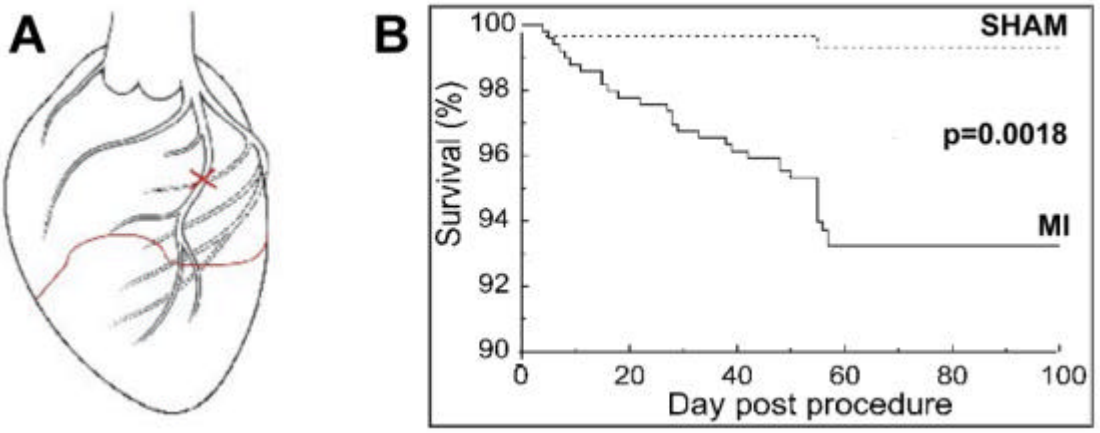

Figure 2-1 – A – schematic diagram of the infarct model. B – Kaplan-Meier survival curve of sham versus MI, demonstrating increased mortality associated with coronary ligation (from (94)**) .**

2.3 In vivo electrocardiogram recordings

In-vivo analysis of the electrocardiogram was carried out to allow determination of RR and PR intervals and QRS duration in the intact animal, and to identify any effect of LVD on these parameters. Recordings were taken immediately after echocardiography therefore no additional sedation or anaesthesia was required. Three electrodes were positioned subcutaneously and the electrocardiogram recorded from lead II.

2.3.1 Analysis of in-vivo electrocardiograms

The ECG data were acquired using a MP100A data acquisition unit (Biopac Systems Inc, Santa Barbara, California) which converted the ECG signals to digital format. Signals were recorded using software associated with the MP100 system, AcqKnowledge (version 3.5.3, Biopac Systems Inc, Santa Barbara, California). Data files were then viewed using locally developed software (ECG Explore, Dr FL Burton, University of Glasgow) which allowed conversion to text files, which could be imported into the ECG analysis program. Analysis of the RR and PR intervals and the QRS duration was carried out using commercially available software (Chart, version 5, ADInstruments). A representative sample of 1000 beats at steady state (as determined by the lack of significant variation in the RR interval (less than 10ms) over the recording period) were selected from each experimental condition. From this, the mean RR interval, mean PR interval and mean QRS duration were determined. Comparisons were made between the sham and ligated animals. To identify the presence of a correlation, the PR interval versus the RR interval was also plotted for each condition, as was the PR interval versus the QRS duration.

2.4 The isolated atrioventricular node

2.4.1 Tissue preparation

Under terminal anaesthesia with sodium pentobarbitone 200mg/kg (Rhone Merieux) mixed with 500IU of heparin, hearts from adult male New Zealand White rabbits were rapidly excised and placed in ice cold Tyrode's solution, of the following composition (mmol/L): Na^+ 134.5, Mg^{2+} 1.0, K^+ 5.0, Ca^{2+} 1.9, Cl^- 101.8, SO_4 1.0, H_2PO_4 0.7, HCO_3 20, acetate 20 and glucose 50. The pH of the solution was maintained at 7.4 by continuous bubbling with mixed gas of 95% oxygen and 5%

carbon dioxide. The isolated AV node preparation was created by the removal of all ventricular tissue, followed by an incision around the crest of the right atrial appendage, which when folded open exposed the endocardial surface of the right atrium and inter-atrial septum. Remaining left atrial tissue was removed, leaving a section of tissue containing the triangle of Koch, the Crista Terminalis, the right atrial appendage and a small section of right ventricle and inter-ventricular septum (Figure 2-2). The sinus node was left intact. This tissue was pinned onto a Sylgard plate and superfused with oxygenated Tyrode's solution. A constant superfusion rate of 40ml/min was maintained using a Gilson Minipuls 3 peristaltic pump. Temperature was maintained at 37ºC. Figure 2-3 illustrates the isolated atrioventricular node superfusion system.

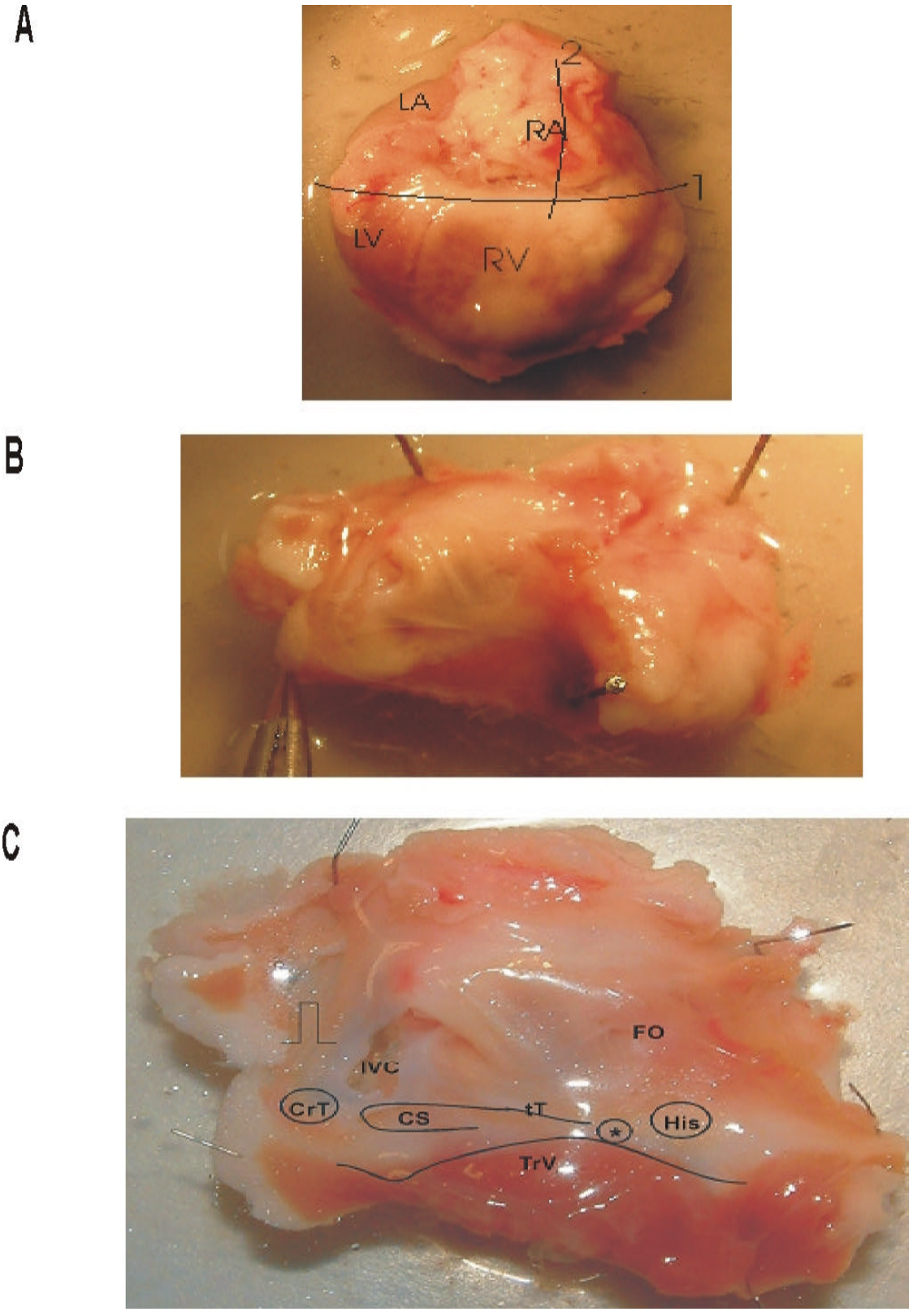

Figure 2-2 – Dissection of the isolated AV node preparation. A. The ventricles are removed via an incision distal to the AV groove (1). Then an incision around the crest of the right atrial appendage (2) allows exposure of the endocardial surface of the interatrial septum. B. With the ventricles removed, the triangle of Koch can be identified and the remaining left atrium and ventricular tissue can be removed safely. C. The isolated AV node pinned out on Sylgard, demonstrating the structures of the triangle of Koch and the position of the stimulus and His and atrial electrodes. (CrT: crista terminalis (atrial electrode position), IVC: inferior vena cava, CS: coronary sinus, tT: tendon of Todaro, FO: fossa ovalis, TrV: tricuspid valve, His: His bundle electrode position, *: AV node region.

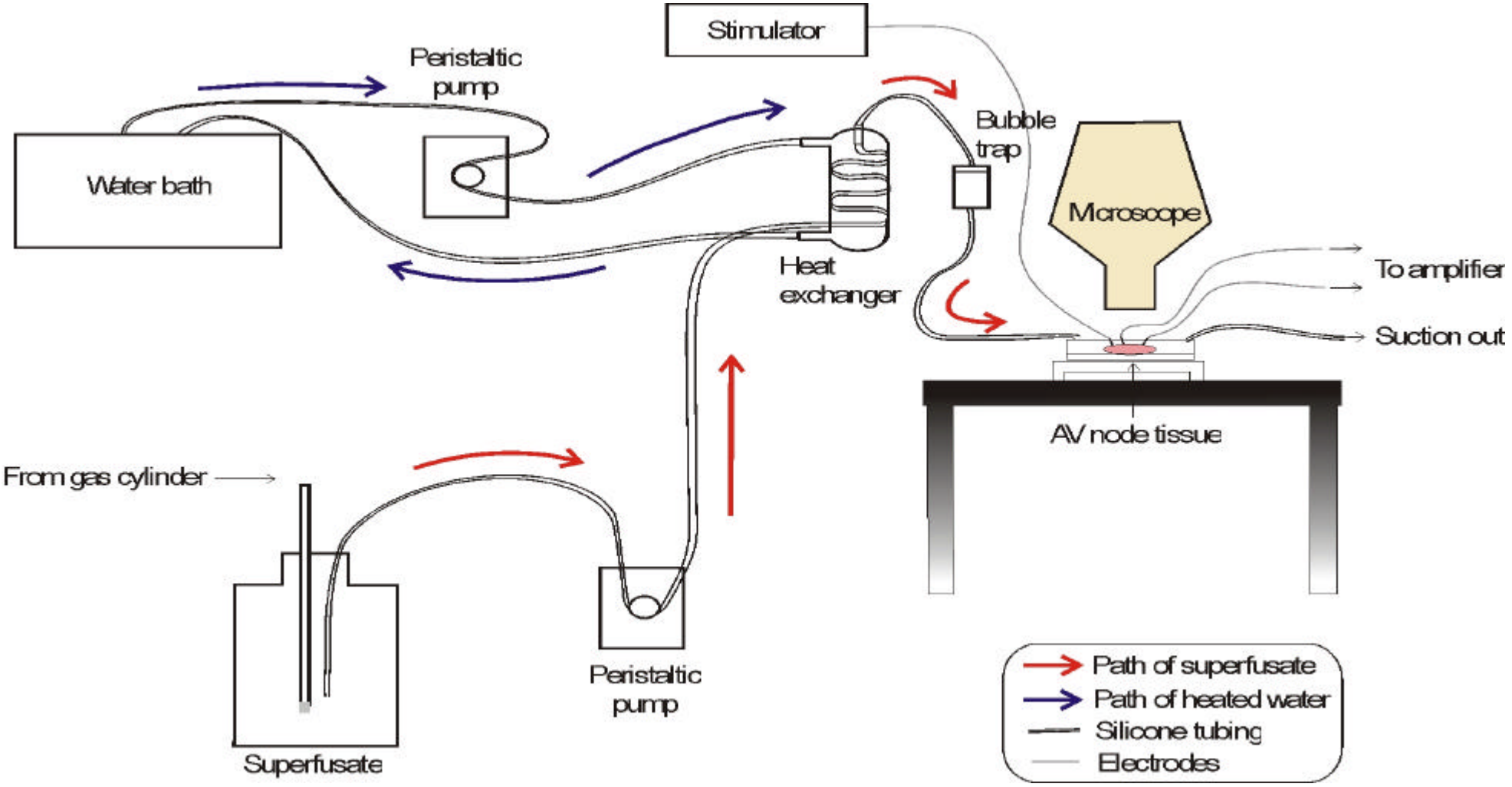

Figure 2-3 – Isolated AV node superfusion apparatus

2.4.2 Surface electrogram recording and pacing protocols

A bipolar silver wire stimulating electrode was positioned on the endocardium at the right atrial appendage near the sinus node. The atrium was driven by a Digitimer DS2 stimulator that provided twice threshold 2ms wide rectangular voltage pulses. Timing of the pulse was computer controlled using locally developed software (Dr FL Burton, University of Glasgow).

Two silver wire bipolar extracellular recording electrodes were developed to allow surface electrograms from the low inter-atrial septum and the His bundle region to be acquired. The distance between each pair of bipolar electrodes was 14mm. Atrial and His bundle electrodes were positioned on the endocardial surface using a Narishige micromanipulator. Effort was made to ensure consistent distance between the electrodes to ensure the conduction times were not affected by heart size. The electrodes were connected to a monophasic action potential (MAP) amplifier (custom built by Dr Mark Watts, Glasgow Royal Infirmary). Electrograms underwent high pass (40Hz) filtering within the MAP amplifier, which was connected to an oscilloscope (Nicolet Instruments Corporation, Wisconsin, USA) to allow real-time viewing of the electrograms.

2.4.3 Analysis of surface electrograms from the isolated atrioventricular node

The rate dependent properties of the AV node are determined by standard pacing protocols. Electrograms recorded from the surface of the isolated AV node preparation were recorded using locally developed ECG acquisition software (NMap, Dr FL Burton, University of Glasgow). The basic stimulus cycle length was 300ms or 10% shorter than the spontaneous sinus cycle length. The standard basic stimulus protocol (in which sixteen basic beats were followed by a one second pause, with the cycle length decrementing by 5ms intervals after each pause) allowed atrio-Hisian (AH) intervals and Wenckebach cycle length to be derived. Examples of the signals acquired and the analysis methods are outlined in Figure 2-4.

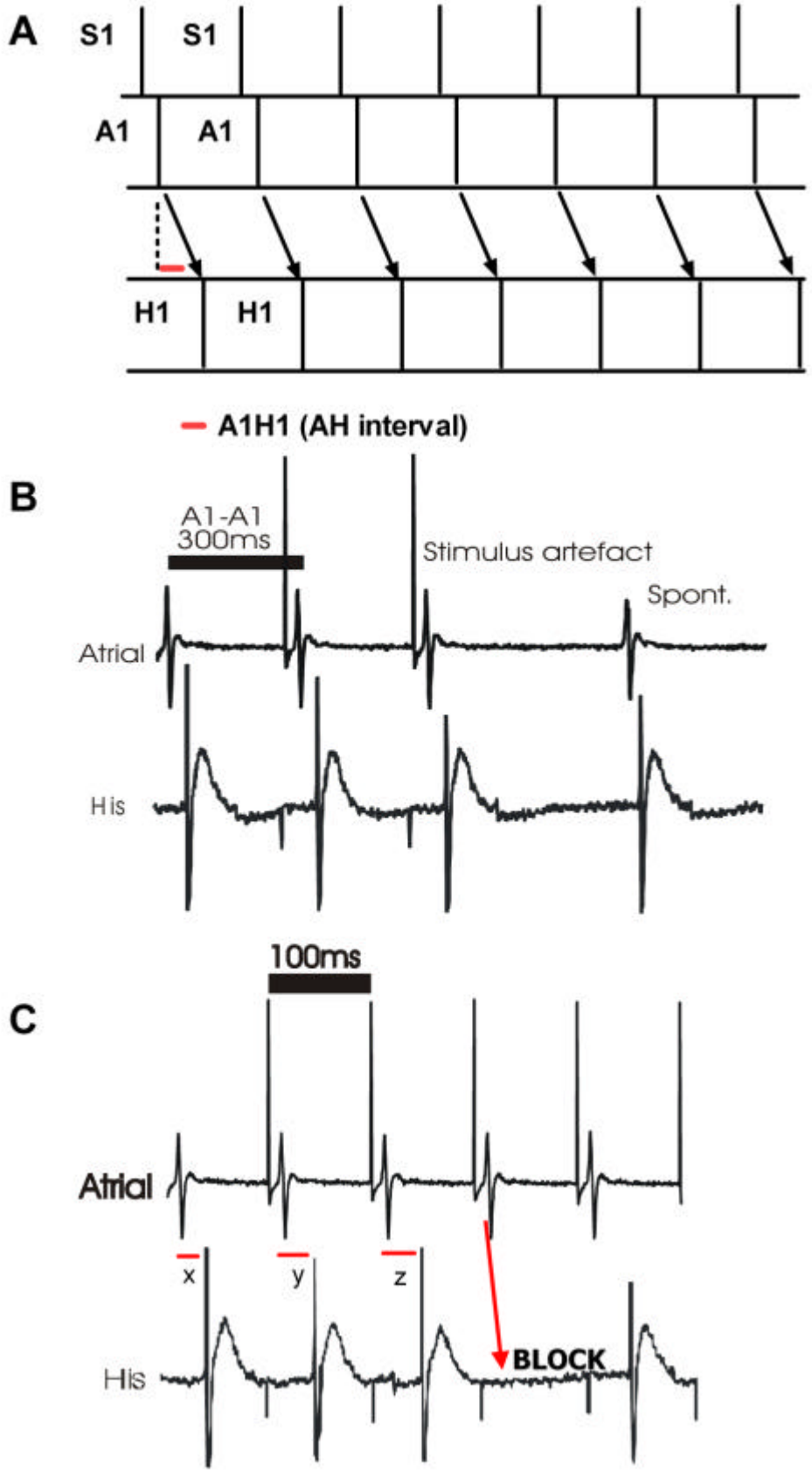

Figure 2-4 – A – Pacing method to derive AH intervals and Wenckebach cycle length at basic pacing cycle length (S1S1 (ms)). B – Surface electrograms derived from the isolated AV node preparation at pacing cycle length S1S1 300ms (thus A1A1 interval = 300ms). C- Progressive prolongation of the AH interval (x=35ms; y=39ms; z=45ms). Rate dependent activation failure of the His bundle occurs at PCL 100ms, i.e. 100ms is the Wenckebach cycle length.

The functional and effective refractory periods of the AV node and the atrial effective refractory periods were derived by a premature stimulation protocol. The AV nodal effective refractory period (ERP) is defined as the longest A1A2 interval that fails to elicit an H2 response. The AV nodal functional refractory period (FRP) is defined as the shortest H1H2 interval achieved by premature stimulation The atrial effective refractory period is defined as the longest S1S2 interval that fails to elicit an A2 response. This protocol consisted of sixteen basic beats followed by one premature beat followed by a one second pause (Figure 2-5A). The premature beat coupling interval was decremented by 5ms steps until atrial refractoriness (defined as the longest S1S2 interval that failed to elicit an A2 response) occurred. These protocols allow consistent and reproducible creation of AV nodal conduction and refractory curves (Figure 2-5B and 2-5C), from which parameters of AV nodal function can be derived. In addition, the spontaneous sinus cycle length was recorded in every experiment.

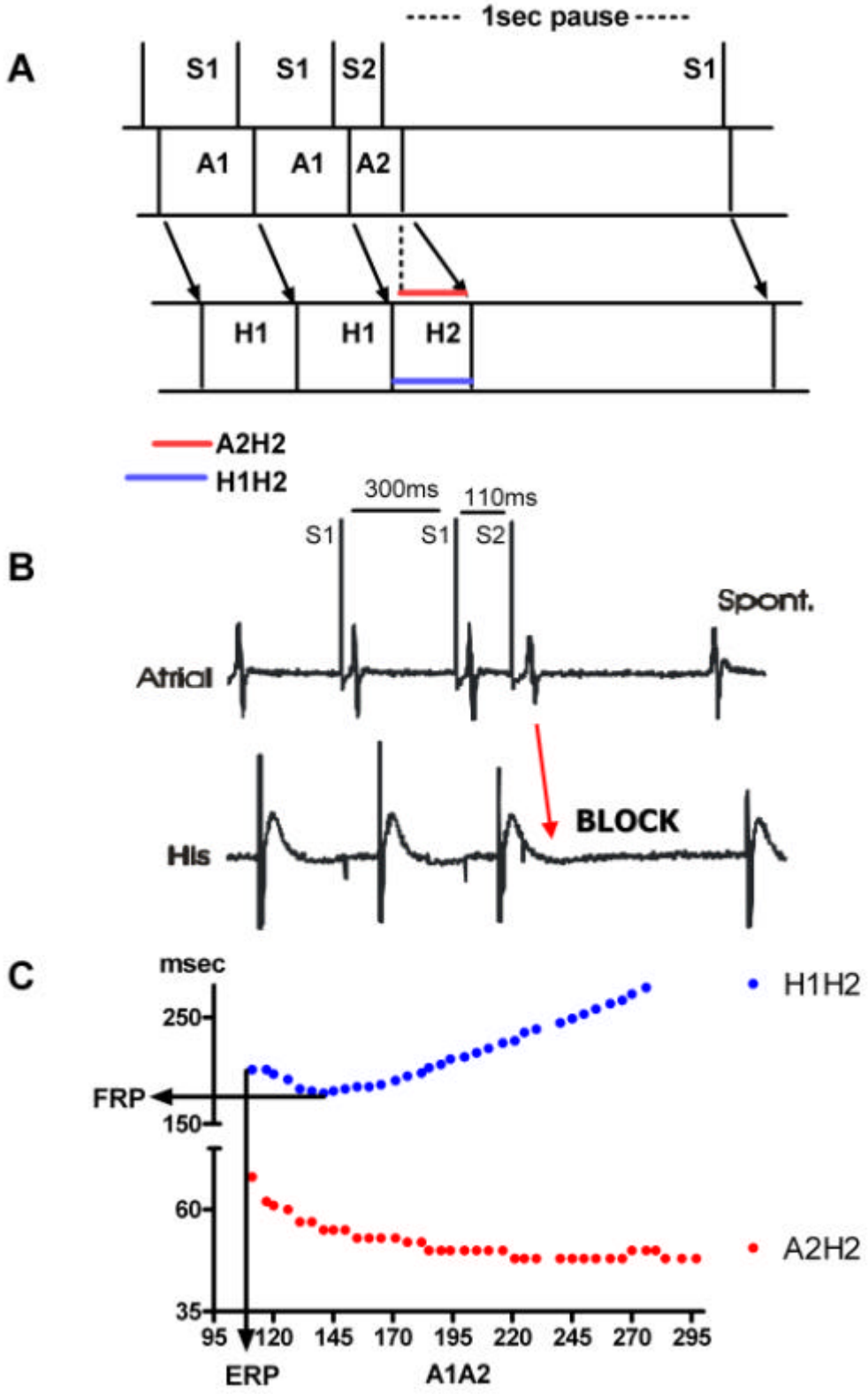

Figure 2-5 – A – Pacing method to derive functional and effective refractory periods of the AV node showing introduction of a premature stimulus after a 16 beat basic drive train at S1S1 300ms. B – Surface electrograms derived from the isolated AV node showing blocked conduction to the His bundle at S1S2 110ms. C – By plotting the A2H2 interval against the A1A2 interval, the AV node conduction curve is create d (red). By plotting the H1H2 interval against the A1A2 interval, the AV node refractory curve is created (blue) and the FRP and ERP can be determined.

2.5 Optical mapping of the atrioventricular node

2.5.1 Principles of optical mapping using fluorescent voltage sensitive dyes

The AV node is an entity of incredible structural and functional complexity (46). The technical challenges of attempting to impale multiple glass microelectrodes into this small region are such that it is difficult to use this technique to characterise, with accuracy, the spread of activation across the inputs and output of the compact nodal region. Imaging of transmembrane potentials using voltage sensitive fluorescent dyes has become a major tool for the study of electrical activation in myocardial tissue. Recent progress in this imaging modality has allowed the study of activation patterns in the AV node, helping to link its functional complexities to its anatomic structure (95-99).

An optical mapping system consists of three main components (Figure 2-6):

1. The heart preparation, stained with a fluorescent voltage sensitive dye;

2. A system of optics, which filters the fluoresced light emitted from the heart preparation, then focuses it on to a photo-detector, and;

3. A photo-detector, which quantifies the emitted light from the preparation.

Optical mapping allows the simultaneous recording of the electrical activity of hundreds to tens of thousands of sites on a cardiac surface (For review see (100;101)). Hearts are first loaded with a voltage-sensitive fluorescent dye (such as RH237) that binds to the myocyte membrane with high affinity. The general principle underlying optical mapping is that photons of an appropriate excitation wavelength are absorbed by the voltage-sensitive dye. The dye forms an unstable state, from which it falls back to its baseline state, emitting photons of a longer wavelength. The key property of voltage sensitive dyes is that the emission spectrum of the dye is voltage dependent. In summary, after being excited by short wavelength light, the dye fluoresces at a longer wavelength (Stokes Law). The spectral characteristics of this fluorescence are altered by the membrane potential of the preparation. Figure 2-7 illustrates how membrane depolarisation results in a shift of RH237's fluorescence spectrum to shorter wavelengths. This spectral shift affects the amplitude of the fluorescence as measured beyond a fixed long

wavelength cut-off. Therefore membrane depolarisation results in a relative fall in fluorescence at longer wavelengths. On membrane repolarisation, the spectrum returns to its original characteristics, resulting in an increase in fluorescence back to pre-activation levels.

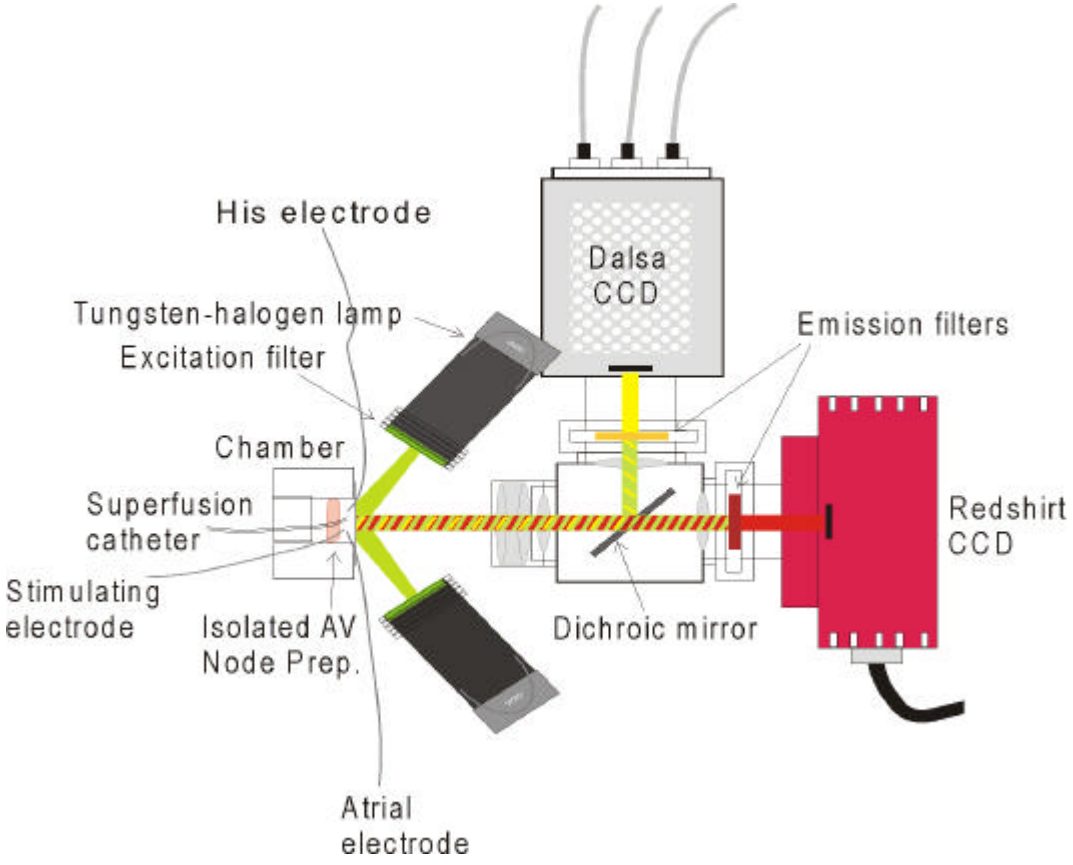

Figure 2-6 - – Schematic diagram of the AV node optical mapping apparatus

The nature of the optical action potential (AP) is different from the transmembrane AP recorded by a microelectrode. For this reason, the optical AP upslope is slower than the simultaneous transmembrane AP. Cells adjacent to each other activate in rapid succession as the wave of excitation spreads. The extent of upstroke slowing depends on the number of cells influencing the membrane potential recording. In optical mapping the extent of slowing of the upstroke of the optical AP is determined by the spatial resolution of the optical system. The spatial resolution is determined by a combination of the optical magnification, and the number of recording sites on the detector. The optical magnification is a limiting factor on the spatial resolution as increasing magnification lowers the signal to noise ratio.

Previously it was thought, that similar to contact electrodes, optical recordings originated from only the very surface layer of the epi/endocardium. Evidence now shows that optical measurements may penetrate deeper. Using a transparent mapping array, Knisley *et al*. compared simultaneously the excitation intervals of optical and extracellular electrical recordings, and demonstrated that the differences between them could be attributed to deeper optical interrogation and the accompanying fibre rotation (102). This 'depth of field' effect is an additional complication, but its dependency on the optical properties of the set-up allows it to be quantified using the standard optical equation (103):

$$\text{Depth of Field} = 1000?m/[(7 \times NA \times \text{magnification}) + ?_{ex}/2(NA)^2$$

(where NA is the numerical aperture of the collecting lens and $?_{ex}$ is the wavelength of the emitted light).

Movement during myocardial contraction alters the site that the detector is focused on, and therefore changes the signal fluorescence for reasons unrelated to the membrane potential (movement artefact). Although electro-mechanical uncoupling agents can be used to reduce or even eliminate movement, evidence is growing that they alter the electrophysiological properties that are being studied (104-107). Motion artefact while imaging the AV junction was minimal as this area is largely composed of fibrous non-contractile myocardium therefore the use of an excitation-contraction un-coupler was not necessary

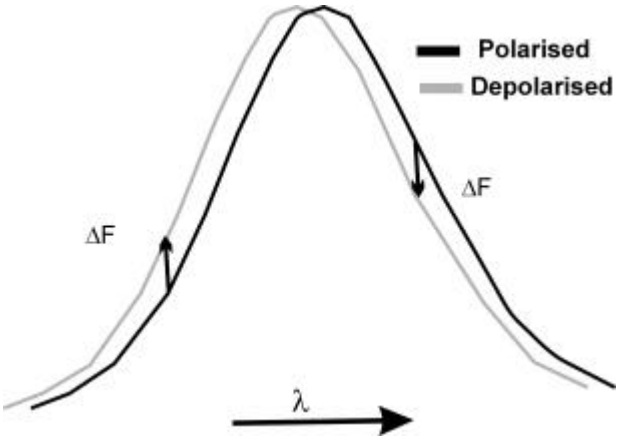

Figure 2-7.- Diagram of voltage-sensitive spectral shift. Depolarisation produces a reduction in fluorescence at the red end of the spectrum e.g. RH237. (Adapted from (108)).

2.5.2 Langendorff perfusion

Under terminal anaesthesia with sodium pentobarbitone 200mg/kg (Rhone Merieux) mixed with 500IU of heparin, hearts from adult male New Zealand White rabbits were rapidly excised and placed in ice cold Tyrode's solution, of the following composition (mmol/L): Na^+ 134.5, Mg^{2+} 1.0, K^+ 5.0, Ca^{2+} 1.9, Cl^- 101.8, SO_4 1.0, H_2PO_4 0.7, HCO_3 20, acetate 20 and glucose 50. The pH of the solution was maintained at 7.4 by continuous bubbling with mixed gas of 95% oxygen and 5% carbon dioxide. The solution was filtered through a 5µm filter (Whatman). The heart was mounted on the aortic cannula for Langendorff perfusion. The temperature was maintained at 37°C. A constant perfusion rate of 40ml/minute was maintained using a Gilson Minipuls 3 peristaltic pump. Perfusion pressure was monitored with a transducer in series with the aortic cannula. While undergoing Langendorff perfusion, hearts were loaded with a 200µl bolus of the voltage sensitive dye RH237 (Molecular Probes) dissolved in DMSO (1mg/ml) administered by slow injection into the coronary circulation via an injection port in the bubble trap. The fractional fluorescence change caused by an action potential has previously been shown to be in the range 2 to 6% at 514.5 nm excitation (109). In preliminary experiments, in keeping with previous work undertaken by other groups (43;95;97), the voltage sensitive dye di-4-ANEPPS was used. However I found superior signal amplitudes and signal to noise ratios using RH237 and therefore used this consistently throughout the remainder of the study. Hearts were then removed from the Langendorff cannula and returned to ice-cold Tyrode's solution to induce cardioplegia before dissection of the isolated AV node preparation as described above.

2.5.3 Optical imaging of AV nodal conduction

A schematic diagram of the optical mapping apparatus is shown in Figure 2-6. The isolated AV node preparation was dissected as described above and mounted onto a Sylgard base within a custom made imaging chamber, designed to allow superfusion of the AV node preparation and simultaneous programmed stimulation, recording of surface electrograms from the atrial and His bundle regions as well as imaging of patterns of activation from optically derived action potentials. The preparation was superfused with oxygenated Tyrode's solution at a rate of 40ml/min maintained by a Gilson Minipuls 3 peristaltic pump. The temperature was maintained at 37°C. Light emitted from four 75W tungsten-halogen bulbs was passed through short-pass (535±50nm) filters and directed onto the endocardial surface of the AV node preparation. Light emitted from the tissue was collected by the camera lens (Nikon

50mm) and focused onto the charged coupled device (CCD) array (Dalsa, Canada) via a 695nm high-pass filter. This system affords flexibility in the choice of mapping area and spatial resolution (80x80, 40x40 or 26x26 pixels), traded off against maximum temporal resolution (1kHz, 3kHz & 5kHz respectively) and signal-to-noise ratio. Recordings of up to 5 seconds (limited by RAM) were saved to computer disk for later analysis. The image of the AV node region was focused onto the array such that an area of 14.5x14.5mm^2 at a spatial resolution of 40x40 pixels (3kHz) was imaged. This was found to be optimum for imaging AV nodal activation, allowing mapping of AV nodal inputs and output to the His bundle, as identified by the surface electrograms.

2.5.4 Analysis of optically derived action potentials from the isolated AV node preparation.

Analysis of optically derived action potentials (AP) from the isolated AV node preparation was carried out on locally developed software ("Optiq", Dr Francis Burton, University of Glasgow). Surface electrograms recorded during optical mapping experiments could be concurrently visualised and analysed using this program. This in addition to the integrated functionality allowing direct import of the CCD image from each experiment allowed accurate anatomical and functional characterisation of optical signals.

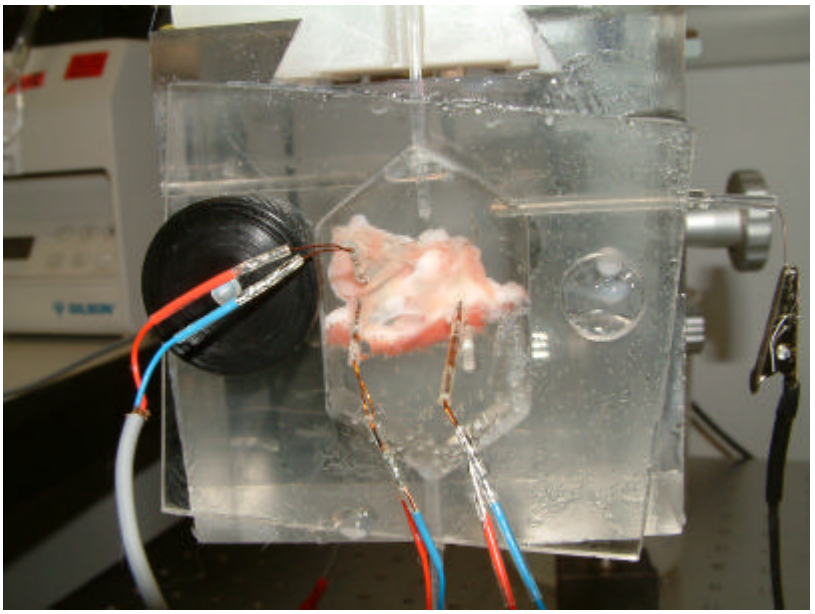

Figure 2-8 – Photograph of isolated AV node preparation in optical imaging chamber.

A bipolar silver wire stimulating electrode was positioned on the endocardium at the right atrial appendage near the sinus node. The atrium was driven by a Digitimer DS2 stimulator that provided twice threshold 2ms wide rectangular voltage pulses. Timing of the pulse was computer controlled using locally developed software (Dr FL Burton, University of Glasgow). Surface electrograms were recorded using a pair of bipolar silver electrodes positioned at the Crista terminalis (for the atrial electrogram) and at the central fibrous body (for the His bundle electrogram). The distance between the electrodes remained consistent throughout each experiment due to fixed holes in the imaging chamber front plate (Figure 2-8). Adjustment of the position of the front plate allowed fine adjustment of electrode position without altering the inter-electrode distance. The electrodes were connected to a MAP amplifier (custom built by Dr Mark Watts, Glasgow Royal Infirmary). Electrograms underwent high pass (40Hz) filtering within the MAP amplifier, which was connected to an oscilloscope (Nicolet Instruments Corporation, Wisconsin, USA) to allow real-time viewing of the electrograms. Furthermore, electrograms were recorded and digitised by the Redshirt imaging system and could be visualised and analysed simultaneously with the optically derived signals. There was no evidence of alteration of the AV nodal conduction time with the addition of voltage sensitive dye, as illustrated by Figure 2-9. At PCL 250ms there was no significant change in the AH interval over an 80 minute period regardless of fluorescence and in spite of the addition of a further bolus of RH237 to improve fluorescence signals.

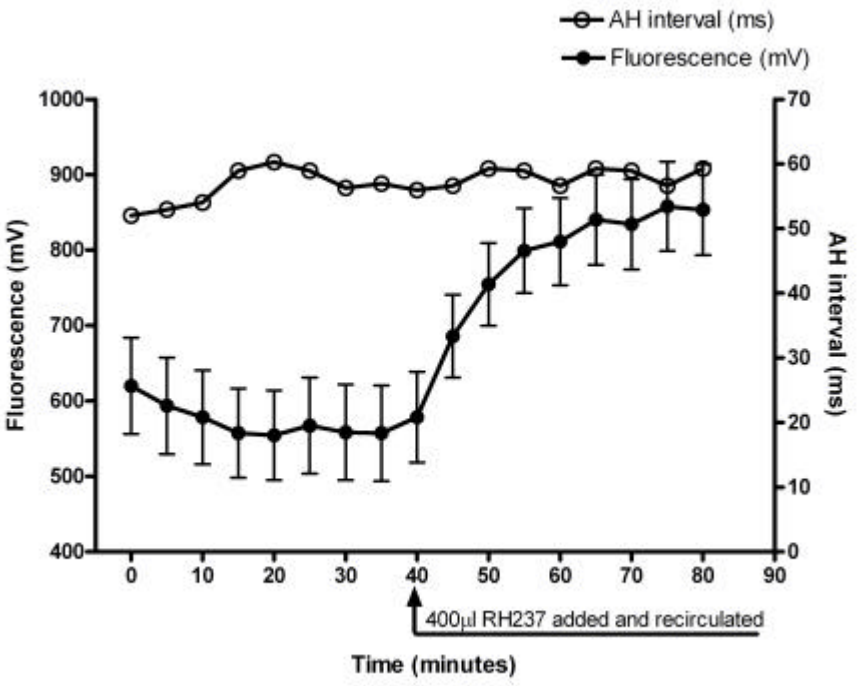

Figure 2-9 – Association of fluorescence over time versus AH interval with RH237 (at baseline 200µl RH237 injected via Langendorff followed by a further bolus of 400µl added to the effluent for re-circulation).

Optically derived action potentials result from fluorescent signals emitted from a group of cells within the three dimensional volume of myocardium aligned with the photodiode. The image of the AV node was magnified such that each pixel represented signals derived from a 0.36x0.36mm area of endocardium. The depth of field of the collecting lens restricted the fluorescence measurements to a layer of cells up to 500µm from the surface.

Three measures of activation derived from optical signals were studied, each analysed relative to the onset of the atrial electrogram:

- T_{act} (activation time). Tact was defined as the time point of the maximum rate of rise of the AP upstroke (dF/dt_{max}), defined as the first derivative of the fluorescence signal.

- T_{peak} (time to peak of the AP). Tpeak was defined as the time in milliseconds from the defined start point (the first peak of the atrial electrogram) to the peak amplitude of the AP.

- T_{actM} . TactM was defined as the activation time point midway between the baseline and the peak of the AP.

The mean ± SEM of each parameter defined above was determined in 4 distinct regions of the preparation, consisting of 10-15 pixels each. Region 1 represented the signals derived from atrial myocytes, region 2 the proximal AV node, region 3 the compact AV node and region 4 the His bundle region/AV nodal output (Figure 2-10). Regions were defined anatomically for each individual preparation. Absolute values of mean ± SEM T_{act}, T_{peak} and T_{actM} were then plotted and values compared between control and LVD samples. Furthermore, the conduction times between regions (atrial to AV node input, AV node input to compact node, compact node to His bundle) were determined and plotted. Activation time (T_{act}) was found to be the most reliable measurement and therefore data from the analyses of T_{peak} and T_{actM} are not shown.

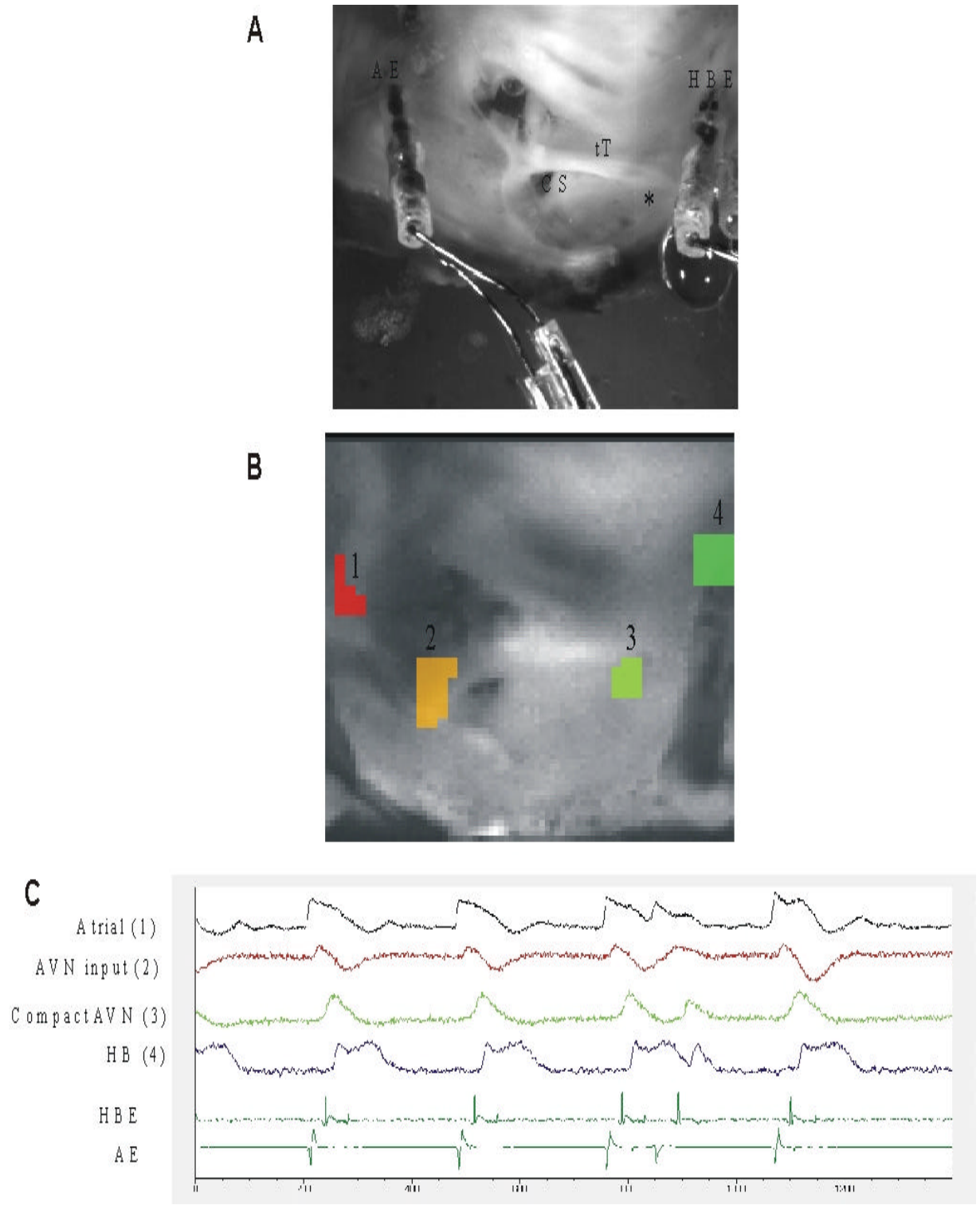

Figure 2-10- Analysis of optical signals derived from the AV node. A – Photograph of the preparation in situ (AE – atrial electrode, CS – coronary sinus, tT – tendon of Todaro, HBE –His bundle electrode, * - compact AV node. B – CCD image of optically imaged region (1 – atrial tissue, 2 – AVN input/proximal AVN, 3 – compact AVN, 4 – His bundle region). C – Optically derived action potentials from regions 1-4. Note also atrial and His bundle surface electrograms (AE and HBE).

2.6 Histological analysis of the AV node

Dr Patrizia Camelliti (University of Oxford) has undertaken histological analysis of the isolated AV node preparation to determine the expression of gap junction proteins (connexins) and their distribution in AV nodal tissue, and to determine the presence of any changes in connexin expression and/or distribution caused by LVD in our experimental model.

At the end of the electrophysiology experiments, the isolated AV node preparations were further dissected to remove excess atrial tissue and remaining ventricular myocardium. The tissue was then placed on a coverslip rendered hydrophobic by coating with Repelcote. A fixative solution was then applied to the tissue and a further coverslip placed on top. The tissue sample was then snap frozen in liquid nitrogen and packaged in dry ice for transportation to the laboratory of Dr Camelliti, where it was sectioned and immuno-labelled for connexins 40, 43 and 45 and neurofilament NF-160.

2.7 Statistical analysis

Power calculations predicted the estimated sample size required (N) at 10 rabbits/group to detect a 20ms (20%) difference in the AH intervals between the control and LVD groups. (N=(2.SD2.power index)/?2, where power index is equal to 7.9 for 80% power to detect 2-sided significance at P<0.05)(110) .

Data were expressed as the mean ± standard error of the mean (SEM). Comparisons between two groups of data were made using Student's t-test (paired where appropriate). Two-way ANOVA was used where appropriate to compare differences in the response of the controls versus LVD samples to interventions, such as the administration of a drug as well as to compare region by region conduction times in optical mapping experiments. A two-tailed p-value of less than 0.05 was considered statistically significant.

Chapter 3 - Atrioventricular nodal function in a rabbit model of left ventricular dysfunction

3 Atrioventricular nodal function in a rabbit model of left ventricular dysfunction

3.1 Introduction

3.1.1 Conduction abnormalities in CHF

The prognosis in chronic heart failure is affected by conduction abnormalities affecting both the AV node and the His-Purkinje system (5-7;9;17). The mechanisms by which this occurs are not fully understood. Previous work from this laboratory has demonstrated delay in AV conduction in a rabbit model of left ventricular dysfunction (LVD)/heart failure due to chronic myocardial infarction (81). In this model, the infarct is localised to the left ventricular apex and there is no direct ischaemic insult to the basal myocardium. Using optical mapping, a mean increase of 20ms (20%) was found in the interval between right atrial stimulation and left ventricular epicardial activation in LVD hearts compared with controls (Figure 3-1). There was no decrease in left ventricular transmural or epicardial conduction velocity. The AV conduction delay increased with increasing pacing rates, suggesting that the site of increased delay was most likely to be the atrio-ventricular node. Initial histological analysis failed to demonstrate any gross changes in the tissue architecture of the AV node to account for this. The purpose of this study was to confirm that the exaggerated delay observed in LVD with respect to epicardial activation following right atrial stimulation was due to conduction delay within the AV node. Furthermore, this study aimed to study the effects of LVD on atrial and AV nodal refractory periods. Also, using standard pacing protocols, this study aimed to determine the prevalence of dual pathway AV nodal physiology in rabbit, and to identify any differences in slow or fast pathway conduction that might explain any exaggerated AV nodal delay in LVD.

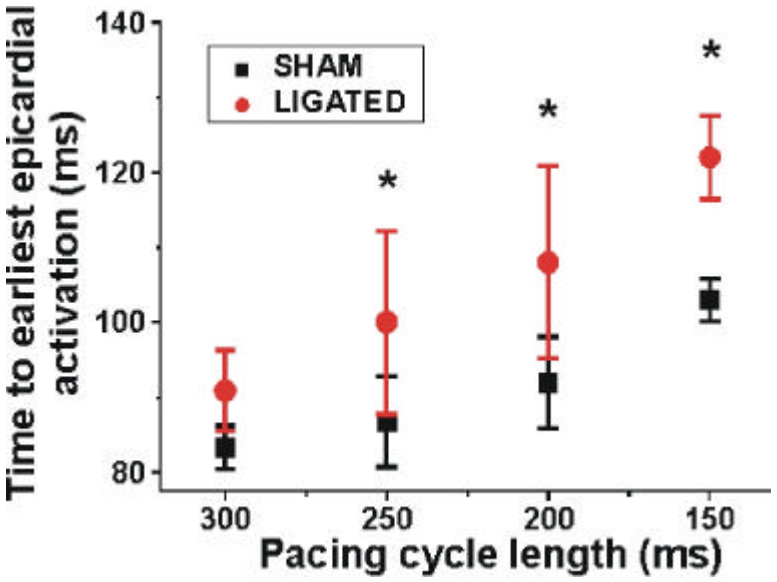

Figure 3-1 –Time to earliest epicardial activation from right atrial pacing (reproduced from (81) with permission. This demonstrates the increase in delay of time from right atrial stimulus to epicardial activation in LVD, which increases with shorter pacing cycle lengths.

3.1.2 Age as a contributor to AV nodal delay in CHF

Atrioventricular conduction disorders have been recognised to occur with increased frequency with increasing age. Both cross-sectional and longitudinal studies of apparently healthy men and women have shown progressive prolongation of the PR interval on the electrocardiograph with advancing age (111;112). A further study, aiming to correlate the presence of ECG abnormalities with co-existing cardiac disease, showed that even in the absence of apparent underlying coronary or hypertensive heart disease, atrio-ventricular block occurred in patients = 65 years old (113). The prevalence was increased in men compared to women, and further increased in the presence of co-existing heart disease.

Non-invasive investigation by means of high resolution signal averaged ECG in the context of age-related PR interval prolongation showed that the increase appeared to be due entirely to prolongation of the interval between the onset of the P wave to the His bundle signal, with no increase in the H-V interval. This suggests that age associated PR interval prolongation reflects delay at the level of the AV node (114).

AV conduction is highly dependent on heart rate and autonomic tone, which is difficult to control for in human studies. Schmidlin *et al* (115) studied the effects of physiological aging on the cardiac electrophysiology of isolated, Langendorff

perfused Fischer 344 rat hearts, in the absence of potentially confounding autonomic influences. They demonstrated a significant decrease in heart rate with aging. Furthermore, spontaneous AV conduction times and AV conduction time during programmed stimulation increased significantly with aging. Wenckebach cycle length was also prolonged in senescent rats compared to younger animals. Histological analysis of the tissues demonstrated increased intercellular distance and increased collagen in the AV node, His bundle and summit of the interventricular septum. In 1995, another group studied the effect of aging on AV conduction in human subjects in the presence of autonomic blockade with atropine and propranolol (116). The findings concur with the animal study by Schmidlin *et al*. They found that in the presence of double autonomic blockade, the RR, PR, paced AV intervals and AV block cycle length were longer in older subjects. This confirms that in humans, heart rate and AV conduction prolongation exists with increasing age, and are independent of ß-adrenergic and/or parasympathetic influences.

In the present study, there is progressive prolongation of the AH interval at all pacing cycle lengths in animals at 32 weeks post ligation (LVD (32)) compared to younger animals at 8 weeks post ligation (LVD (8)). As discussed above, age-related AV nodal conduction disturbance has been identified in both human and animal studies. The aim of this study was to examine the AV nodal conduction characteristics in a series of sham operated controls at 32 weeks post sham operation, and compare this with stock control animals (aged approximately 12 weeks) to determine if age is a contributor to the more pronounced AV delay observed in LVD (32) compared to LVD (8).

3.2 Methods

3.2.1 Rabbit model of LVD

The rabbit model of LVD due to apical myocardial infarction induced by coronary artery ligation as detailed in General Methods (Chapter 2) was used in this study. Sham operated animals underwent thoracotomy but not coronary ligation. Procedures were undertaken in accordance with the United Kingdom Animals (Scientific Procedures) Act 1986 and conform to the Guide for the Care and Use of Laboratory Animals published by the US National Institutes of Health (NIH Publication No. 85-23, revised 1985). Echocardiography was carried out prior to sacrifice to assess left ventricular systolic function determined by ejection fraction (LVEF) measured in long axis by M-mode. At 32 weeks, sham operated animals showed no evidence of left ventricular dysfunction, with a mean LVEF of 72.75 ± 1.89%.

Stock control animals did not undergo thoracotomy or echocardiography.

Sham-operated animals, studied at 32 weeks post sham ligation (n=4), were compared to younger stock control animals, which were between 12 and 20 weeks old (n=14). Sham operations were performed at an age of 12-20 weeks, therefore the effective age of the Sham (32) animals was 44-52 weeks old. The results are discussed in detail below.

3.2.2 The isolated AV node preparation

The isolated AV node preparation was created as described in Chapter 2.

3.2.3 Surface electrogram recording

Electrograms recorded from the surface of the isolated atrioventricular node preparation were recorded using locally developed ECG acquisition software as previously described (NMap, Dr FL Burton, University of Glasgow). The spontaneous sinus cycle length was recorded in every experiment. The basic stimulus cycle length was 300ms. Atrio-Hisian (AH) intervals, Wenckebach cycle length, functional and effective refractory periods of the AV node and the atrial effective refractory periods were derived using standard pacing protocols and analysed as described earlier.

3.2.4 Optical mapping of activation

The pattern of activation through the right atrial/AV node preparation was studied in a further series of 4 controls and 4 LVD samples (at 8 weeks post infarct) using the optical mapping methodology described earlier (see Chapter 2, General Methods). Hearts excised under terminal anaesthesia were loaded with RH237 via the coronary circulation via Langendorff perfusion. Thereafter the isolated right atrial preparation was prepared as previously described and mounted in a custom made chamber to allow superfusion with Tyrode's solution of the above composition. The preparation was paced using protocols previously described to derive AH intervals and WCL. Surface electrograms and optically derived action potentials were recorded simultaneously.

3.2.5 Analysis of optically derived action potentials

Activation time (T_{act}) was defined as the time point of the maximum rate of rise of the AP upstroke (dF/dt_{max}), defined as the first derivative of the fluorescence signal. The mean ± SEM of T_{act} (ms) was determined in 4 distinct regions of the preparation, consisting of 10-15 pixels each (Figure 3-2). Region 1 represented the signals derived from atrial myocytes (around the pacing electrode), region 2 (A) the proximal AV node/AVN input, region 3 (B) the compact AV node and region 4 (C) the His bundle region/AV nodal output. Regions were defined anatomically and confirmed by the simultaneous presence of surface electrograms at the atrial and His bundle regions for each individual preparation. Absolute values of mean ± SEM T_{act} were then plotted and values compared between control and LVD samples. Furthermore, the conduction times between regions (atrial to AV node input, AV node input to compact node, compact node to His bundle) were determined and plotted.

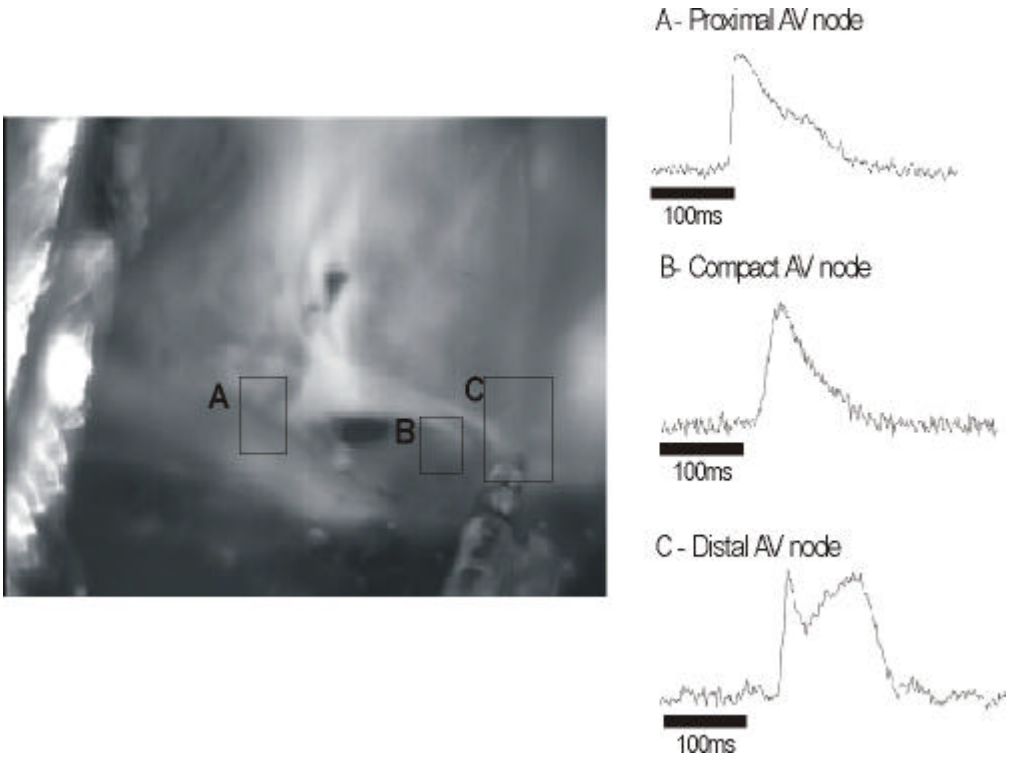

Figure 3-2 – Typical optically derived action potentials from the isolated AV node preparation. Pacing electrode can be seen in the top left corner (atrial region). A – Proximal AV node/AVN input; B – Compact AV node; C – Distal AVN/His bundle.

3.2.6 Statistical analysis

3.2.6.1 Surface electrogram studies

Results are expressed as mean ± SEM unless otherwise stated. Unless otherwise stated, comparisons between data derived from controls versus ligated preparations were made using an unpaired Student's t-test. A two-tailed p-value of less than 0.05 was considered statistically significant.

3.2.6.2 Optical mapping studies

A series of 4 LVD animals at 8 weeks post ligation were studied and compared to 4 control animals. Results are expressed as mean ± SEM unless otherwise stated. Statistical analysis was based on analysis of variance (ANOVA) followed by *t*-tests corrected for multiple comparisons unless otherwise stated. A two-tailed p-value of less than 0.05 was considered statistically significant.

3.3 Results: In vivo data

3.3.1 Baseline characteristics

Previous work has shown that there are no significant differences in the haemodynamic or electrophysiological characteristics of stock animals versus sham operated controls studied at 8 weeks post sham ligation (81). "Control" animals were therefore stock animals, which had not undergone sham ligation. Baseline characteristics (body weight and left ventricular ejection fraction (LVEF)) of animals studied are summarised in Table 3-1. The mean body weight (Figure 3-3A) of the controls was 3.36 ± 0.6kg. The animals studied 8 weeks post coronary ligation (LVD (8)) weighed 3.56 ± 0.6kg ($P<0.05$), and those studied at 32 weeks post coronary ligation (LVD (32)) weighed 4.0 ± 0.2kg ($P<0.01$ when compared to LVD (8) and $P<0.001$ compared to control). A series of sham operated controls were studied at 32 weeks post sham ligation (Sham (32)) to exclude age as a possible confounding factor. These animals weighed 3.91 ± 0.1kg (P=NS compared to LVD (32)).

In keeping with previous studies (86), coronary ligation resulted in left ventricular systolic dysfunction as defined as a reduction in LVEF measured in short axis by M-mode echocardiography (Figure 3-3B). Stock controls did not undergo echocardiography. Mean LVEF in LVD (8) was 44.88 ± 0.76% and in LVD (32) 43.56 ± 0.99%. At 32 weeks, sham operated controls had a mean LVEF of 72.75 ± 1.89% ($P<0.001$ when compared to LVD (8) and (32)).

	Control (n=60)	**LVD (8) (n=34)**	**LVD (32) (n=9)**	**Sham (32) (n=4)**
Body weight (kg)	3.36 ± 0.6	3.56 ± 0.6	4.0 ± 0.2	3.91 ± 0.1
Ejection fraction (%)	*	44.88 ± 0.76	43.56 ± 0.99	72.75 ± 1.89

Table 3-1 - Baseline characteristics of the MI model as compared to stock and sham operated controls. LVD/Sham (8/32) – 8/32 weeks post infarct/sham ligation. Results expressed as mean ± SEM. (* control animals did not undergo echocardiography)

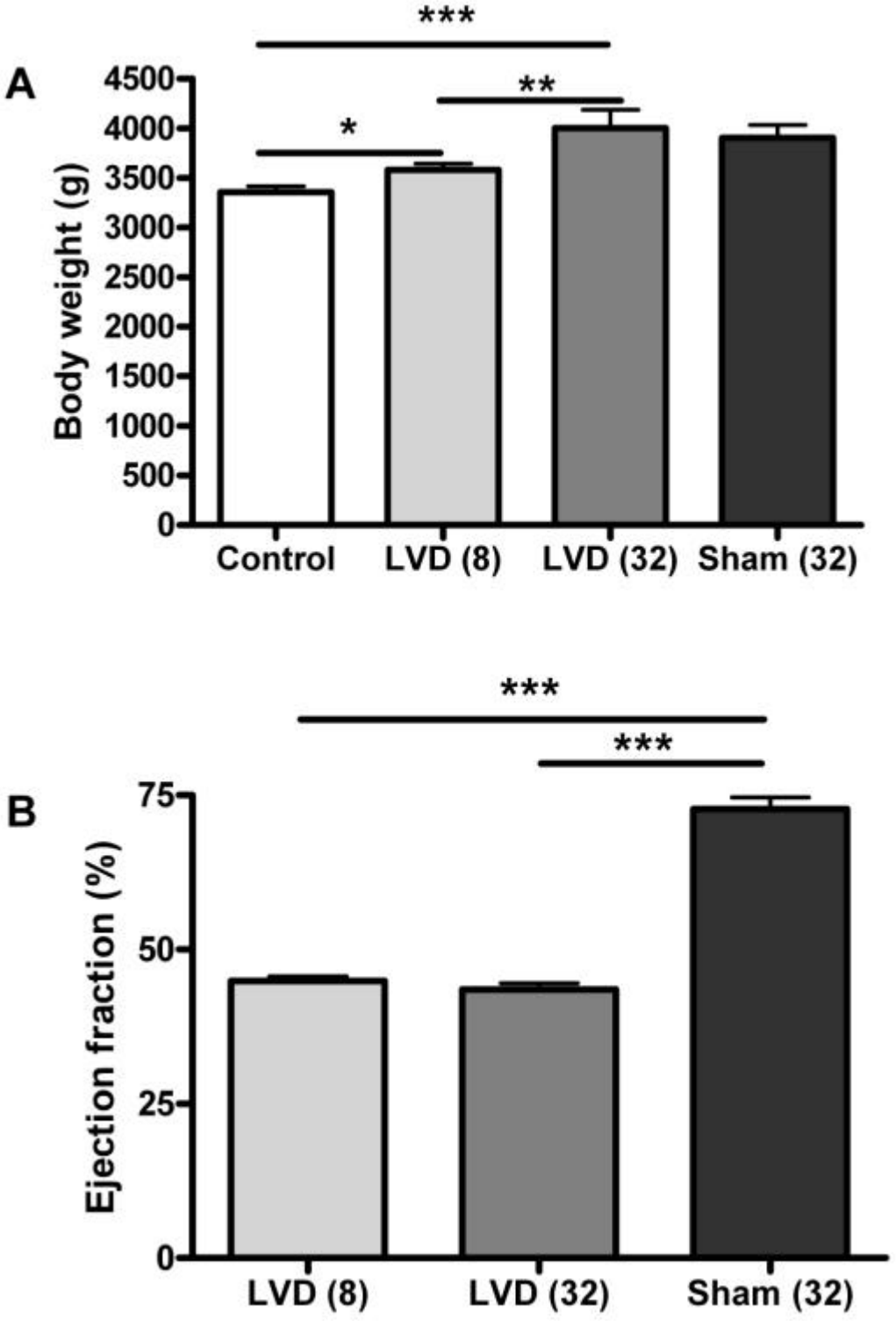

Figure 3-3– A – Bar chart of body weights of MI model animals compared to stock and sham operated controls. B – Bar chart of left ventricular ejection fraction in MI model as compared to sham operated controls. Results expressed as mean ± SEM. * P<0.05; ** P<0.01; *** P< 0.001.

3.3.2 Effect of LVD on the electrocardiographic markers of AV delay in vivo

Surface ECG recordings (Figure 3-4) were carried out in a series of 8 sham operated animals and 8 LVD animals at 8 weeks post infarct to study the effect of coronary ligation on the in vivo markers of AV delay (namely PR interval). The data acquired allowed the analysis of the heart rate and therefore allowed the correlation of PR interval with RR interval across the series.

Figure 3-4 – Example of surface ECG acquired from rabbits in this study. Paper speed 20ms per box on x-axis.

There was a tendency towards higher heart rates in the LVD group compared to sham operated animals (Figure 3-5). The RR interval in the sham series was 143 ± 24ms. In LVD the RR interval was 115 ± 10ms. The difference did not reach statistical significance. There was no difference in the mean PR interval between sham and LVD (Figure 3-5) (sham 26 ± 2ms and LVD 26 ± 2ms).

Figure 3-6 shows a scatter plot of the mean ± SEM of the PR interval plotted against the corresponding RR interval for each animal in both sham and LVD series. This demonstrates the wider range of baseline RR intervals in the sham series compared to LVD. Linear regression analysis comparing sham with LVD failed to demonstrate any statistically significant difference in the relationship between RR and PR interval between the groups.

To determine whether there is any difference in the PR interval of LVD animals compared to sham at a given RR interval, a direct beat to beat comparison was made at a range of RR intervals between 130-135ms. This showed that the mean PR interval at RR 130-135ms was significantly longer in LVD compared to sham (31ms vs. 28ms, P<0.001, Figure 3-7). However, this should be interpreted with caution, as when analysed sample by sample (as opposed to beat to beat) there was no significant difference. It was not possible to analyse all samples at this heart rate due to the variation in baseline RR intervals. Further samples require to be studied at the given RR interval to provide enough power to detect a significant difference sample by sample.

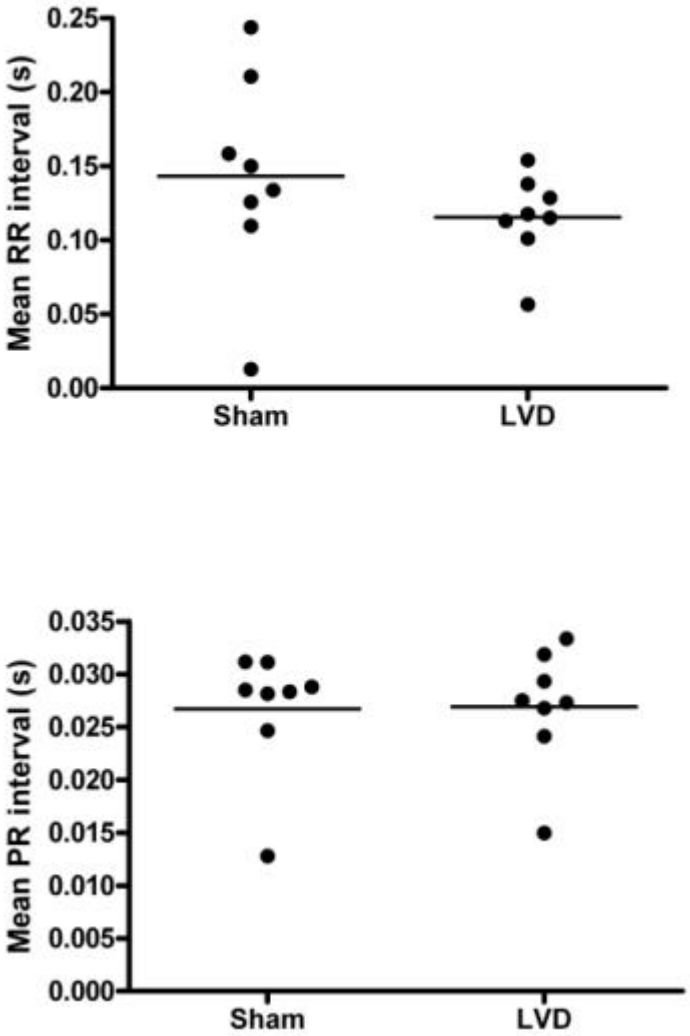

Figure 3-5 - Mean RR and mean PR interval on the surface ECG in vivo of sham versus LVD animals (n=8 in each group). P=NS.

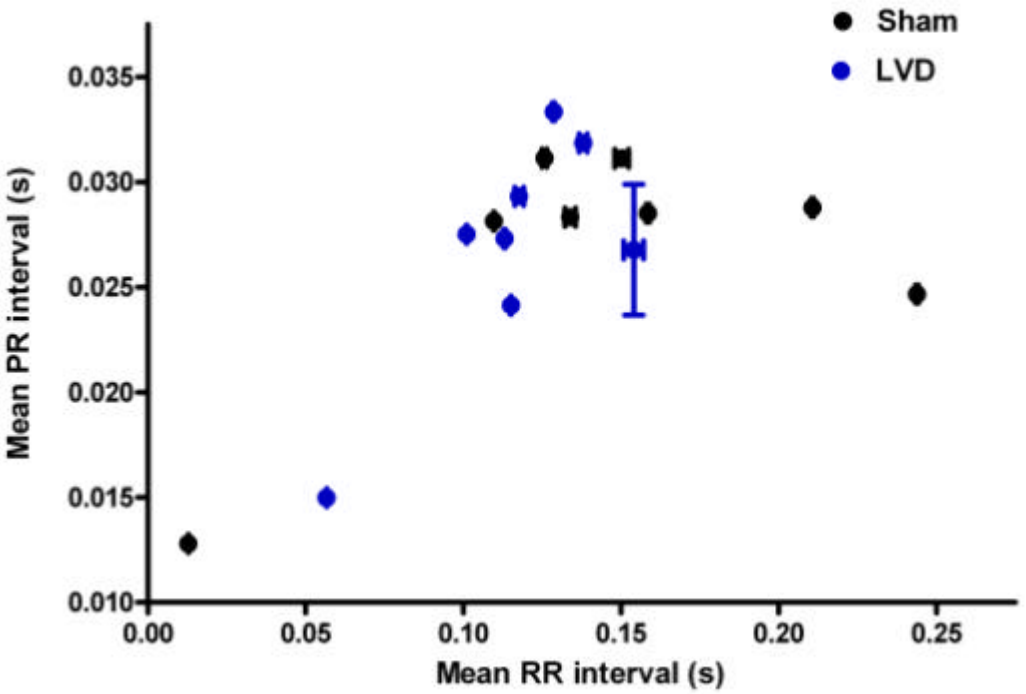

Figure 3-6 - Correlation between the mean (± SEM) RR interval and the mean (±SEM) PR interval on the surface ECG in vivo for sham and LVD animals (n=8 in each group).

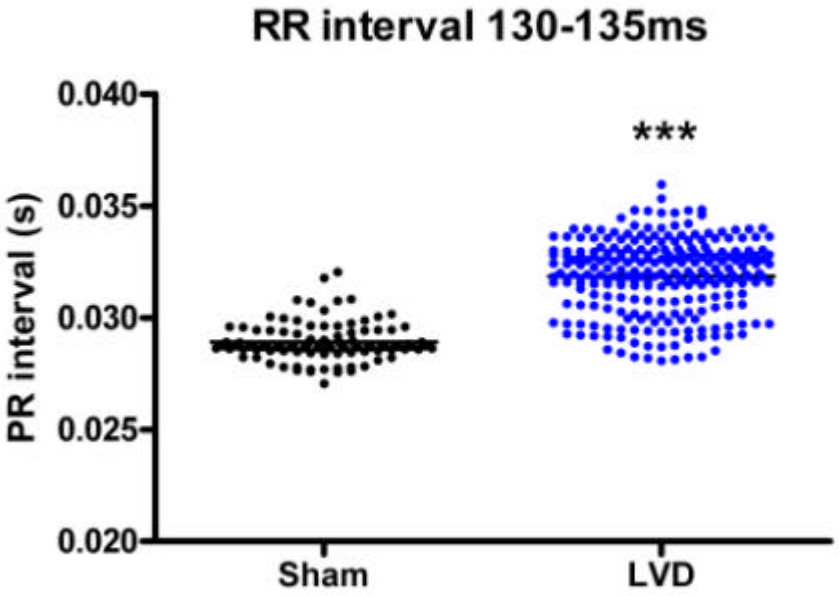

Figure 3-7 - Beat to beat variation in PR interval on the surface ECG in vivo in sham versus LVD over range of RR intervals between 130-135ms. (Sham n=102 beats (4 animals); LVD n=243 beats (4 animals). ***P<0.001).

3.4 Results: The isolated AV node preparation

3.4.1 Effect of LVD on spontaneous sinus cycle length

The sinus node was kept intact to allow comparison of the spontaneous sinus cycle length (SSCL) between controls and LVD groups. There were no significant differences in the SSCL between controls and any other group, as summarised in Figure 3-8. The mean SSCL was: control 378.1 ± 13.6ms; LVD (8) 373.1 ± 23.2ms; LVD (32) 348.4 ± 23.5ms, and Sham (32) 354.3 ± 6.0ms.

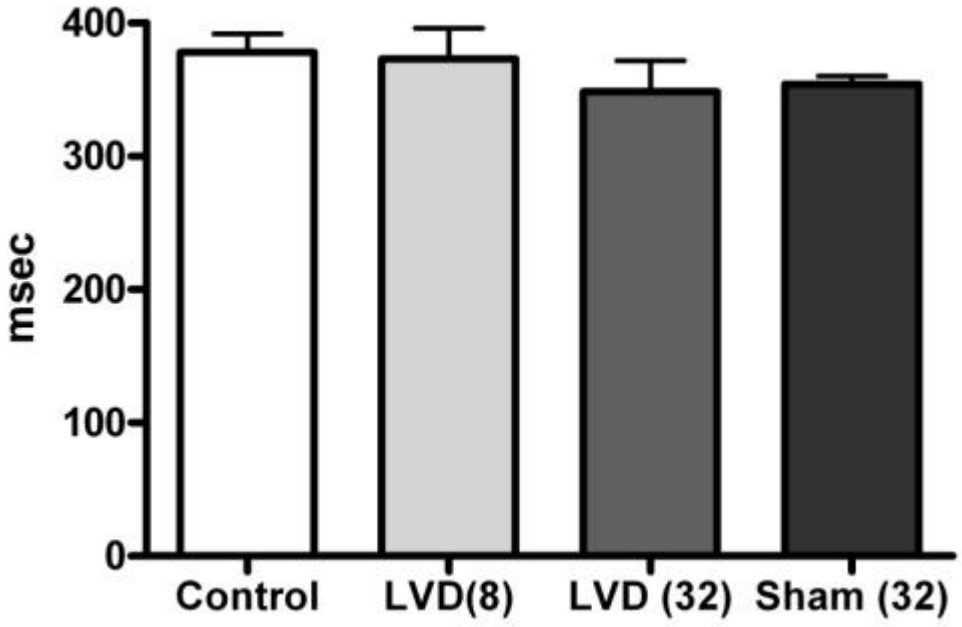

Figure 3-8 - – Spontaneous sinus cycle length in MI model compared to stock and sham operated controls. No significant differences were observed between any groups. Results expressed as mean ± SEM.

3.4.2 Effect of LVD on AV node conduction characteristics

The effects of LVD on AV node conduction characteristics were studied in a series of 14 controls, 14 LVD (8) and 8 LVD (32) animals. AV node conduction was measured by plotting the A1H1 (AH) interval against the A1A1 interval using a pacing protocol of a drive train of 16 stimuli at a constant S1S1 interval of 300ms (Figure 3-9A) followed by a 1 second pause, before the S1S1 interval is decremented by 5ms. When the mean A1H1 interval for each corresponding A1A1 interval is plotted,

compared to controls there is an upwards shift of the AH interval in LVD (8), with a further upward shift in LVD (32) (Figure 3-9B). This represents prolongation of the AH interval at all tested pacing cycle lengths (PCL) in LVD compared to controls. The effect appears magnified at 32 weeks post ligation.

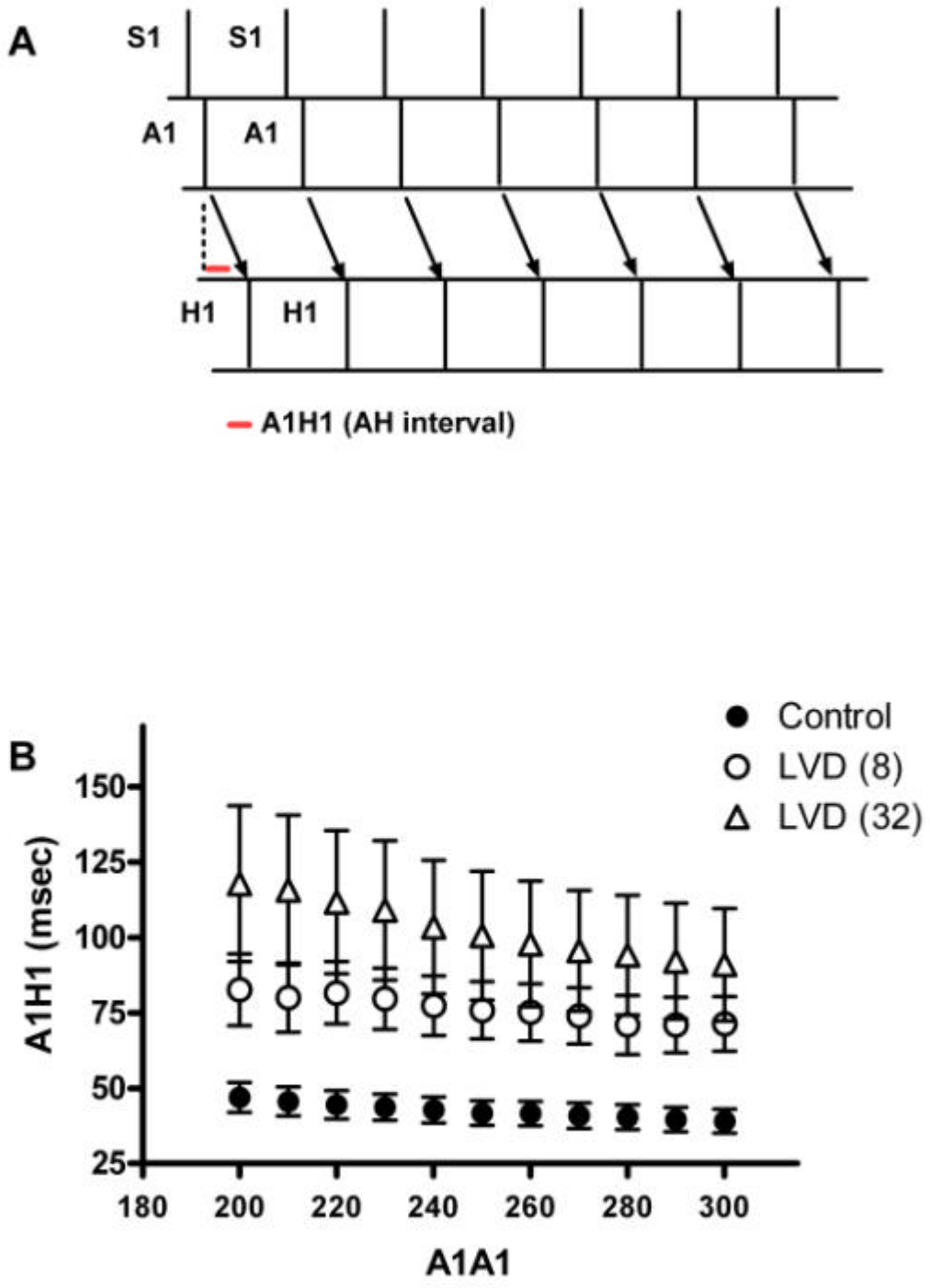

Figure 3-9 – A – Ladder diagram of pacing protocol used to derive AV node conduction curves. B – AV node conduction curves of controls (n=14) and LVD at 8 (n=14) and 32 (n=8) weeks post infarct. Results expressed as mean ± SEM A1H1 at a range of pacing cycle lengths (A1A1).

In addition to an upwards shift in the AH interval in LVD, the Wenckebach cycle length is significantly longer in the LVD groups compared to controls. The effects of LVD on Wenckebach cycle length and AH intervals are summarised in Table 3-2. This demonstrates the statistically significant prolongation of the AH interval in LVD at both 8 and 32 weeks post ligation compared to controls at PCLs of 300ms and 200ms and the effect of LVD on Wenckebach cycle length.

	Control	LVD (8)	Sham (32)	LVD (32)
WCL	129.3 ± 8.3	172.0 ± 13.6*	172.3 ± 12.8*	167.5 ± 13.7*
AH300	43.6 ± 4.4	69.7 ± 8.8*	57.3 ± 8.9	77.4 ± 10.5**
AH200	51.3 ± 5.3	77.5 ± 8.3*	68.3 ± 9.9	100.5 ± 15.6**

Table 3-2 – Effect of LVD on AV node conduction characteristics. WCL - Wenckebach cycle length; AH300 - AH interval at PCL 300ms; AH200 - AH interval at PCL 200ms. Results expressed as mean ± SEM (ms). *P<0.05 **P<0.01.

3.4.3 Effect of LVD on atrial and AV nodal refractory periods

The functional (FRP) and effective (ERP) refractory periods of the AV node and the atrial effective refractory period were derived using the S1S2 pacing protocol described previously and illustrated in General Methods Figure 2-5. Samples which showed evidence of dual pathway AV nodal physiology were excluded from analysis of AV node refractory periods (excluded n=1 control, n=4 LVD (8) and n=2 LVD (32)).

The effects of LVD on AV nodal FRP and ERP and atrial ERP are summarised in Table 3-3. In LVD (8), the FRP was prolonged compared to controls, although this difference did not reach statistical significance. There was significant prolongation of the FRP in LVD (32) compared to controls. The ERP was prolonged in LVD (8) and (32) compared to controls, however there were no statistically significant differences between the groups.

Atrial effective refractory period was determined in all samples and was not significantly prolonged in LVD compared to controls.

	Control	LVD (8)	Sham (32)	LVD (32)
FRP	145.1 ± 8.1	162.6 ± 15.6	140.6 ; 201.0	175.0 ± 8.4*
ERP	110.6 ± 7.9	135 ± 12.1	121.0 ; 145.0	122.5 ± 10.7
Atrial ERP	93.9 ± 6.5	84.8 ± 4.7	97.3 ; 63.3	94.3 ± 7.7

Table 3-3 – Effects of LVD on AV nodal functional (FRP) and effective (ERP) refractory periods and atrial ERP. Results expressed as mean ± SEM, except where n=2 (individual values shown). *P<0.05.

3.5 Results – Effects of ageing

3.5.1 Effect of age on spontaneous sinus cycle length

The sinus node was again kept intact to allow comparison of the spontaneous sinus cycle length (SSCL) between stock controls and 32 week sham operated controls. There were no significant differences in the SSCL between controls and Sham (32), as summarised in Figure 3-10. The mean SSCL was: control 378.1 ± 13.6ms and Sham (32) 354.3 ± 6.0ms.

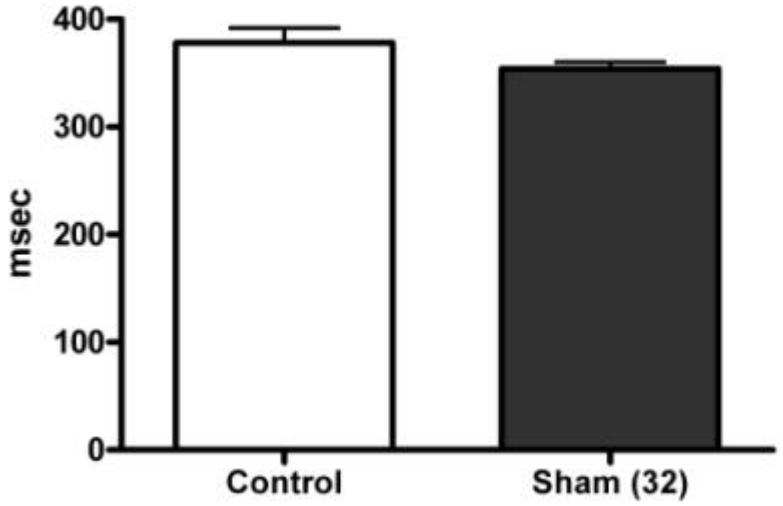

Figure 3-10 – Spontaneous sinus cycle length in 32 week sham operated animals (n=4) versus 12 week controls (n=14). No significant differences were observed between the groups. Results expressed as mean ± SEM.

3.5.2 Effect of age on AV node conduction characteristics

The effect of aging on AV node conduction characteristics was studied in a series of 4 sham operated controls at 32 weeks post procedure, and compared with 12 week controls as detailed above. The AH intervals at pacing cycle length 300 and 200ms were prolonged in Sham (32) compared to 12 week controls, but this difference was not statistically significant. There was, however, significant prolongation of the Wenckebach cycle length in Sham (32) compared to 12 week controls (172.3ms vs. 129.3ms, $P<0.05$). The results are detailed in Table 3-4.

	12 week Control	Sham (32)
WCL	129.3 ± 8.3	172.3 ± 12.8*
AH300	43.6 ± 4.4	57.3 ± 8.9
AH200	51.3 ± 5.3	68.3 ± 9.9

Table 3-4 – Effect of aging on AV node conduction characteristics. WCL - Wenckebach cycle length; AH300 - AH interval at PCL 300ms; AH200 - AH interval at PCL 200ms. Results expressed as mean ± SEM (ms). *P<0.05.

3.5.3 Effect of age on atrial and AV nodal refractory periods

The functional (FRP) and effective (ERP) refractory periods of the AV node and the atrial effective refractory period were derived using the S1S2 pacing protocol described previously and illustrated in Chapter 2, Figure 2-5. Samples which showed evidence of dual pathway AV nodal physiology (n=1 12 week control, n=2 Sham (32)) were analysed separately to allow comparison of the refractory periods of both the slow and fast AV nodal pathways.

The AV nodal FRP and ERP of Sham (32) was prolonged compared to control, however the results were not statistically significant due to the small number of samples. Only 4 Sham (32) animals were studied, and 2 of these showed evidence of dual pathway AV nodal physiology and were therefore excluded from the analysis

outlined in Table 3-5 below. Atrial ERP was not significantly different in the Sham (32) group compared to controls.

	12 week Control	Sham (32)
FRP	145.1 ± 8.1	140.6 ; 201.0
ERP	110.6 ± 7.9	121.0 ; 145.0
Atrial ERP	93.9 ± 6.5	97.3 ; 63.3

Table 3-5 - Effects of aging on AV nodal functional (FRP) and effective (ERP) refractory periods and atrial ERP. Results expressed as mean ± SEM (ms) (except where n=2 where individual values shown). Due to dual pathway AV nodal physiology, n=13 controls and n=2 Sham (32).

The refractory periods of the slow and fast AV nodal pathways were then analysed in the remaining 2 Sham (32) animals and values were compared to the one control animal with evidence of dual pathway AV nodal physiology. Results are detailed in Table 3-6 below. There were no significant differences in slow or fast pathway FRP or ERP between the groups, although in the context of such small numbers statistical analysis must be interpreted with caution.

	FRP		ERP	
	Fast pathway	**Slow pathway**	**Fast pathway**	**Slow pathway**
12 week Control (n=1)	161	276	145	116
Sham (32) (n=2)	206 ; 214	273 ; 245	137 ; 186	127 ; 142

Table 3-6 - Refractory periods of fast and slow AV nodal pathways in 32 week sham controls versus stock controls exhibiting dual pathway AV nodal physiology. Individual values shown due to small sample size.

3.6 Results: Optical mapping of AV nodal conduction

3.6.1 Effect of LVD on AV nodal conduction determined by optical mapping of activation

Analysis of surface electrograms recorded during optical mapping experiments allowed measurement of the spontaneous sinus cycle length, AH intervals and Wenckebach cycle length in samples stained with RH237 with simultaneous optical data acquisition. Experiments were carried out in 4 controls and 4 LVD samples at 8 weeks post infarct. As in previous studies there was no significant difference in the SSCL of controls versus LVD samples (Figure 3-11A). There was significant prolongation of WCL and AH interval across all PCLs in LVD compared to controls (Figure 3-11B and 3-11C).

Figure 3-12 shows the surface electrograms and corresponding optical action potentials acquired during optical mapping experiments. Figure 3-13 documents the results of analysis of optically derived action potentials recorded from the isolated AV node preparation. Activation time (T_{act}) is significantly longer at the compact node and His bundle regions in LVD versus controls ($P<0.001$ by ANOVA). There is no significant difference in T_{act} at the atrial and AVN input regions between LVD and controls. The conduction times between regions ($? T_{act}$) are shown in Figure 3-13B, where 1= conduction time between the atrial and AVN input regions, 2= conduction time between the AVN input and compact AVN regions, and 3= conduction time between the compact AVN and His bundle regions. There is significant delay in conduction between the AVN input and compact nodal region in LVD compared to controls. When expressed as a ratio, there is an almost 4-fold increase in conduction time between AVN input and compact node in LVD compared to control, and a 3-fold increase in conduction time between compact node and His bundle in LVD compared to control (Figure 3-13C).

Figure 3-14 shows isochronal maps of activation at all three regions in one example each of control and LVD. It demonstrates conduction delay occurring initially at the proximal to compact nodal region in LVD with further delay between the compact node and His bundle of a greater extent in LVD compared to control. It is worth noting that the gap in the isochronal map corresponding to region 2 in control is a result of the position of the coronary sinus in the example analysed.

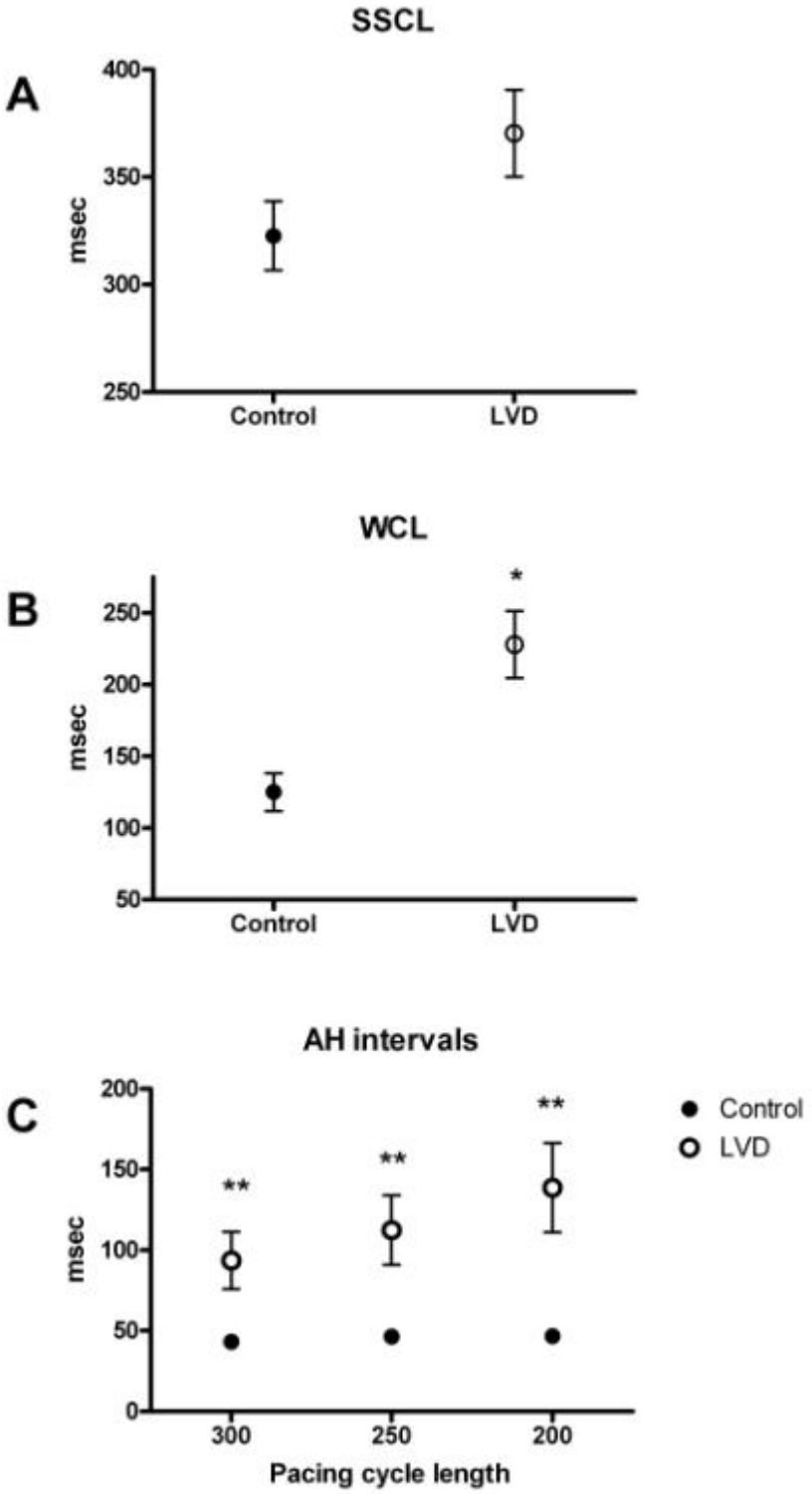

Figure 3-11 - Sinus rate and AV nodal conduction parameters from surface electrogram recordings during optical mapping experiments. A – Spontaneous sinus cycle length (SSCL); B – Wenckebach cycle length (WCL); C – AH intervals. Results expressed as mean ± SEM (msec). *P<0.05; **P<0.01. n=4 control and 4 LVD.

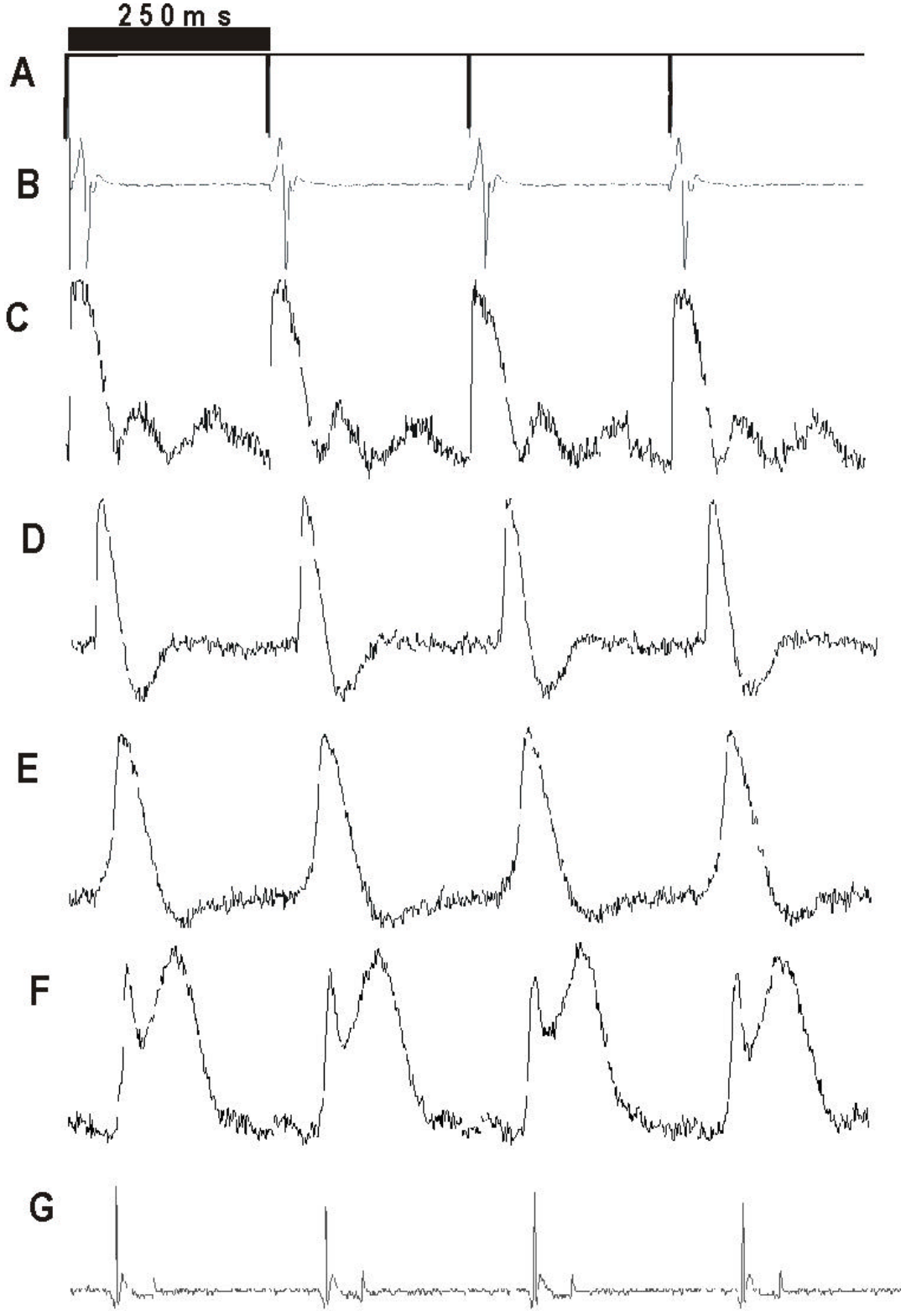

Figure 3-12 - Surface electrograms and optical action potentials (OAP) during regular pacing at 250ms. A – stimulus artefact; B – atrial electrogram; C – OAP from atrial region; D – OAP from proximal AVN; E – OAP from compact AVN; F – OAP from His bundle region; G – His bundle electrograms followed by low amplitude ventricular signal. In F, the second peak of the OAP corresponds to the ventricular signal following the His electrogram as shown in G.

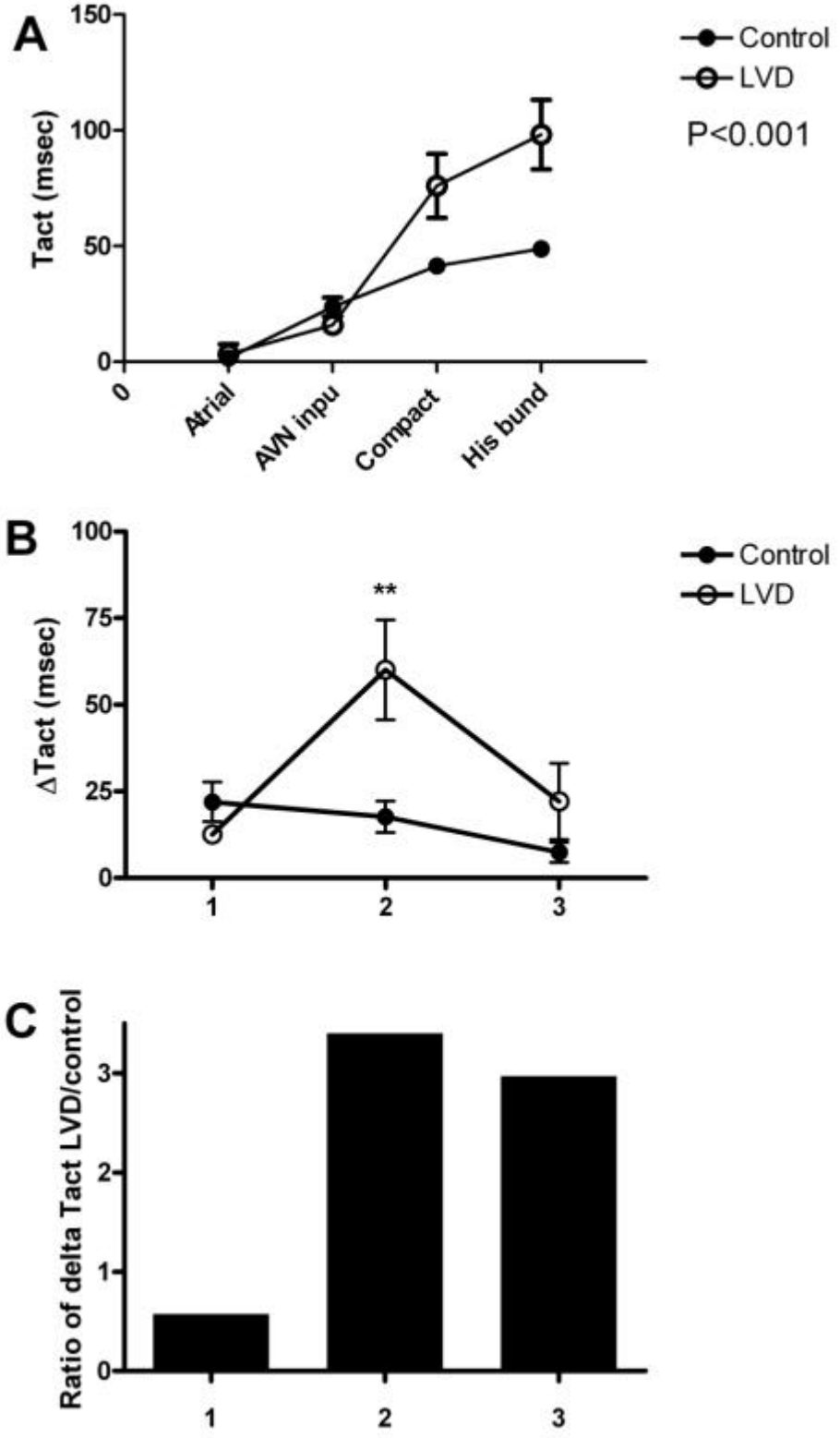

Figure 3-13 - A – Activation time (T_{act}) region by region. B – Change in activation time (?Tact) between adjacent regions. Results expressed as mean ± SEM (msec); n=4 control and 4 LVD. C - ?T_{act} LVD / ? T_{act} Control. 1 = atrium to AVN input; 2= AVN input to compact AVN; 3 = Compact AVN to His bundle. There is significant prolongation of Tact in LVD at the compact node and His bundle regions compared to controls (ANOVA P<0.001). This is predominantly a consequence of significant delay in conduction between the AVN input and compact nodal region as shown in B above. ** P<0.01.

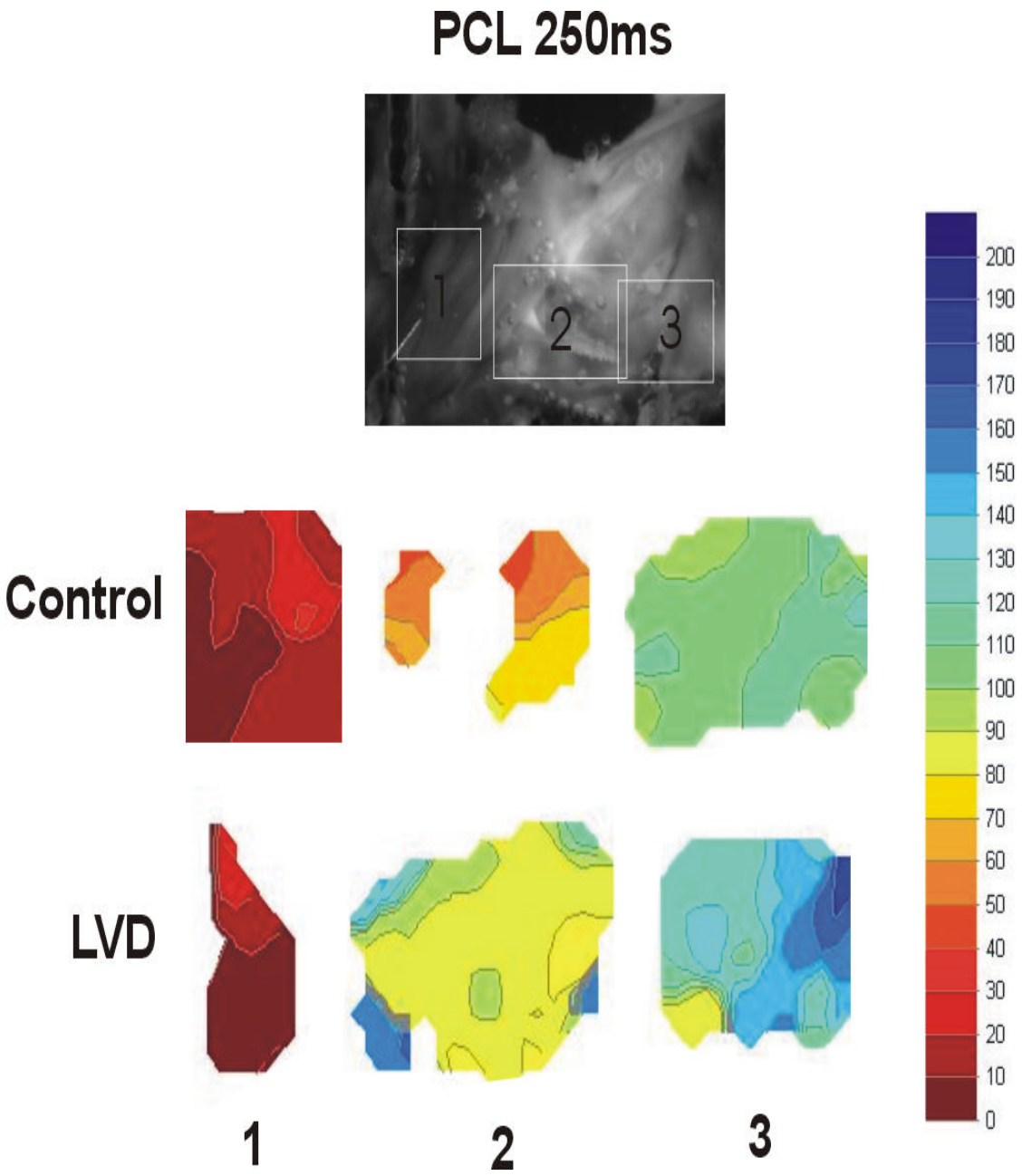

Figure 3-14 – Isochronal maps of activation in one example of control and LVD showing conduction slowing at region 2 (Proximal to compact AVN) and region 3 (Compact AVN to His bundle) in LVD compared to control. The key on the right is in milliseconds. Activation times are relative to the onset of the atrial electrogram.

3.7 Results: Evidence of dual pathway AV nodal physiology in rabbit

In keeping with previous studies (42-44), we identified evidence of dual pathway AV nodal physiology in a number of animals, based on the presence of discontinuity of the AV nodal conduction curve, and functionally defined as an abrupt increase in the A2H2 interval of = 20ms in response to a 5ms decrement in A1A2 (Figure 3-15).

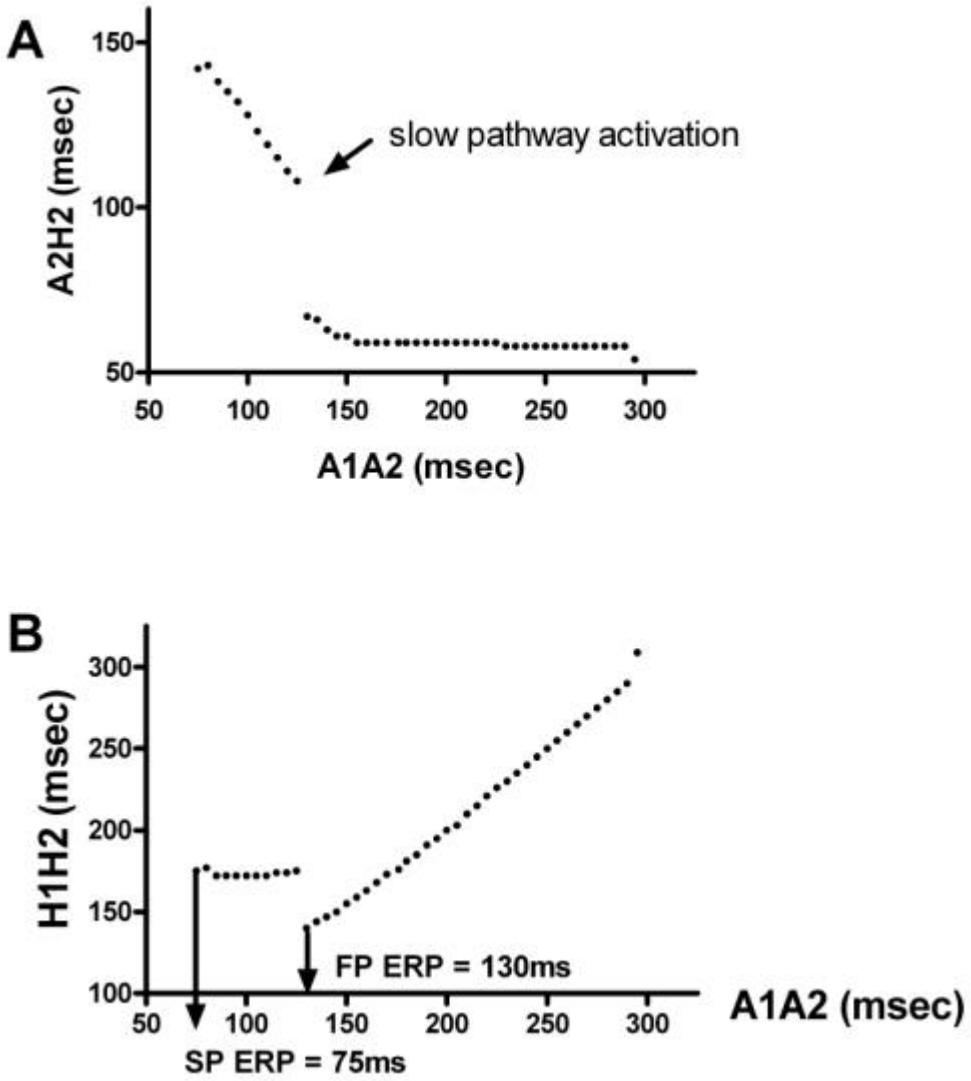

Figure 3-15 – AV nodal conduction and refractory curves showing evidence of dual pathway AV nodal physiology. A – Discontinuity of the AV nodal conduction curve identifies slow pathway activation. B – Refractory curve identifies the fast pathway (FP) with an effective refractory period (ERP) of 130ms, and the slow pathway (SP) with an ERP of 75ms.

Dual pathway AV nodal physiology could be identified in both controls (22%) and LVD (33%) animals as summarised in Figure 3-13 (Chi-square, P=ns). When controls were subdivided into stock controls and sham operated controls, and LVD animals were subdivided into 8 and 32 weeks post ligation, there were no significant differences in the proportions of animals demonstrating evidence of dual pathway AV nodal physiology (Figure 3-16, Chi-square, P=ns).

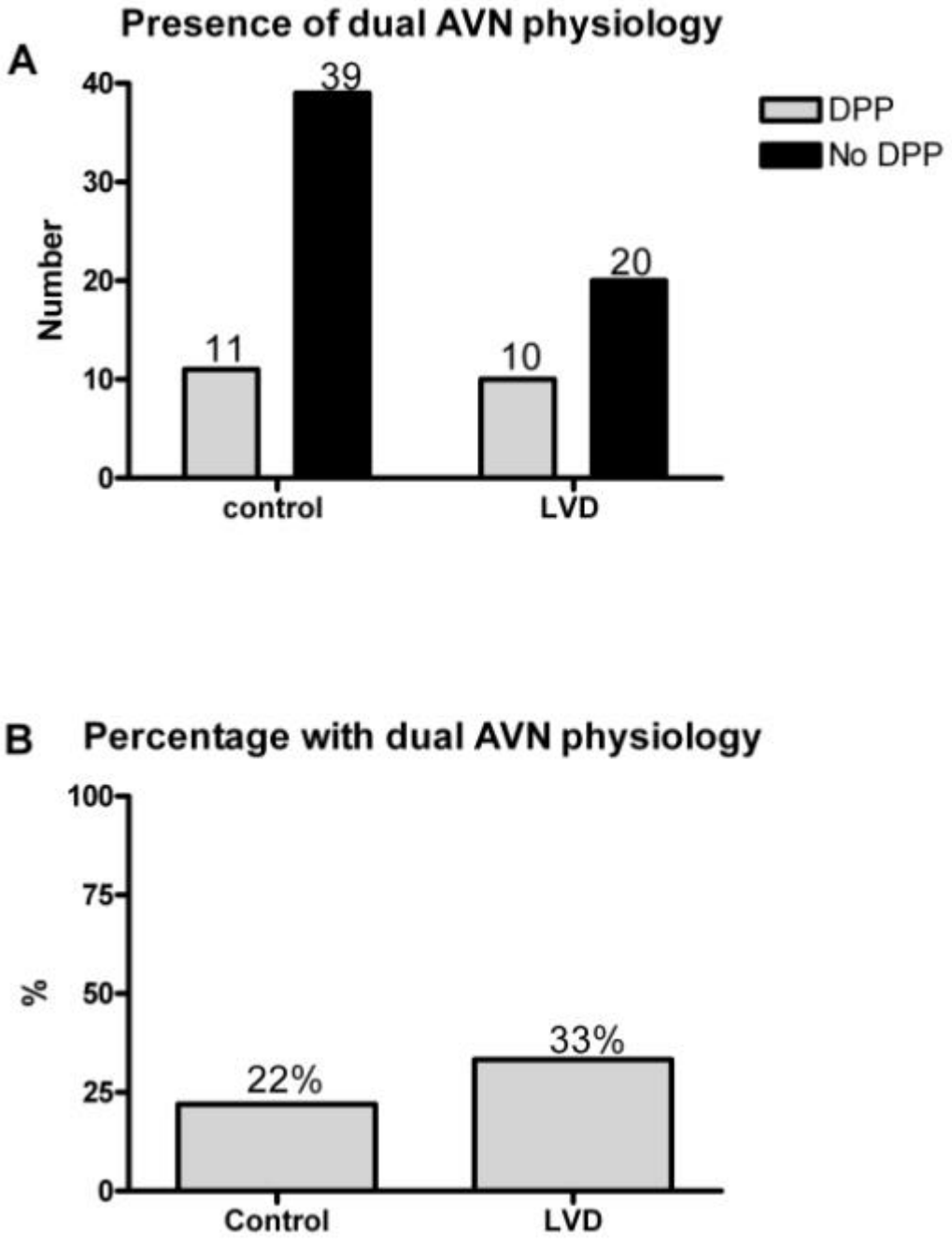

Figure 3-16 – A – Absolute numbers of samples displaying evidence of dual AV nodal physiology in controls (stock and sham operated) and LVD (8 and 32 weeks post infarct). B – expressed as a percentage of the total. P = ns.

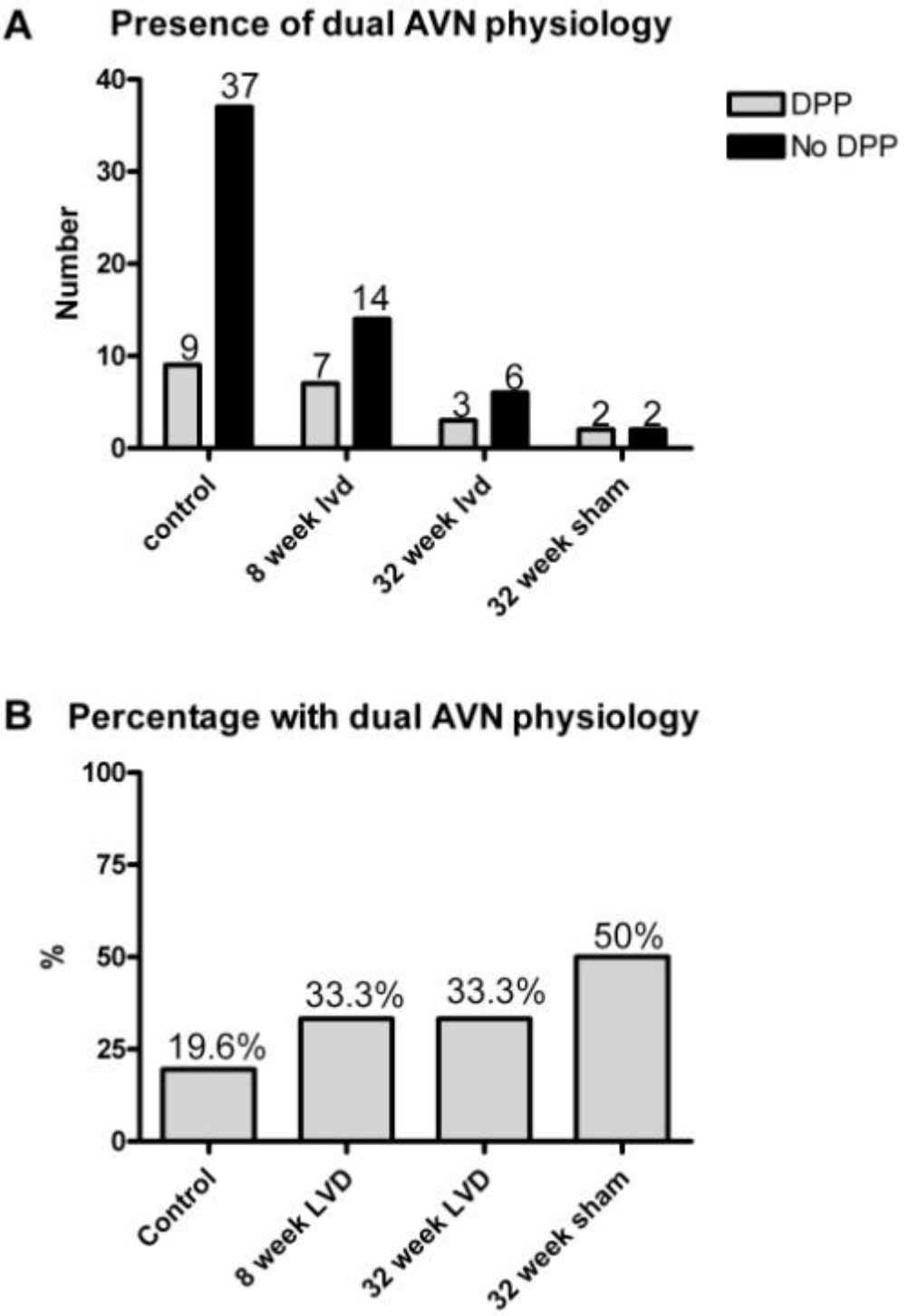

Figure 3-17 – A - Absolute numbers of samples displaying evidence of dual AV nodal physiology subdivided by procedure: controls (stock and sham operated) and LVD (8 and 32 weeks post ligation). B – expressed as a percentage of the total. P = ns.

In the study of the effect of LVD on AV nodal conduction characteristics, a number of samples were excluded from AV node refractory period analysis as explained above due to the presence of dual pathway AV nodal physiology. In these samples

the effective and functional refractory periods of the slow and fast pathways were determined, and are summarised in Table 3-7.

	FRP		ERP	
	Fast pathway	**Slow pathway**	**Fast pathway**	**Slow pathway**
Control (n=1)	161	276	145	116
LVD (8) (n=4)	139.8 ± 9.4	186.8 ± 18.3	110.0 ± 9.4	80.3 ± 3.2
LVD (32) (n=2)	122	152	105	80
	143	161	115	98

Table 3-7 – Refractory periods of fast and slow AV nodal pathways. Data expressed as mean ± SEM (ms) except where n=2 where individual data values shown.

3.8 Discussion

In a rabbit model of LVD due to apical myocardial infarction, this study has confirmed that there is significant prolongation of AV nodal conduction delay at both 8 and 32 weeks post infarct. There was no effect of LVD on sinus node automaticity. The results and possible mechanisms underlying the findings are discussed in detail below.

3.8.1 Effect of LVD on in vivo markers of AV delay

A study of surface electrocardiograms from sham and LVD animals has demonstrated a non- significant increase in baseline heart rate in LVD but no difference in the overall mean PR intervals between the groups. Also, there was no significant difference in the overall relationship between the mean PR interval versus the mean RR interval between sham and LVD. When compared at a defined RR interval, there appears to be significant prolongation of the PR interval in LVD compared to sham. Further work on additional samples is required to study in more detail the relative difference in PR interval at each defined RR interval to confirm or refute this latter observation.

In the isolated AV node preparation, in this rabbit model of LVD due to apical myocardial infarction, this study has confirmed that there is significant prolongation of AV nodal conduction delay at both 8 and 32 weeks post infarct. There was no effect of LVD on sinus node automaticity. The results and possible mechanisms underlying the findings are discussed in detail below.

3.8.2 Effect of LVD on sinus node automaticity

In the isolated right atrial/AV node preparation used in this study, the mean spontaneous sinus cycle length was not significantly altered by LVD, either at 8 or 32 weeks post infarct. This is in contrast to findings of a previous study, in which a significant increase in the SSCL was observed in the presence of heart failure (117). However, the heart failure model in the study by Opthof *et al* (117) was induced by combined pressure and volume overload and not myocardial infarction as in the present study.

3.8.3 Effect of LVD on parameters of AV nodal function

3.8.3.1 Effect of LVD on conduction time (AH interval and Wenckebach cycle length)

In the present study, there is evidence of electrical remodelling of the AV node of rabbits with LVD due to chronic apical myocardial infarction. This was manifest by significant prolongation of the AH intervals at all tested pacing cycle lengths, with an upwards shift of the AV node conduction curve in LVD at both 8 and 32 weeks post infarct as illustrated by Figure 3-6B. The mean ± SEM AH intervals at all pacing cycle lengths in LVD (32) were further prolonged compared to LVD (8), but this difference was not statistically significant. Furthermore, there was significant prolongation of the Wenckebach cycle length in the LVD model at both 8 and 32 weeks post infarct compared to controls. There was no progressive prolongation of the WCL at 32 weeks post infarct compared to 8 weeks post infarct.

Given the heterogeneity of the AV node, the possible mechanisms by which conduction delay through the AV node is prolonged in LVD are likely to be multiple and complex.

3.8.3.2 Beta-adrenergic down-regulation in heart failure

In chronic heart failure, excess norepinephrine levels lead to downregulation and desensitisation of myocardial beta-adrenoceptors (74-76). The negative inotropic effect of chronic catecholamine excess and subsequent beta-adrenoceptor downregulation has been demonstrated in rabbit models using chronic isoprenaline infusion via the implantation of an osmotic minipump (77;78). Furthermore, previous work in our laboratory has demonstrated evidence of reduced ?-adrenoceptor sensitivity to the inotropic effects of isoprenaline in papillary muscles from rabbits with LVD compared with sham operated controls (79). AV node conduction time depends on the interaction between the prevailing heart rate and the level of sympathetic tone, both of which exert opposite effects on AV conduction (118). In vivo, if the heart rate is held constant by artificial pacing, sympathetic stimulation decreases AV conduction time. However, an increase in heart rate by atrial pacing prolongs AV conduction time. Therefore, in response to chronic catecholamine excess in CHF, it may be that beta-adrenoceptor downregulation results in a reduction in the conduction velocity through the AV node. This hypothesis is explored further in a subsequent chapter.

3.8.3.3 Endogenous adenosine effects on the AV node

Adenosine may signal conditions that are detrimental to the organism such as hypoxia. In cardiac hypoxia or ischaemia, adenosine formation occurs in both the cytosol of the cardiomyocyte and also in the extracellular space, possibly in the capillary endothelium (119). It reduces AV nodal excitability by inactivation of $I_{Ca,L}$ and activation of a time-dependent inwardly rectifying potassium current (120-122). Furthermore, adenosine inhibits the potentially detrimental inotropic and metabolic effects of catecholamines released in response to myocardial ischaemia (123;124). Adenosine reduces myocardial oxygen demand by reducing sinus node automaticity and AV node conduction velocity via the adenosine A1 receptor subtype. This protective negative feedback mechanism is of importance in conditions of low oxygen supply to demand ratio. In the presence of a chronic myocardial infarction and left ventricular dysfunction, chronic excess endogenous adenosine release may explain the increase in AV nodal delay observed in this rabbit model. This hypothesis is also explored in more detail in subsequent chapters.

3.8.3.4 Effect of LVD on atrial and AV nodal refractory characteristics

The presence of LVD due to apical myocardial infarction did not alter the refractory characteristics of the atrial tissue, with no significant differences being observed in the atrial ERP of LVD at 8 or 32 weeks compared to control. The effect of LVD on conduction time from atrial to proximal AV nodal tissue and its contribution to the increase in AV conduction time in the rabbit model of LVD is explored using the technique of optical mapping, as discussed later.

In the present study, mean AV nodal ERP and FRP were prolonged in LVD at 8 and 32 weeks post infarct, however the results did not reach statistical significance (other than the AVN FRP in LVD (32) compared to control). This is likely to be a consequence of the lack of statistical power to detect the small increase in AV nodal refractoriness that occurs in LVD in the present series. Original power calculations were based on previous observations from this laboratory (81), namely a 20% increase in the AH interval in LVD, and did not account for changes in the FRP or ERP in the absence of preliminary observations.

Reduction in conduction velocity through the AV node with a minimal effect on AV nodal refractoriness could occur as a consequence of reduced intercellular coupling. Connexin 43 is the major connexin in the working myocytes of the atria and

ventricles (125;126). Connexin 40 and 45 are the major connexins contributing to the spread of depolarisation through the AV conduction system (127-130).

Hyperpolarisation-activated and cyclic nucleotide-gated channel 4 (HCN4), which has characteristic pacemaker activity, has been shown to be most abundant in the posterior nodal extension ((61;68). More recently, Yoo *et al* (68) confirmed the presence of the Na^+ channel isoform $Na_v1.5$ at the posterior nodal extension and the transitional zone between atrial and AV nodal cells. The gene responsible for $Na_v1.5$ is the SCN5A gene and inherited AV conduction disorders have been linked recently to mutations in this gene (64;65;67). In addition, $SCN5A^{+/-}$ mice exhibit impaired AV conduction (66). Alterations in connexin expression and/or distribution in AV nodal tissue in the context of LVD are a possible mechanism for the observed increase in AV delay in the present study. In collaboration with Dr Patrizia Camelliti, University of Oxford, this hypothesis is under investigation.

3.8.4 Effect of ageing

Another purpose of this chapter was to explore the possibility that age of the animal may be a contributor to the prolongation of AV delay observed in the LVD (32) group, given that there appeared to be progression of conduction delay compared to the LVD(8) group. Sham-operated animals, studied at 32 weeks post sham ligation, were compared to younger stock control animals, which were between 12 and 20 weeks old. Sham operations were performed at an age of 12-20 weeks, therefore the effective age of the Sham (32) animals was 44-52 weeks old. The results are discussed in detail below.

3.8.4.1 Effect of age on sinus node automaticity

The isolated right atrial / AV nodal preparation used in this study removes the possibility of sympathetic/parasympathetic influence on the automaticity of the sinus node, therefore the sinus rate observed is truly "intrinsic". In the present study, there were no significant differences in the spontaneous sinus cycle length in the stock controls versus the Sham (32) group. This is in contrast to the study of the effect of aging on Fischer 344 rats by Schmidlin *et al* (115) in which they demonstrated a significant decrease in heart rate in senescent rats. Human studies have also demonstrated prolongation of the RR interval with increasing age (116), even in the absence of autonomic influences. The lack of effect of age on the SSCL of the Sham (32) rabbit compared to younger animals in the present study may

represent a species specific difference compared to smaller rodents. Another possibility is that the age difference between the control group (12-20 weeks old) and the sham operated controls (44-52 weeks) may not be sufficient to affect sinus node automaticity in rabbit. The life expectancy of a healthy New Zealand White rabbit is between 5 and 7 years. Further studies in senescent rabbits may demonstrate an increase in the SSCL as has been observed in other species.

3.8.4.2 Effect of age on parameters of AV nodal function

In the present study there was a modest increase in the AH interval at PCL 300 and 200ms in sham operated animals at 32 weeks compared to younger stock controls. The increase in AH interval was not statistically significant and was not of the same magnitude as that observed in animals that had undergone coronary ligation, at either 8 or 32 weeks post ligation. The Wenckebach cycle length was prolonged in Sham (32) compared to stock controls, and the increase was similar to that observed in both ligated groups (see Table 3-2, Chapter 3). Of note, in the study of the effects of LVD on AV nodal conduction, the Wenckebach cycle length did not get progressively longer at 32 weeks post ligation compared to that at 8 weeks post ligation.

The AV nodal functional and refractory periods were prolonged in Sham (32) compared to stock controls, but due to the small sample size the results did not reach statistical significance. Previous authors have demonstrated age related prolongation of AVN ERP (131), although in this study the autonomic status of the patients was not controlled.

Although every effort was made during experiments to minimise the ischaemic insult to the tissue, increased sensitivity to hypoxia in older samples may contribute to the observed prolongation of AV nodal conduction delay and WCL. The effects of graded hypoxia on AV nodal conduction in isolated perfused rabbit hearts was studied by Young *et al* (132). They compared adult and neonatal hearts and observed that in 95% O_2 the WCL was longer in adult compared to neonatal hearts, and increased much further in response to hypoxia in adult versus neonatal hearts. AH intervals began to increase at a higher O_2 saturation (20%) in adult hearts versus neonatal (10%).

The mechanisms whereby aging results in prolongation of AV nodal conduction delay have been explored in a number of studies of human AV nodal function. Wu *et al*

(133) showed that the cycle length of AV nodal re-entrant tachycardia was longer in an elderly population. Anselme *et al* (134) further investigated the modification of anterograde and retrograde activation associated with the aging process. The main finding of this study was that of slower retrograde conduction times in older patients due to selective regional slowing of conduction. There did not appear to be slowing of conduction in the "slow" pathway region but longer retrograde conduction occurred at all other recording areas. They concluded by suggesting that the delayed retrograde activation of the atrium is due to "transverse, non-uniform anisotropic conduction both in the circuit itself and between the exit from the circuit and the recorded atrial sites". This may be a consequence of age-related microfibrosis within the AV nodal tissues.

Age related microfibrosis of atrial tissue was found to result in reduction of transverse conduction velocity in a study by Spach and Dolber in 1986 (70). Using atrial tissue derived from humans at the time of cardiac surgery (chosen because of the anisotropic properties of the atrial pectinate bundles) they analysed both transverse and longitudinal extracellular and transmembrane action potentials to elucidate mechanisms of cardiac conduction disturbances that may ultimately lead to re-entry. They studied differences in waveforms between young and old patients. They found a smooth contoured waveform during transverse propagation in young patients but complex polyphasic waveforms in older patients. This was thought to be due to electrical uncoupling of the side-to-side connections of myocardial fibres with aging, resulting in a zigzag course of transverse propagation. Furthermore they observed collagenous septa separating groups of fibres. Consequently, there was a decrease in transverse conduction velocity with age, making it possible for re-entry to occur in small regions of cardiac tissue with apparently normal cellular electrophysiological properties.

Lenegre or Lev's disease (idiopathic progressive cardiac conduction disease) was initially described in 1963 (135;136). It is characterised by progressive age related AV conduction slowing, which may ultimately result in complete AV block necessitating permanent pacemaker implantation. Initially considered a primary degenerative disease of the conduction system, recently it has been linked to a loss of function mutation in the *SCN5A* gene encoding a cardiac Na^+ channel (64). Studies of families carrying the gene revealed that the conduction defect worsened with age, and life threatening AV block occurring only in older patients. In order to study this in more detail a mouse model with targeted disruption of *SCN5A* was developed (137). Heterozygous mice (*SCN5A*$^{+/-}$) demonstrate slowed conduction similar to that

in Lenegre's disease patients, with progressive worsening of conduction defects (including P-wave, PR and QRS prolongation) with aging. Furthermore, histological analysis demonstrated fibrosis and expression of hypertrophy markers in older animals. In addition, connexin 40 expression was reduced by approximately 50% in *SCN5A*$^{+/-}$ mice compared to WT, which may explain slowed atrial and AV nodal conduction.

In the present study of older, sham operated controls studied at age 44-52 weeks old, there was a modest but not statistically significant increase in the AH interval at PCL 300 and 200ms, and in AV nodal FRP and ERP compared to younger stock controls (age 12-20 weeks). Wenckebach cycle length was significantly longer in the older animals. There was no difference in the spontaneous intrinsic sinus cycle length between the groups. The lack of significant prolongation of SSCL, AH intervals and refractory periods is in contrast to previous human and animal studies. The rabbits used in this study were not senescent therefore age-related prolongation of SSCL and AV nodal conduction delay may still occur but may only be observed at an older age.

3.8.5 Site of maximal AV delay – evidence from optical mapping studies

Analyses of the surface electrograms acquired during optical mapping experiments confirmed the significant increase in AH interval and WCL in LVD compared to controls. It is interesting to note that the AH intervals at each PCL in LVD during this series of experiments appear strikingly longer than the intervals at corresponding PCLs in the surface electrograms series. The reason for this is not clear. Overall there is no statistically significant difference when the AH intervals in LVD from optical experiments are compared with the same from surface electrogram experiments. The lack of a similar discrepancy in the control AH intervals between the two series of experiments makes experimental technique (for example, use of the voltage sensitive dye, ischaemic time, duration of recordings) unlikely to be implicated.

The results of optical mapping experiments show that the prolongation of AH interval in LVD compared to controls occurs as a result of conduction delay predominating between the AVN input and the compact node. There is also prolongation of conduction time between the compact node and the His bundle but this did not reach statistical significance. There is no difference in conduction time

from the atrial tissue to the AVN inputs. This strengthens the original hypothesis that the prolonged AV delay observed in LVD is due to conduction delay originating within the AV node, and is not a consequence of changes in conduction characteristics within atrial tissue.

3.8.6 Evidence of dual pathway AV nodal physiology in rabbit

Anatomical and functional studies of the rabbit AV node have confirmed the presence of two distinct input pathways into the AV node (40-44). In this study, there is also evidence of dual pathway AV nodal physiology in rabbit.

Figure 3-17 illustrates the number and percentage of animals with evidence of dual pathway AV nodal physiology across all animals used for each study in this thesis. There was no significant difference in the proportion of animals exhibiting dual pathway AV nodal physiology between controls (33%) and LVD (22%) at either 8 or 32 weeks post infarct. Activation of both slow and fast pathways was evident in both controls and LVD at 8 and 32 weeks post infarct. Therefore conduction block in the fast pathway with preferential slow pathway conduction is unlikely to explain the observed increase in AV delay in LVD.

In the series of animals used to study the effect of LVD on AV nodal conduction characteristics, 1 control, 4 LVD (8) and 2 LVD (32) showed dual pathway AV nodal physiology. These animals were excluded from the analysis of AV nodal refractory periods. However, if the FRP and ERP of the fast pathway were input into the analysis, there were still no significant differences in refractory characteristics of the AV node between the groups. When the FRP and ERP of the fast and slow pathways were compared across the groups, there were no significant differences observed. This conclusion must be interpreted with caution in view of the small number of samples on which it is based. In particular there appeared to be an unusually long FRP and ERP in the control sample in which dual AV nodal physiology was observed (Table 3-7). This is inconsistent with data obtained from control animals compared to LVD animals shown previously, which suggested prolongation of the refractory periods of the AV node (although failing to reach statistical significance in most analyses) in LVD. This would suggest that the prolonged FRP and ERP in the control sample with dual AV nodal physiology was a spurious result that should be excluded from any conclusions.

3.8.7 Conclusion

In summary, this study has confirmed that the exaggerated AV delay observed in the presence of LVD in this rabbit model is due to conduction delay at the level of the AV node. This occurs in the absence of significant prolongation of AV nodal functional or effective refractory periods. Atrial effective refractory period is not affected. There is no change in the conduction time between the atrium and the AVN input but significant delay in conduction between the AVN input and compact node and His bundle regions in LVD. The presence of dual pathway AV nodal physiology in similar proportions of controls and LVD hearts rules out preferential conduction via the slow pathway in LVD as a mechanism for the observation. Other hypotheses include a negative dromotropic effect on the AV node due to beta-adrenoceptor down-regulation or chronic endogenous adenosine excess. The absence of significant prolongation of AV node refractory periods suggests reduction in conduction velocity due to changes in the electrotonic interaction between the cells of the AV conduction system, possibly through altered connexin expression. Subsequent chapters will investigate and discuss these hypotheses in more detail.

Age related AV nodal delay may contribute to the observed further prolongation of AH intervals in LVD (32) animals compared to LVD (8). Indeed, mechanisms known to result in age-related AV nodal conduction delay may play a role in LVD induced AV nodal conduction delay. Histological analysis is being carried to identify the presence of microfibrosis and immunohistochemical analysis to determine the expression of connexins known to have a role in AV nodal conduction

Chapter 4 - Response of the sinus and AV nodes to beta-adrenergic stimulation in the rabbit model of LVD

4 Response of the sinus and AV nodes to beta-adrenergic stimulation in the rabbit model of LVD

4.1 Introduction

In chronic heart failure, excess norepinephrine levels lead to downregulation and desensitisation of myocardial ?-adrenoceptors (74-76;138;139). The negative inotropic effect of chronic catecholamine excess and subsequent ?-adrenoceptor downregulation has been demonstrated in rabbit models using chronic isoproterenol infusion via the implantation of an osmotic minipump (77;78). Furthermore, previous work in our laboratory has demonstrated evidence of reduced ?-adrenoceptor sensitivity to the inotropic effects of isoproterenol in papillary muscles from rabbits with LVD compared with sham operated controls (79).

In the present study I have confirmed the presence of excessive AV nodal delay in the rabbit model of LVD due to apical myocardial infarction. The mechanisms underlying this conduction delay are uncertain but may include downregulation of ?-adrenoceptors in AV nodal tissue. This would potentially have a negative dromotropic effect. The purpose of this study was to evaluate the chronotropic and dromotropic response to ?-adrenoceptor stimulation in controls and LVD animals at 8 weeks post ligation (LVD (8)), and then to compare the responses to determine whether ?-adrenoceptor downregulation has a mechanistic role in the observed abnormal AV nodal delay in LVD.

4.2 Methods

4.2.1 Rabbit model of left ventricular dysfunction due to apical myocardial infarction

A well-characterised model of myocardial infarction (MI) induced by coronary artery ligation was used in this study as previously described (82-88). Procedures were undertaken in accordance with the United Kingdom Animals (Scientific Procedures) Act 1986 and conform to the Guide for the Care and Use of Laboratory Animals published by the US National Institutes of Health (NIH Publication No. 85-23, revised 1985).

4.2.2 Isolated atrioventricular node preparation

The isolated AV node preparation was created as described in Chapter 2.

4.2.3 Isoproterenol concentration response study

After 20-30 minutes of superfusion with normal Tyrode's solution to allow equilibration, samples were superfused with isoproterenol in Tyrode's solution of the above composition. The ?AH interval in response to isoproterenol reached steady state after 10 minutes of superfusion. Concentration response relationships for the chronotropic and dromotropic effects of isoproterenol were studied at increasing concentrations from $1x10^{-9}$M to $1x10^{-6}$M.

4.2.4 Surface electrogram recording and pacing protocols

Electrograms recorded from the surface of the isolated AV node preparation were recorded using locally developed ECG acquisition software (NMap, Dr FL Burton, University of Glasgow). The spontaneous sinus cycle length was recorded in every experiment. The basic stimulus cycle length was 300ms. Atrio-Hisian (AH) intervals, Wenckebach cycle length, functional and effective refractory periods of the AV node and the atrial effective refractory periods were derived using standard pacing protocols as described earlier.

4.2.5 Statistical analysis

Results are expressed as mean ± standard error of the mean unless otherwise stated. The $logEC_{50}$ of isoproterenol for each parameter was determined in each experiment. In addition, mean ± SEM values were determined for each parameter in response to each isoproterenol concentration increment. Overall response to isoproterenol was analysed by ANOVA. The values were then plotted against the log[isoproterenol] to generate the concentration response curve for each parameter. Unless otherwise stated, comparisons between data derived from controls versus ligated preparations were made using an unpaired Student's *t*-test. A two-tailed p-value of less than 0.05 was considered statistically significant.

4.3 Results

The chronotropic and dromotropic effects of isoproterenol were studied in a series of 7 control and 7 LVD (8) samples. This study was carried out in different animals to those reported in Chapter 3. Results are discussed in detail below.

4.3.1 Chronotropic response to isoproterenol

The spontaneous sinus cycle length at baseline was not significantly different between the control and LVD (8) groups (362.2 ± 27.75ms versus 343.9 ± 11.87ms) (Figure 4-1A). There was a progressive reduction in the spontaneous sinus cycle length with increasing isoproterenol concentration in both controls (ANOVA P<0.001) and LVD (8) (ANOVA P<0.001) (Figure 4-1B). There was no significant difference in the EC_{50} for isoproterenol between controls and LVD (8) (Table 4-1). Furthermore, the maximal response to isoproterenol was not significantly different between controls and LVD (8) (percent reduction in SSCL (mean ± SEM): control 33.55 ± 3.15% versus LVD (8) 40.65 ± 3.50%).

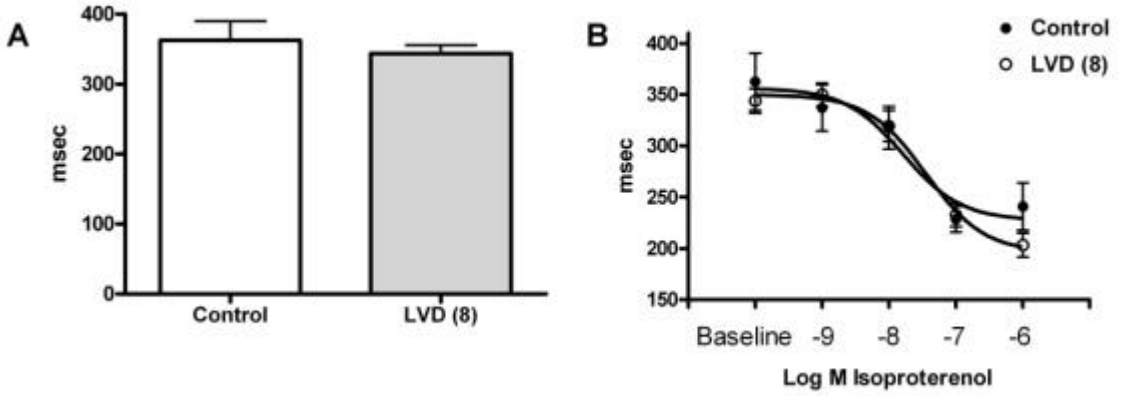

Figure 4-1 – Chronotropic response to isoproterenol. A – SSCL at baseline in controls versus LVD (8). B – Concentration response curves of SSCL to isoproterenol in controls versus LVD (8). Results expressed as mean ± SEM. N=7 controls and 7 LVD (8).

4.3.2 Isoproterenol effects on parameters of AV nodal function

Preliminary data confirmed that the time to steady state AH interval at PCL 300ms in both control and LVD (8) was no longer than 10 minutes. Data were therefore recorded after 10 minutes of superfusion with each incremental concentration of

isoproterenol. Of note, the effects of isoproterenol at higher concentrations ($3.1x10^{-7}$M and above) became unpredictable, particularly in the control samples, possibly because at this concentration the spontaneous sinus rate was faster than the PCL, affecting pacing capture. Due to this loss of pacing capture at PCL 300ms in $3.1x10^{-7}$M isoproterenol and above, data were excluded from the concentration response curve as illustrated in Figure 4-2B.

At baseline, the mean ± SEM AH interval at PCL 300ms in control was 44.00 ± 4.48ms and in LVD (8) was 77.57 ± 16.35ms ($P < 0.05$, Figure 4-2A). Furthermore, at PCL 200ms, the baseline AH interval was significantly longer in LVD (8) compared to control (control 58.00 ± 6.07ms versus LVD (8) 84.00 ± 12.59ms, $P < 0.05$, Figure 4-2C). There was a progressive reduction in the AH intervals at both PCL 300ms (ANOVA control P=0.05; LVD (8) P=0.03) and 200ms (ANOVA control P=NS; LVD (8) P=0.04) with increasing isoproterenol concentration in both controls and LVD (8) (Figure 4-2B and 4-2D). The maximal response to isoproterenol was significantly greater in LVD (8) compared to controls at PCL 300ms (percent reduction in AH interval (mean ± SEM): control 9.98 ± 3.02% versus LVD (8) 23.69 ± 5.10%, $P < 0.05$). There was no significant difference, however, in the maximal response to isoproterenol at PCL 200ms between controls and LVD (8) (percent reduction in AH interval (mean ± SEM): control 13.96 ± 4.43% versus LVD (8) 18.81 ± 4.30%, P = ns). There was no significant difference in the EC_{50} for isoproterenol between controls and LVD (8) at either PCL 300ms or 200ms (Table 4-1).

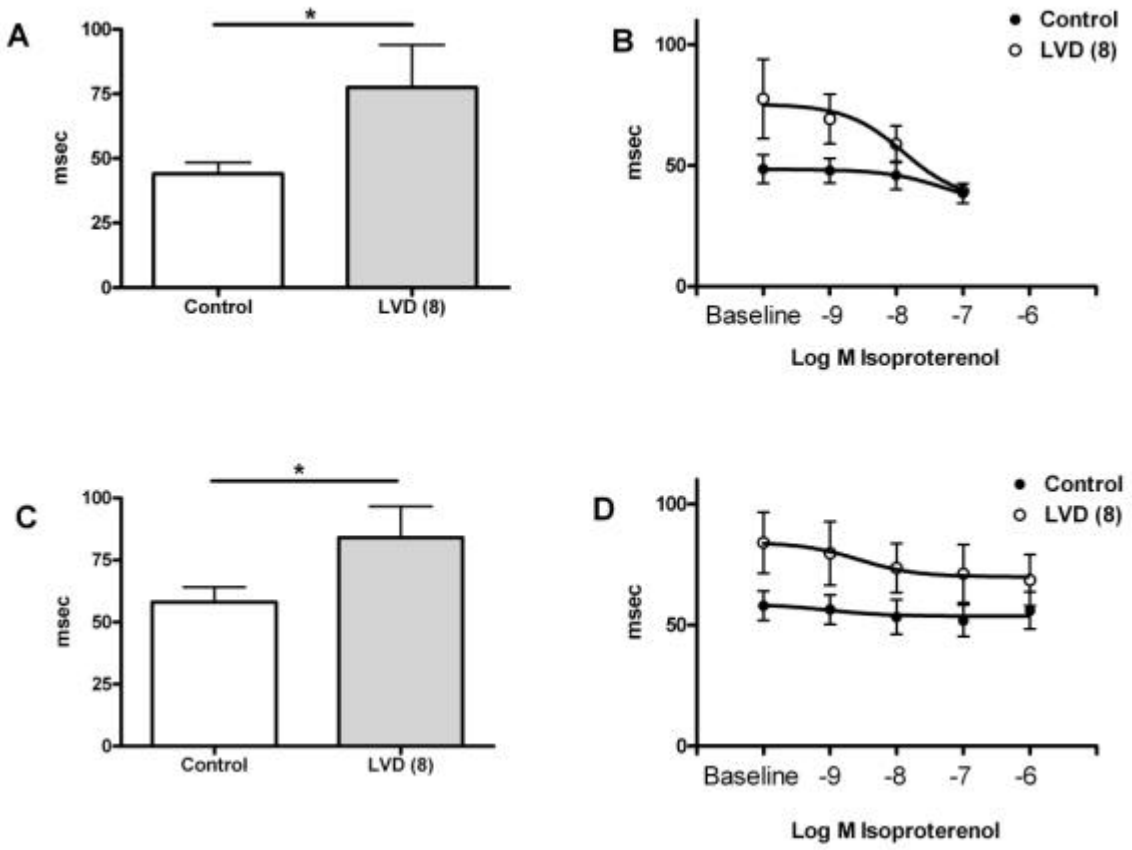

Figure 4-2 – Effect of isoproterenol on AH intervals. A – Baseline AH intervals at PCL 300ms. B – Concentration response curve showing the effect of isoproterenol on AH interval at PCL 300ms. C - Baseline AH intervals at PCL 200ms. D – Concentration response curve showing the effect of isoproterenol on AH interval at PCL 200ms. Results expressed as mean ± SEM (ms). * P < 0.05. N=7 controls and 7 LVD (8).

The Wenckebach cycle length at baseline was significantly longer in LVD (8) compared to control (191.4 ± 23.5ms versus 135.7 ± 9.4ms, P < 0.05) (Figure 4-3A). There was a progressive reduction in the Wenckebach length with increasing isoproterenol concentration in both controls (ANOVA P=NS) and LVD (8) (ANOVA P<0.001) (Figure 4-3B). There was no significant difference in the EC_{50} for isoproterenol between controls and LVD (8) (Table 4-1). However, the maximal response to isoproterenol was significantly greater in LVD (8) compared to controls (percent reduction in WCL (mean ± SEM): LVD (8) 27.3± 5.8% versus control 11.7 ± 2.6%, P < 0.05).

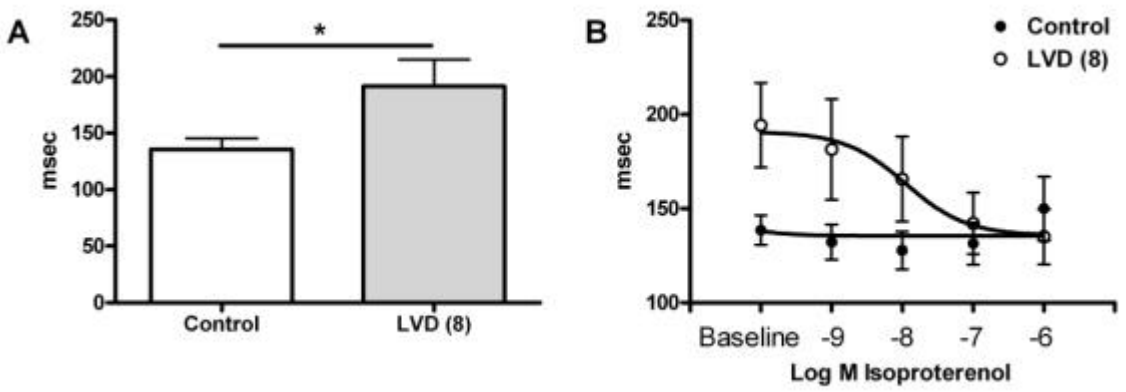

Figure 4-3 – Effect of isoproterenol on Wenckebach cycle length. A – WCL at baseline in controls versus LVD (8). B - Concentration response curves of WCL to isoproterenol in controls versus LVD (8). Results expressed as mean ± SEM (ms). * P < 0.05. N=7 controls and 7 LVD (8).

Due to the increase in spontaneous sinus cycle length in response to isoproterenol, refractory periods were determined at PCL 200ms. There were no significant differences in the AVN FRP, AVN ERP or atrial ERP at baseline between controls and LVD (8). There was no significant decrease in the AVN FRP, ERP or atrial ERP with increasing concentrations of isoproterenol. The EC_{50} of isoproterenol for all refractory periods was not significantly different between controls and LVD (8) (Table 4-1).

	Log EC_{50} Isoproterenol (M)		P - value
	Control	LVD (8)	
SSCL	-7.78 ± 0.19	-7.74 ± 0.18	0.11
WCL	-8.93 ± 1.08	-8.22 ± 0.49	0.55
AH300	-8.89 ± 1.88	-8.59 ± 0.80	0.92
AH200	-7.15 ± 1.85	-8.98 ± 0.57	0.39
AVN FRP	-7.39 ± 0.53	-8.02 ± 0.45	0.40
AVN ERP	-7.73 ± 1.29	-9.49 ± 0.43	0.20
Atrial ERP	-7.33 ± 0.66	-6.15 ± 1.61	0.50

Table 4-1 – Log EC_{50} of isoproterenol. Results expressed as mean ± SEM (M). N=7 controls and 7 LVD (8).

4.4 Discussion

4.4.1 Evidence for ß-adrenoceptor downregulation in human studies and animal models of chronic heart failure

Neurohormonal derangement has a central role in the pathogenesis of chronic heart failure. Increased circulating levels of catecholamines, especially norepinephrine, have been observed in the plasma of patients with CHF, and are strongly related to prognosis (140). In CHF, excess norepinephrine levels lead to downregulation and desensitisation of myocardial ?-adrenoceptors, the latter occurring by inhibition of receptor signalling pathways, increase in inhibitory G-proteins and decrease in adenylate cyclase and cAMP levels (74-76). The negative inotropic effect of chronic catecholamine excess and subsequent ?-adrenoceptor downregulation has been demonstrated in rabbit models using chronic isoprenaline infusion via the implantation of an osmotic minipump (77;78). Furthermore, previous work in our laboratory has demonstrated evidence of reduced ?-adrenoceptor sensitivity to the inotropic effects of isoprenaline in papillary muscles from rabbits with CHF compared with sham operated controls (79). Another group has shown evidence of progressive reduction in ß-adrenoceptor density in human ventricle (obtained via right ventricular endomyocardial biopsy or from LV free wall in explanted hearts of patients undergoing transplantation) with degree of LVSD, beginning with mild-moderate LVSD (141). Furthermore, Ginsburg *et al* (142) demonstrated decreased response of failing human hearts to isoproterenol in RV papillary muscles isolated from normal and failing hearts. There was a significant decrease in the maximum tension generated by the failing hearts compared with normal. The EC_{50} for isoproterenol was fivefold higher in failing muscle compared with normal.

4.4.2 Response of the sinus node to isoproterenol in the rabbit model of chronic heart failure

The results of the present study show that isoproterenol had a positive chronotropic effect, with a concentration-dependent reduction in the spontaneous sinus cycle length. These findings are in keeping with other studies. Toda *et al* (143) studied the effect of sympathetic stimulation on transmembrane potentials in the SAN. Sympathetic nerve stimulation resulted in an increase in the pacemaker firing rate and in the slope of the slow depolarisation of the AP during diastole, as well as a decrease in the APD_{90}. Similar effects were seen with the application of

norepinephrine, namely a concentration dependent decrease in the SAN cycle length with norepinephrine. Furthermore, Hewitt and Rosen (144) also observed a concentration dependent increase in sinus rate in isolated rabbit SAN tissue superfused with isoproterenol. The maximal reduction in SCL was comparable to the present study, at approximately –40% of baseline value.

There is a paucity of literature reporting the effect of heart failure on the response of the sinus node to ß-adrenergic stimulation, although the effect of isoproterenol on sinus node rate has been studied in a rat model of cardiac hypertrophy induced by volume loading secondary to aortic incompetence (AI) (145). In isolated right atria, they observed a higher basal rate and a smaller effect of isoproterenol in AI animals compared to controls, suggesting down regulation of the ß-adrenoceptor pathway in this model (without overt heart failure). However, in this model, it has previously been shown that there was no alteration of the effect of isoproterenol on contractile force of papillary muscles and an unchanged number of ß-adrenoceptors in the ventricles of AI animals compared to controls, therefore this model is not really comparable to the MI model used in the present study. In the present study, the concentration response-relationship did not differ between the control group and the LVD group, with no significant difference being observed in the EC_{50} for isoproterenol between the groups. Furthermore, the maximal increase in the sinus node firing rate with isoproterenol was not significantly different between the groups.

4.4.3 Effect of isoproterenol on dromotropic function in the atrioventricular node in the rabbit model of chronic heart failure

Sympathetic stimulation results in an increase in conduction velocity through the AV node via ß-2 adrenoceptor mediated positive dromotropic effects (146). Given the evidence of ?-adrenoceptor downregulation and its potential therapeutic reversibility in respect of inotropic function, what evidence is there of analogous mechanisms affecting dromotropic function in the AV node? Elnatan *et al* (147) demonstrated a higher proportion of ?-adrenoceptors in the AV node than in the His bundle in hearts explanted from patients with idiopathic dilated cardiomyopathy and ischaemic heart disease. The lack of disease-free hearts prevented any comparison of the relative abundance of ?-adrenoceptors in disease states compared to controls. We hypothesised that ?-adrenoceptor downregulation may

result in a reduction in the conduction velocity through the AV node in CHF, and this may be evidenced by a relative reduction in the sensitivity of isolated AV nodal tissue from LVD animals to isoproterenol.

The results of the present study confirm that superfusion with isoproterenol resulted in a concentration-dependent reduction in AV nodal conduction time (AH interval) in both controls and LVD samples. This finding was not influenced by heart rate as the intrinsic spontaneous sinus rate was overdriven by pacing at the Crista Terminalis. With this, there remained a concentration dependent reduction in the AH interval at both PCL 300ms and 200ms. Due to the increase in the spontaneous sinus rate at higher isoproterenol concentrations, there was failure of pacing capture at PCL 300ms in concentrations of isoproterenol greater than $1x10^{-7}$M, precluding analysis of the AH interval under these conditions. The EC_{50} for the isoproterenol effect on AH interval was not significantly different between the groups, regardless of PCL. However, at the slower rate of PCL 300ms, the magnitude of the reduction in the AH interval with increasing isoproterenol concentration was significantly greater in the LVD group (24%) compared to control (10%). No similar difference was observed at PCL 200ms. This may reflect the inability of the rabbit AV node to facilitate a further increase in conduction velocity at this faster constant pacing rate in the presence of maximal ß-adrenergic stimulation, given that nodal conduction time is dependent on the complex interaction of a number of factors including the recovery time elapsed since the last activation and cumulative time and rate-dependent fatigue (148). During Wenckebach cycles, however, fatigue does not affect nodal conduction time and in fact facilitation increases from beat to beat allowing conduction at very short recovery intervals (55;148). In the present study the maximal reduction in Wenckebach cycle length was also significantly greater in the LVD group (27%) compared to control (12%).

There have been no previous studies of the effect of isoproterenol on AV nodal conduction in the presence of AV nodal conduction delay in rabbit. Previous studies of the effects of isoproterenol on AV nodal conduction in patients with and without evidence of AV block have shown that AV nodal conduction delay may be reduced with ß-adrenergic stimulation (149). The AH interval was reduced with isoproterenol in both patients with normal and prolonged AV nodal conduction time. In two patients with second degree AV block proximal to the His bundle, 1:1 conduction was observed with isoproterenol. In individuals with normal AH interval at baseline, the AH interval was reduced by 21% with isoproterenol. In those with prolonged AH interval, the reduction with isoproterenol was 22%. There was no significant

difference in the magnitude of the effect of isoproterenol on AH interval in the presence of conduction delay compared to those with normal conduction, however conduction disease was not in the context of chronic myocardial infarction or heart failure.

4.5 Conclusion

This study suggests that the sensitivity of the rabbit AV node to exogenous ß-adrenergic stimulation is in fact greater in the LVD model compared to controls when paced at cycle lengths similar to the spontaneous sinus cycle length. This novel finding is in contrast to the evidence of ß-adrenoceptor downregulation in the left ventricle of the same model as discussed above. There are a number of possible mechanisms which may underlie this, including the possibility of changes in the signalling system or an increase in the overall number of ?-adrenoceptors in the AV node. An alternative explanation could be that in LVD there is tonic depression of AV nodal conduction, for example due to endogenous adenosine, which is overcome by the action of exogenously applied isoproterenol. Further work is required to clarify this. The lack of a difference in the EC_{50} for isoproterenol across the two groups suggests that the affinity of the AV nodal ß-adrenoceptors for the agonist was not different. However, the increase in the maximal reduction in AH interval and WCL may be due to enhanced efficacy of the agonist in LVD. This apparent up-regulation of AV nodal ß-adrenoceptors in LVD due to apical MI may play an important role in the prevention of high degree AV block in vivo.

Chapter 5 - Influence of endogenous and exogenous adenosine on AV nodal conduction in the rabbit model of LVD

5 Influence of endogenous and exogenous adenosine on AV nodal conduction in the rabbit model of LVD

5.1 Introduction

It has been shown conclusively by many investigators that adenosine influences conduction time through the AV node (51;122;123;150-153). Conduction is slowed or even blocked as a consequence of the inhibitory action of adenosine on the action potential of nodal cells. Acting via the adenosine A_1 receptor (119), adenosine hyperpolarises the membranes of AV nodal cells, reduces the slope of the upstroke and diminishes the amplitude of the AV nodal cell action potential (154;155).

Adenosine is ubiquitous, as it is involved in the metabolism and catabolism of ATP (156;157). Release of adenosine may signal conditions that are detrimental to the organism, such as hypoxia (119), during which adenosine acts to minimise further tissue injury by reducing the myocardial oxygen demand, by reducing the sinus node automaticity and increasing conduction time through the AV node. Belardinelli *et al* (158) confirmed that release of endogenous adenosine was implicated in hypoxia induced AV conduction disturbances in the isolated perfused guinea pig heart, observing reversal of the hypoxia induced prolongation of the AH interval with the adenosine antagonist aminophylline. Further studies on adenosine and hypoxia effects on the rabbit AV node have also suggested that endogenous adenosine release is implicated in hypoxia induced AV nodal conduction delay (132). However, the magnitude of AH prolongation with hypoxia was significantly greater than that with even high (millimolar) concentrations of adenosine, suggesting that other factors may contribute to AV nodal delay in acute hypoxia. To date, no studies have been published investigating the role of endogenous adenosine in conduction abnormalities persisting after an acute hypoxic insult, such as the observed prolongation of the AH interval in our rabbit model of LVD due to chronic myocardial infarction.

AV nodal conduction is determined in part by the balance of activation (by ß-adrenergic stimulation) and inhibition (by adenosine) of adenylyl cyclase (159;160). As discussed in a previous chapter, in rabbits with AV nodal delay in the context of chronic myocardial infarction there is an increase in the maximal response of the AH

interval and Wenckebach cycle length to isoproterenol when compared to controls with normal AV conduction. The mechanism for this is unclear. Assuming that adenosine and ß-adrenergic agonists modulate AV nodal conduction by acting at the same point in the signalling pathway, i.e. at adenylyl cyclase (161), tonic conduction delay may have been caused by excess endogenous adenosine, which was then overcome in vitro by the application of a high concentration of isoproterenol.

The aim of the present study was to determine whether chronic excess endogenous adenosine release is implicated in the observed prolongation of AV nodal conduction. This is investigated through the application of the selective adenosine A_1 receptor antagonist 8-cyclopentyl-1,3-dipropylxanthine (CPX), and comparison of its effects on the AV nodal functional characteristics in LVD (8) samples versus controls. A further aim of this study was to determine the presence of any differential response to exogenous adenosine in the LVD (8) samples compared to control.

5.2 Methods

5.2.1 Rabbit model of left ventricular dysfunction due to apical myocardial infarction

The rabbit model of LVD due to apical myocardial infarction induced by coronary artery ligation as detailed in Chapter 2 was used in this study. Sham operated animals underwent thoracotomy but not coronary ligation. Procedures were undertaken in accordance with the United Kingdom Animals (Scientific Procedures) Act 1986 and conform to the Guide for the Care and Use of Laboratory Animals published by the US National Institutes of Health (NIH Publication No. 85-23, revised 1985).

5.2.2 The isolated AV node preparation

The isolated AV node preparation was created as described in Chapter 2.

5.2.3 Surface electrogram recording

Electrograms recorded from the surface of the isolated AV node preparation were recorded using locally developed ECG acquisition software (NMap, Dr FL Burton, University of Glasgow). The spontaneous sinus cycle length was recorded in every experiment. The basic stimulus cycle length was 300ms. Atrio-Hisian (AH) intervals, Wenckebach cycle length, functional and effective refractory periods of the AV node and the atrial effective refractory periods were derived using standard pacing protocols as described earlier.

5.2.4 Effect of 8-cyclopentyl-1,3-dipropylxanthine (CPX) – a selective adenosine A_1 receptor antagonist.

The selective adenosine A_1 receptor antagonist 8-cyclopentyl-1,3-dipropylxanthine (CPX) (Sigma, St Louis) was applied to preparations to determine whether release of endogenous adenosine contributes to AV nodal delay in this isolated right atrial preparation in vitro. After 20-30 minutes of superfusion with normal Tyrode's solution to allow equilibration, samples were superfused with CPX in Tyrode's solution of the above composition. The relative change in spontaneous sinus cycle length, Wenckebach cycle length, AH interval, and atrial and AV nodal functional

and effective refractory periods were determined after superfusion for 5 minutes with CPX. Responses were determined at baseline, and in CPX concentrations of 0.01, 0.1 and 1µM.

5.2.5 Effect of exogenous adenosine on AV nodal conduction

In a further series of controls and LVD (8) samples the effect of exogenous adenosine (Sigma, St Louis) on AV nodal conduction was studied. After 20-30 minutes of superfusion with normal Tyrode's solution to allow equilibration, samples were superfused with adenosine in Tyrode's solution of the above composition. Preliminary studies confirmed that the maximal ?AH interval reached steady state after 15 minutes of superfusion with adenosine in both controls and LVD (8) samples. The change in Wenckebach cycle length and AH interval at PCL 300ms and 200ms were therefore determined after superfusion for 15 minutes with adenosine. Responses were determined at baseline, and in adenosine concentrations of 0.1, 1, 5, 10 and 20µM.

To confirm that the response to exogenous adenosine could be reversed, samples were then superfused with progressively increasing concentrations of CPX (0.01, 0.1 and 1µM) following data acquisition in the maximal concentration of adenosine. The changes in Wenckebach cycle length and AH interval were again determined after superfusion for 5 minutes with each incremental dose of CPX.

5.2.6 Statistical analysis

Results are expressed as mean ± standard error of the mean unless otherwise stated. Mean ± SEM values were determined for each parameter in response to each CPX and adenosine concentration increment. Statistical analysis was based on analysis of variance (ANOVA) followed by *t*-tests corrected for multiple comparisons unless otherwise stated. A two-tailed p-value of less than 0.05 was considered statistically significant.

5.3 Results

5.3.1 Effect of 8-cyclopentyl-1,3-dipropylxanthine (CPX) on sinus rate and AV nodal conduction

The effect of CPX on sinus rate and AV nodal conduction and refractory periods was studied in a series of 4 control and 4 LVD (8) samples. Results are expressed as the mean ± SEM percentage change from the baseline value (Table 5-1 and Table 5-2). Figure 5-1A illustrates the effect of CPX on the spontaneous sinus cycle length. There was no significant change in the SSCL compared to baseline with increasing concentrations of CPX in either controls or LVD (8) (Figure 5-1A). There was no significant difference between groups in the effect of CPX on SSCL (ANOVA P = 0.79). Figure 5-1B illustrates the effect of CPX on Wenckebach cycle length. There was no significant change in the WCL compared to baseline with increasing concentrations of CPX in either controls or LVD (8). Furthermore, there was no significant difference between the groups in the effect of CPX on WCL (ANOVA P = 0.73).

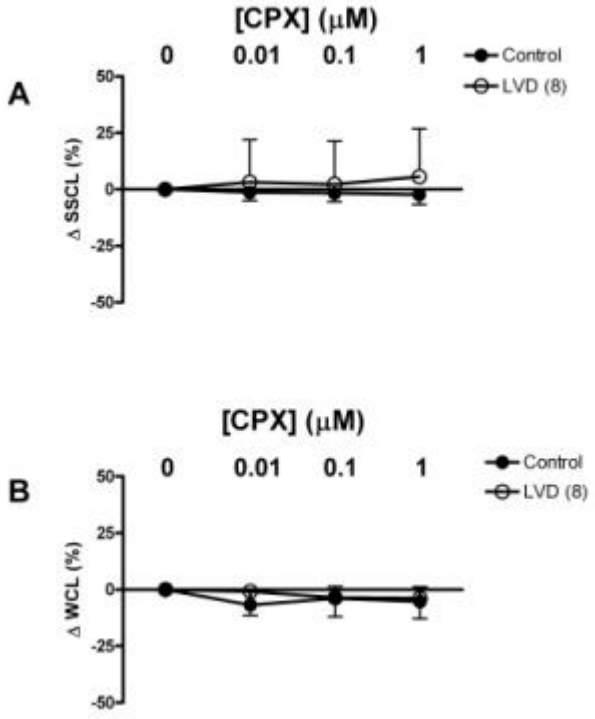

Figure 5-1 – A – effect of CPX on spontaneous sinus cycle length (SSCL) ANOVA P = 0.79. B– effect of CPX on Wenckebach cycle length (WCL) ANOVA P = 0.73. Results expressed as mean ± SEM. N=4 controls and 4 LVD (8).

	[CPX] (μM)	? (mean (SEM) %) from baseline		P value
		Control	LVD (8)	
SSCL	0.01	-1.3 (3.6)	3.2 (18.8)	>0.05
	0.1	-1.7 (3.8)	2.3 (19.1)	>0.05
	1	-2.3 (4.4)	5.6 (21.2)	>0.05
WCL	0.01	-6.8 (4.5)	-0.8 (0.8)	>0.05
	0.1	-3.9 (8.0)	-3.5 (4.9)	>0.05
	1	-5.3 (7.6)	-3.8 (5.0)	>0.05
AH300	0.01	-5.3 (5.0)	-3.6 (3.5)	>0.05
	0.1	-5.9 (5.3)	-5.0 (1.2)	>0.05
	1	-7.3 (4.0)	-7.0 (1.4)	>0.05
AH200	0.01	-1.7 (2.9)	-3.4 (3.4)	>0.05
	0.1	-4.7 (3.9)	-6.5 (1.9)	>0.05
	1	-5.8 (4.2)	-10.1 (2.6)	>0.05
AH100	0.01	-16.2 (9.9)	-7.4 (4.2)	>0.05
	0.1	-16.7 (9.0)	-5.6 (4.0)	>0.05
	1	-18.5 (7.0)	-7.7 (7.7)	>0.05

Table 5-1 – Response to CPX in controls (n=4) versus LVD (8) (n=4). There were no significant differences between controls and LVD (8) for each parameter at each [CPX] as shown. Results expressed as mean (SEM).

The effect of CPX on the AH interval was determined at 3 pacing rates: PCL 300, 200 and 100ms. Results are shown in Figure 5-2 below. Overall, with increasing concentration of CPX, the mean effect was of a progressive reduction in the AH interval at all tested pacing cycle lengths, although this did not reach statistical significance. At PCL 300ms, there was no significant change in the AH interval compared to baseline with increasing concentrations of CPX in the control group. Analysis of variance showed no significant difference in the magnitude of effect between controls and LVD (8) across all concentrations (P = 0.86).

At PCL 200ms, there was no significant change in the AH interval compared to baseline with increasing concentrations of CPX in controls or LVD (8). Again, analysis of variance showed no significant difference in the magnitude of effect between controls and LVD (8) (P = 0.61).

Due to the onset of conduction block at PCL 100ms, AH interval could not be determined for 1 control and 2 LVD (8) samples at this rate. It was therefore not possible to perform analysis of variance to compare groups. At each concentration, however, an unpaired *t*-test revealed no significant difference between groups.

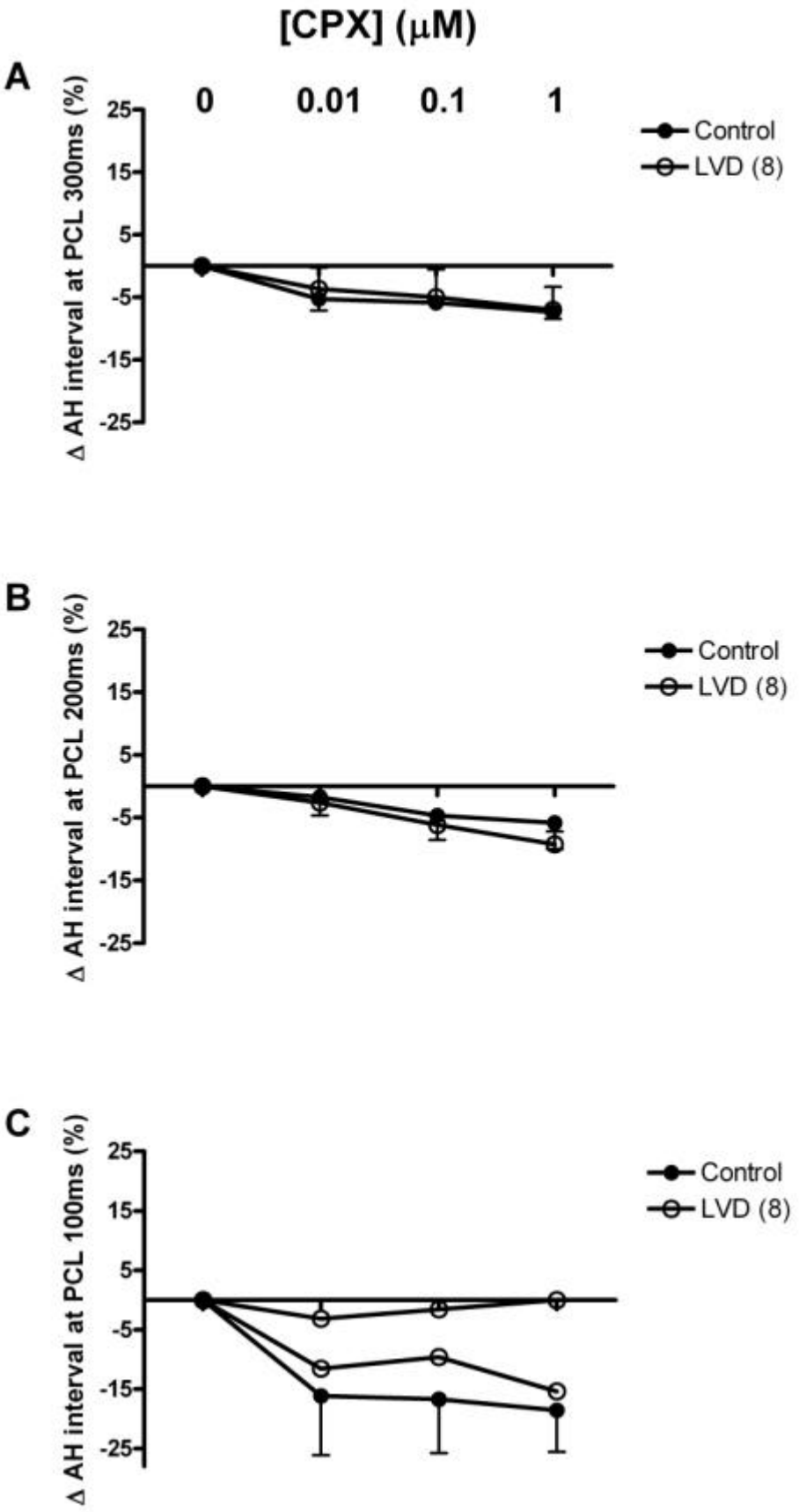

Figure 5-2 – A – effect of CPX on AH interval at PCL 300ms (n=4 control and n=4 LVD (8), ANOVA P = 0.86). B – PCL 200ms (n=4 control and n=4 LVD (8), ANOVA P = 0.61). C – PCL 100ms (n=3 control and n=2 LVD (8) P = ns at each concentration). Results expressed as mean ± SEM (%). Individual data points shown where n=2.

AV nodal functional and effective refractory periods and atrial effective refractory period were determined at a basic PCL of 300ms. Results are shown in Table 5-2 and Figure 5-3 below. CPX did not significantly alter the AVN FRP, ERP or atrial ERP from baseline at any concentration. Furthermore, there were no significant differences in the AVN FRP, ERP or atrial ERP between controls and LVD (8) at any concentration.

	[CPX] (μM)	Δ (mean (SEM) %) from baseline		P value
		Control	LVD (8)	
AVN FRP	**0.01**	-3.5 (10.6)	2.1 (2.2)	>0.05
	0.1	1.0 (9.1)	0.7 (3.0)	>0.05
	1	0.2 (8.3)	0.8 (3.2)	>0.05
AVN ERP	**0.01**	-8.8 (13.3)	14.2 (7.1)	>0.05
	0.1	-13.5 (13.8)	11.2 (4.6)	>0.05
	1	-15.4 (17.5)	13.9 (7.9)	>0.05
Atrial ERP	**0.01**	-2.5 (12.7)	9.5 (4.0)	>0.05
	0.1	3.3 (5.0)	10.5 (3.2)	>0.05
	1	2.5 (6.3)	12.0 (8.1)	>0.05

Table 5-2 – Response to CPX in controls versus LVD (8) – Refractory periods. There were no significant differences between controls and LVD (8) for each parameter at each [CPX] as shown. Results expressed as mean (SEM). N=4 controls and 4 LVD (8).

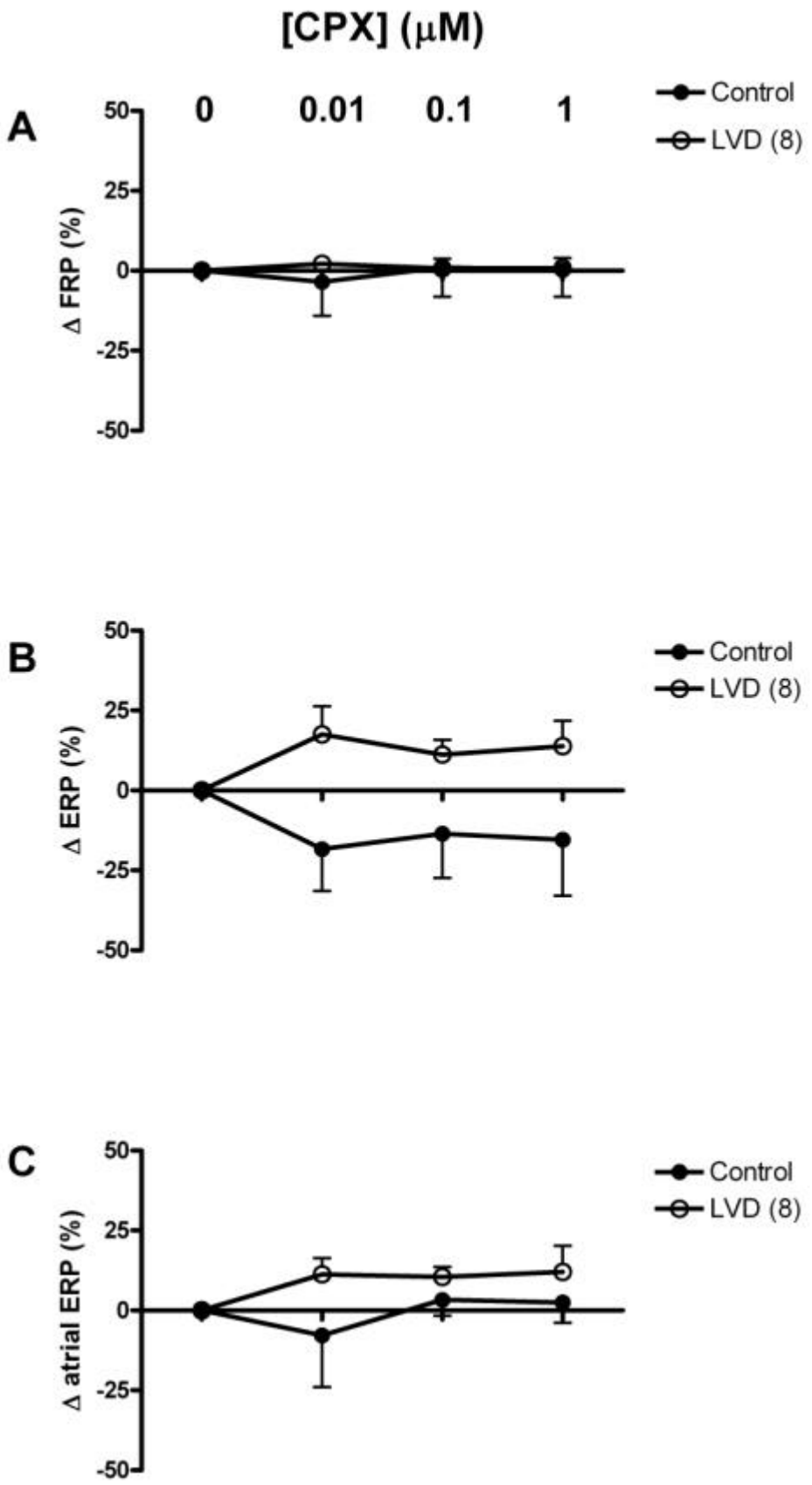

Figure 5-3- A - Effect of CPX on AV nodal FRP (ANOVA P = 0.94). B - Effect of CPX on AV nodal ERP (ANOVA P = 0.15). C – Effect of CPX on atrial ERP (ANOVA P = 0.31). Results expressed as mean ± SEM (%). N=4 controls and 4 LVD (8).

5.3.2 Dromotropic effect of adenosine: comparison between controls and LVD (8)

To characterise the negative dromotropic action of adenosine, and thus identify any difference in response between controls and LVD (8), atrial rate was held constant by pacing at 300ms, 200ms and 100ms cycle lengths (after decrementing the pacing rate to determine the Wenckebach cycle length). Preliminary experiments confirmed that the maximal ?AH interval in response to superfusion with adenosine (concentration 20µM) reached steady state after 15 minutes. Therefore, after 20-30 minutes of superfusion with Tyrode's solution of the composition outlined above to allow equilibration, samples were superfused with adenosine in Tyrode's solution in progressively increasing concentrations (0.1, 1, 5, 10 and 20µM). Data were acquired after 15 minutes of superfusion at each concentration.

Table 5-3 summarises the results of the comparison of the negative dromotropic effect of adenosine on controls (n=6) versus LVD (8) (n=4). The negative dromotropic effect of adenosine was minimal in control samples. At PCL 300ms, the maximum mean ±SEM increase in the AH interval was 2.3 ±1.2ms in [adenosine] 20µM. At PCL 200ms, the maximum mean ± SEM increase in the AH interval was 2.3 ± 0.8ms. The negative dromotropic effect of adenosine was much more pronounced in LVD (8) samples. At PCL 300ms, the maximum mean ± SEM increase in the AH interval was 7.3 ±4.9ms in [adenosine] 20µM. At PCL 200ms, the maximum mean ± SEM increase in the AH interval was 12.5 ± 4.9ms. Overall, adenosine had a significantly greater negative dromotropic effect in LVD (8) compared to controls at both PCL 300 and 200ms (ANOVA $P < 0.05$ and $P < 0.01$, Figure 5-4A and 5-4B respectively). At concentrations > 0.1µM, the magnitude of effect of adenosine was significantly greater in LVD (8) compared to controls at the faster pacing rate of PCL 200ms compared to PCL 300ms. The magnitude of effect of adenosine in prolongation of the Wenckebach cycle length was much greater in LVD (8) than in controls (ANOVA $P < 0.01$, Figure 5-4C). There was no significant change from baseline WCL in controls with increasing concentrations of adenosine. However, in LVD (8), at [adenosine] 5µM and above, there was significant prolongation of the WCL compared to control (Figure 5-4C).

	[Ado] (μM)	? (mean (SEM) (ms)) from baseline		P value
		Control	LVD (8)	
AH300	0.1	-1.2 (1.2)	5.0 (4.0)	> 0.05
	1	0.7 (0.8)	6.5 (5.0)	> 0.05
	5	0.8 (0.5)	7.3 (5.0)	> 0.05
	10	0.7 (0.9)	7.3 (5.3)	> 0.05
	20	2.3 (1.2)	6.3 (4.9)	> 0.05
AH200	0.1	-1.0 (1.3)	0.8 (0.8)	> 0.05
	1	-1.2 (0.8)	8.8 (4.3)	< 0.05
	5	1.2 (1.1)	10.8 (4.5)	< 0.05
	10	1.0 (1.0)	11.0 (4.2)	< 0.05
	20	2.3 (0.8)	12.5 (4.9)	< 0.05
WCL	0.1	2.0 (2.0)	-3.3 (3.3)	> 0.05
	1	0.0 (3.2)	35.0 (22.6)	> 0.05
	5	-3.6 (2.6)	40.0 (20.0)	< 0.05
	10	2.0 (3.4)	53.3 (19.2)	<0.01
	20	2.0 (5.8)	46.6 (20.2)	<0.01

Table 5-3 - Response to Adenosine (Ado) in controls (n=6) versus LVD (8) (n=4). Results expressed as mean (SEM) (ms).

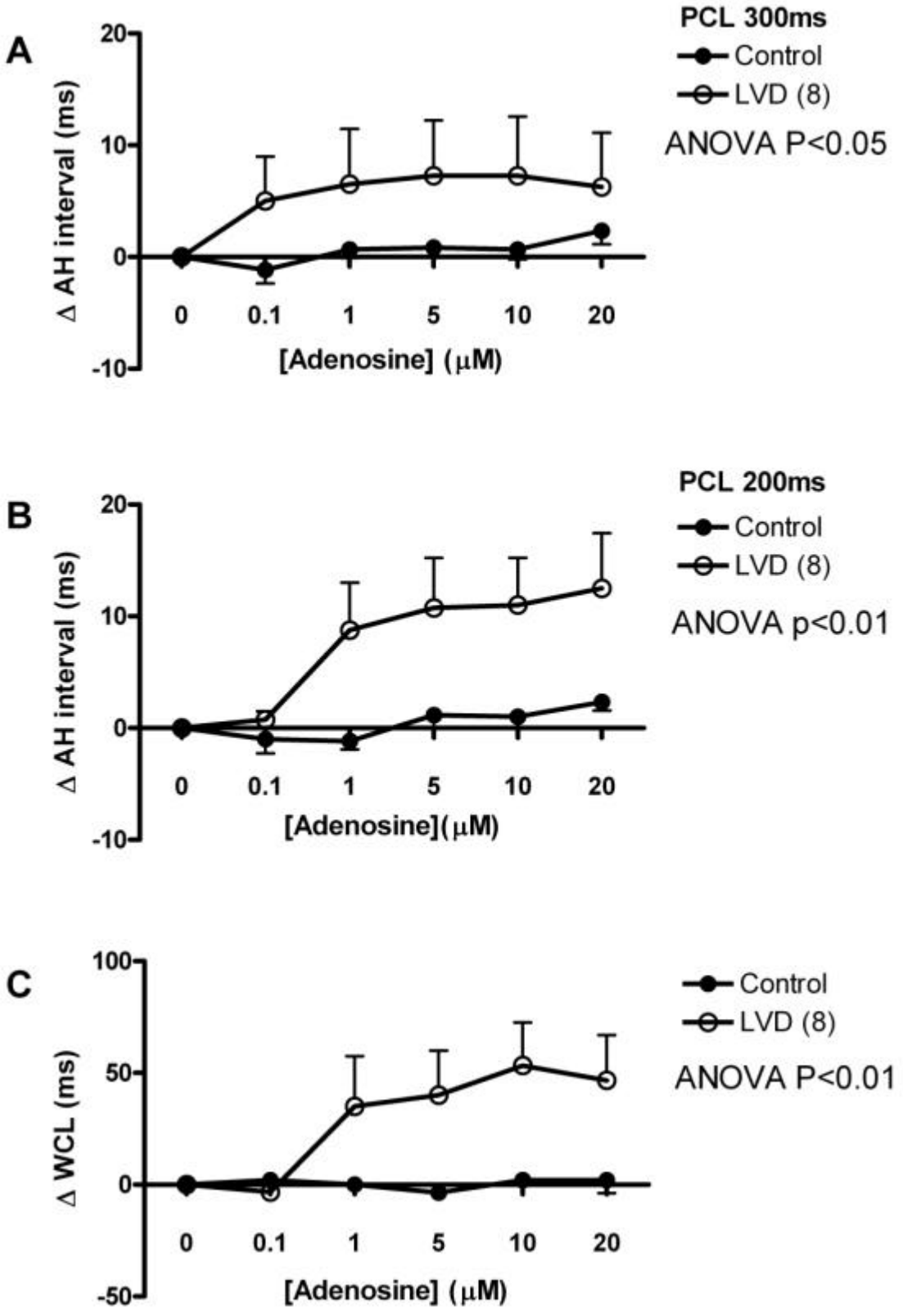

Figure 5-4 – Negative dromotropic effect of adenosine. A – AH interval at PCL 300ms. B – AH interval at PCL 200ms. C – Wenckebach cycle length. Results expressed as mean ± SEM (ms). N=6 controls and 4 LVD (8).

5.3.3 Reversal of the effect of adenosine with CPX

As outlined above, the administration of CPX to this isolated tissue preparation had no significant effect on parameters of sinus rate, AV nodal conduction or refractory periods of the AV node or atrium in either controls or LVD (8) samples. This may have been a result of lack of tissue sensitivity to the concentrations used, or simply because there was insufficient endogenous adenosine present affecting AV conduction time. Therefore to confirm that this preparation was responsive to CPX, namely CPX was capable of reversing the effect of exogenous adenosine, it was added in progressively increasing concentrations (0.01, 0.1 and 1μM) following the adenosine concentration response studies.

Following data acquisition in [adenosine] 20μM, samples were superfused with CPX in Tyrode's solution as outlined in Methods. Data were then acquired after 5 minutes of superfusion with each incremental concentration of CPX. Superfusion with adenosine continued during CPX superfusion. Results are summarised in Figure 5-5 below.

The AH interval prolongation that occurred in response to adenosine at PCL 300ms and 200ms was reversed back to baseline with [CPX] 0.01μM and remained at this level with increasing concentrations of CPX (Figure 5-5A and 5-5B). This effect was seen in both controls and LVD (8) samples.

In controls, Wenckebach cycle length did not change significantly with adenosine or with the addition of CPX. In LVD (8), the prolongation of WCL induced by adenosine was reversed back to baseline with [CPX] 0.01μM and remained at this level with increasing concentrations of CPX (Figure 5-5C).

These results confirm that the isolated AV node preparation was in fact responsive to CPX in the presence of exogenous adenosine. Furthermore, it suggests that the presence of excess endogenous adenosine does not contribute to the observed prolongation of AV nodal conduction time in the rabbit model of LVD.

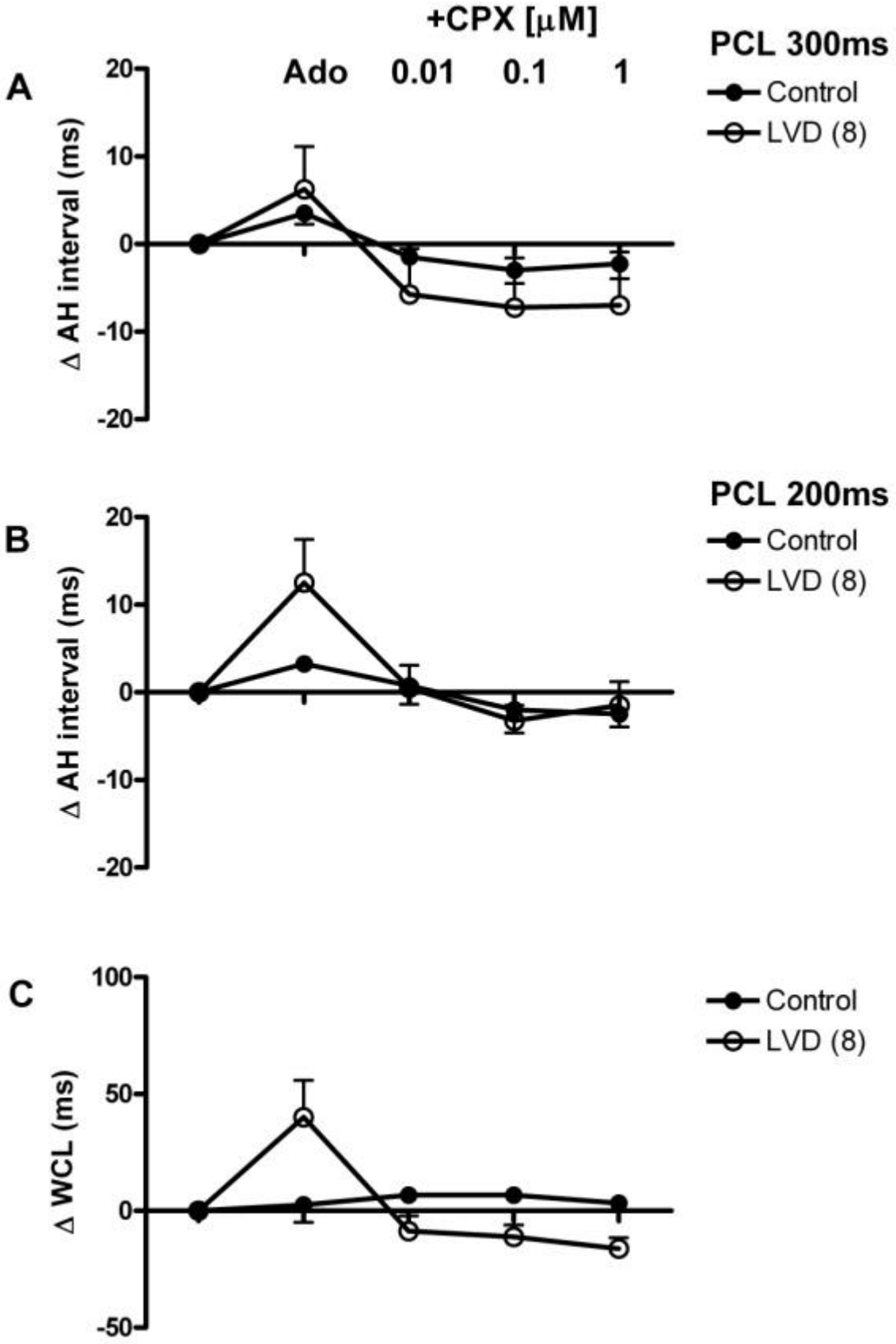

Figure 5-5 – Reversal of the effect of adenosine with CPX. Data at baseline represents pre-adenosine. Superfusion with adenosine 20μM continued during CPX experiments. Results expressed as mean ± SEM (ms). N=6 controls and 4 LVD (8).

5.4 Discussion

5.4.1 Role of endogenous adenosine in abnormal AV nodal delay in the rabbit model of LVD

Adenosine released after acute myocardial ischaemia has an important compensatory role in the inhibition of the detrimental metabolic and inotropic effects of catecholamines (123;124;161;162). To date, no studies have been published investigating the role of adenosine in the development of conduction abnormalities in chronic heart failure, such as may be caused by acute myocardial infarction. The aim of the present study was to determine whether chronic excess endogenous adenosine release is implicated in the observed prolongation of AV nodal conduction time in our rabbit model of LVD due to chronic myocardial infarction. This was investigated by superfusion of a known specific adenosine A_1 receptor antagonist, CPX, onto the isolated AV node preparation in increasing concentrations. There were no significant changes in the SSCL, WCL or AH intervals from baseline with increasing concentrations of CPX. The reasons for the lack of effect of CPX are not clear but are considered in detail below.

It is possible that the lack of effect of CPX reflects simply the absence of tonic excess endogenous adenosine activity in the isolated AV node preparation. Circulating adenosine has a very short half-life of adenosine in plasma and presumably in the interstitial space between cells (1 to a few seconds)(163;164). However, the hypothesis was that local, paracrine adenosine release accounted for the increase in AH interval. The lack of effect of CPX is unlikey to reflect the rapid de-amination or breakdown of endogenous adenosine when the heart is excised and the tissue sample dissected, as this paracrine release of adenosine would be expected to continue. The possibility of a methodological error resulting in the absence of tissue sensitivity to CPX was excluded by the observation of reversal of the effect of exogenously applied adenosine.

The absence of any change in sinus rate or AH interval in the presence of CPX alone provides additional information regarding the integrity of the isolated AV node tissue sample. If the sample were significantly hypoxic, one would expect the release of endogenous adenosine in response to hypoxia, resulting in prolonged SSCL and AV nodal conduction time, effects that would reverse in the presence of CPX.

5.4.2 Differential effect of adenosine on AV nodal conduction in the rabbit model of LVD.

In control samples, adenosine had a minimal effect on the AH intervals and WCL, with a maximal increase in the AH interval of 6ms at the maximum concentration tested (20μM). The protocols in the present study were carried out at 37°C. Previous investigators have confirmed that there is variation in the effect of adenosine across species, with rabbit hearts being less responsive to adenosine than guinea pig hearts (157). In this study, Froldi and Belardinelli observed mean prolongation of stimulus to His bundle interval of less than 10ms in rabbit versus around 30ms in guinea pig hearts in 20μM adenosine. However, the experiments were carried out at 35°C. Other investigators have studied AV nodal responses to adenosine at even lower temperatures (34°C), (158) due to the decreased sensitivity of the preparation to adenosine at higher temperatures (165).

When measured in the effluent of isolated tissue samples, the amount of adenosine released in response to hypoxia is in the sub-micromolar range. The magnitude of AV nodal conduction slowing during hypoxia is much greater than that seen when similar concentrations of exogenous adenosine are applied (121;166). However, when adenosine de-amination and re-uptake are inhibited, the concentration-response relationship becomes similar to that seen in hypoxia (154). In the present study, the magnitude of response to adenosine was much greater in LVD (8) samples compared to controls, and was to the extent seen by previous investigators at cooler temperatures or during hypoxia. This may be a consequence of down-regulation of the signalling pathways responsible for adenosine metabolism in the LVD model.

The maximal increase in the AH interval was greater with increased pacing rate (Figure 5-4A and 5-4B) in keeping with previous investigators observations (157;158). This may be a consequence of the additional effect of endogenous adenosine release during rapid pacing (167). There was a significant prolongation in the WCL in LVD (8) in response to adenosine. This reflects adenosine's action on the N-cells of the AV node, inhibiting $I_{Ca,L}$ and activating of $I_{K,Ado}$ (168) resulting in rate dependent activation failure at lower rates in LVD (8). This increased sensitivity of the AV node of LVD (8) samples to adenosine may have additional anti-arrhythmic properties, protecting the impaired ventricle from rapid atrial rates as may be caused by supra-ventricular tachy-arrhythmias such as atrial fibrillation.

5.5 Conclusion

In summary, in the rabbit model of LVD due to chronic myocardial infarction, there was no evidence of chronic endogenous adenosine excess contributing to prolonged AV nodal conduction time. It is not clear, however, if this represents an absence of endogenous adenosine or rapid reversal of its effects on excision of the heart due to its short half life. There was however an increase in the effect of exogenous adenosine in the LVD model compared to controls, which may be due to adaptive responses serving to protect the impaired ventricle from rapid atrial rates. Further work is required to establish the mechanisms underlying these observations.

Chapter 6 - Effect of acidosis on the electrophysiology of the atrioventricular node

6 Effect of acidosis on the electrophysiology of the atrioventricular node

6.1 Introduction

6.1.1 Clinical significance of myocardial acidosis

It has been recognised that for over 100 years a decrease in extracellular pH has detrimental effects on cardiac function (169), being negatively inotropic (170) and potentially arrhythmogenic (171). Clinical disturbances of acid-base status can result in global myocardial acidosis, such as the metabolic acidosis associated with diabetic ketoacidosis or the respiratory acidosis associated with hypoventilation and hypercapnia. Furthermore, myocardial hypoperfusion, irrespective of aetiology, can result in global myocardial acidosis. Regional myocardial acidosis occurs as a consequence of myocardial ischaemia, most commonly as a result of acute occlusion of a coronary artery. Abrupt cessation of blood flow and therefore oxygen supply to the myocardium results in a profound decrease in intracellular pH by the mechanisms outlined below.

6.1.2 Cellular response to acidosis induced by ischaemia

Two processes contribute to the electrophysiological changes in ischaemia, namely loss of oxygen and nutrient supply, and failure to clear the cell's extracellular space of its metabolites (172). Normally cardiomyocytes derive energy from oxidative metabolism of glucose and fatty acids, with a minimal contribution from anaerobic glycolysis. Ischaemia shifts the cell metabolism to anaerobic glycolysis due to loss of oxygen, which halts the tricarboxylic acid cycle. This transition has several important consequences (173). The breakdown of glycogen produces pyruvic acid, which cannot enter the TCA cycle. htracellular pH falls as protons are produced during hydrolysis of ATP and accumulate during production of lactic acid. Extracellular pH falls as intracellular protons move into the extracellular compartment via the Na^+/H^+ exchanger, $Na^+/HCO3^-$ co-transporter, lactate transport and lactic acid and CO_2 diffusion. This results in intracellular and extracellular acidosis which if severe may result in complete cessation of anaerobic glycolysis. There are a number of possible sites within the cardiomyocyte at which H^+ may have an effect as summarised in Figure 6-1. Initially, during the early stages of hypoxia

and anaerobic glycolysis, ATP levels are maintained by phosphocreatine breakdown due to the large capacity of the phosphocreatine pool, but ATP levels eventually become depleted, and adenine nucleotides may also be lost from the cell, which may compromise the cells recovery from anoxia. Certain rate-limiting glycolytic enzymes are inhibited by acidosis, and therefore the accumulation of intracellular H^+ acts as a negative feedback mechanism to limit further acidification of the cell. Furthermore, the fall of ATP and the accumulation of ADP, Pi, and H^+, results in inhibition of energy-dependent regulation of transmembrane ion gradients such as the Na^+/K^+ pump and sarcoplasmic reticulum Ca^{2+} cycling. Overall this results in a net accumulation of intracellular Na^+ and Ca^{2+} in acidosis. Acidosis and membrane depolarisation associated with extracellular K^+ accumulation slows conduction and these changes act both as a protective mechanism (174) and also contribute to the substrate for re-entry

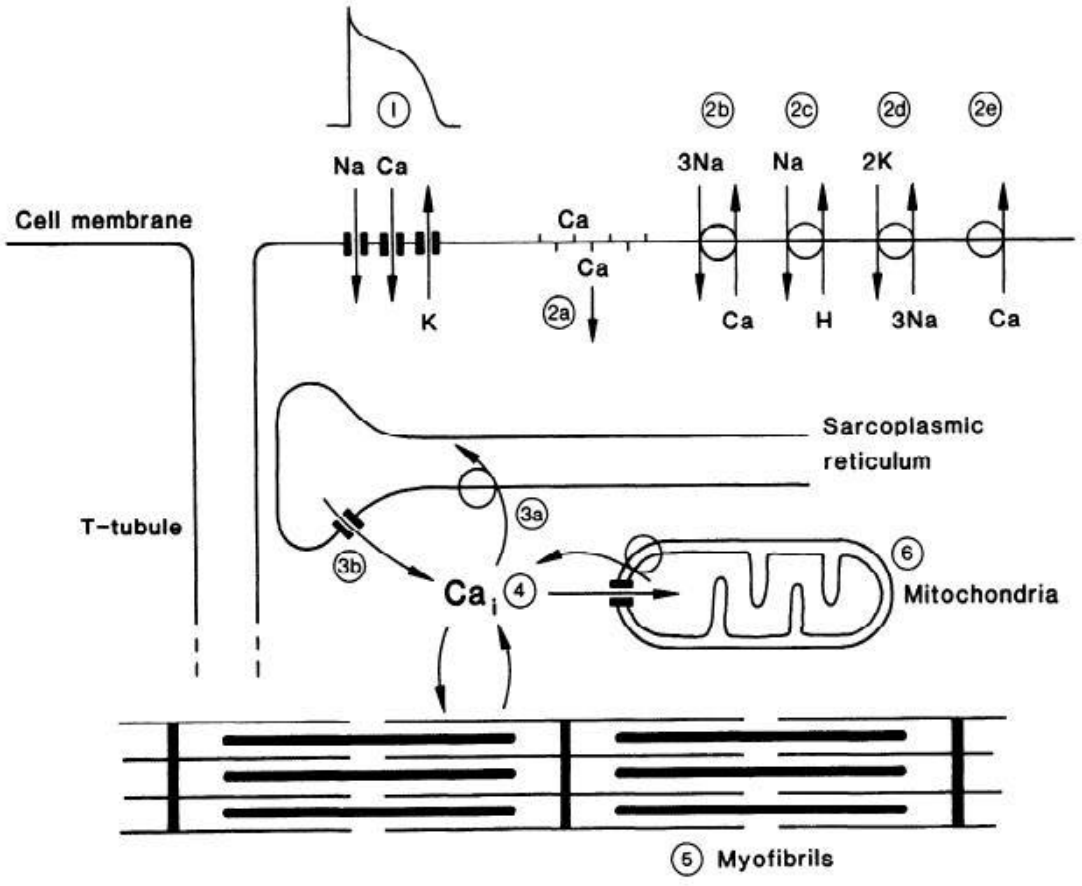

Figure 6-1 – Possible sites of action of H^+ in the cardiomyocyte. 1 – ion channels and currents; 2a – sarcolemmal bound Ca^{2+}; 2b – Na^+/Ca^{2+} exchanger; 2c – Na^+/H^+ exchanger; 2d – Na^+-K^+ ATPase; 2e – Ca^{2+} ATPase; 3a – SR Ca^{2+} uptake; 3b – SR Ca^{2+} release; 4 – cytoplasmic Ca^{2+} during acidosis; 5 – contractile proteins; 6 – cell metabolism and mitochondrial function. (Adapted from (170)).

6.1.3 Slowed conduction velocity in ischaemia and acidosis

Conduction velocity slows in ischaemia by two mechanisms, namely by a decrease in the inward sodium current and also by cellular electrical uncoupling (172;173). The latter occurs as a consequence of the intracellular acidosis that occurs during ischaemia, increasing the resistance of gap junctions, which are composed of connexins. Connexins provide aqueous conduits between cells for current flow. Gap junctional conductance is decreased in response to increased H^+, Ca^{2+} and decreased ATP with resultant slowing of the longitudinal spread of current through cardiac tissue (175). This is not purely a consequence of hypoxia, however, as demonstrated by Turin and Warner (176). They observed that when embryonic cells of Xenopus were exposed to 100% CO_2 the intracellular pH was reduced from 7.7 to 6.4, the resting potential was decreased, the electrical coupling of the cells was abolished and the input resistance was increased. Similar results were found using mixtures of 40%CO_2/60% O_2, suggesting the uncoupling is not purely due to hypoxia but at least partly due to a fall in pH.

6.1.4 Effect of acidosis on the action potential and excitation-contraction coupling

Acidosis inhibits excitation-contraction coupling by a number of mechanisms (177-180), namely inhibition of $I_{Ca,L}$, inhibition of the ryanodine receptor, inhibition of the sarcoplasmic reticulum calcium ATPase, reduction in amplitude of I_{to} and increase of the I_{Kss} and inwardly rectifying Cl^- currents. Because of regional differences in the expression of ion channels underlying membrane currents, the effect of acidosis on the action potential will not be the same in all regions of the heart. In isolated rat atrial cells, reducing the pH of the bathing solution from 7.4 to 6.5 resulted in shortening of the action potential, increased the inward current at –80mV and depolarised the resting membrane potential (179). They concluded that an acidosis-induced increase in the steady state outward K^+ current underlies the shortening of the action potential and an increase in the inwardly rectifying Cl^- current underlies the depolarisation of the resting membrane potential. In rat ventricular myocytes, isolated from both epi- and endocardium, acidosis resulted in prolongation of the APD50 and depolarisation of the resting membrane potential. Before acidosis, there was heterogeneity of the APD between epi- and endocardial cells, with APD shorter in epicardial myocytes.The response to acidosis was also heterogeneous. Furthermore, the degree of prolongation of the APD in acidosis was

greater in endocardial cells than in epicardial cells (Figure 6-2) (178). This heterogeneity of the effect of acidosis on the action potential in different regions of the heart, including the dispersion of effect across the transmural surface of the ventricle, may further contribute to the substrate for conduction abnormalities and arrhythmias.

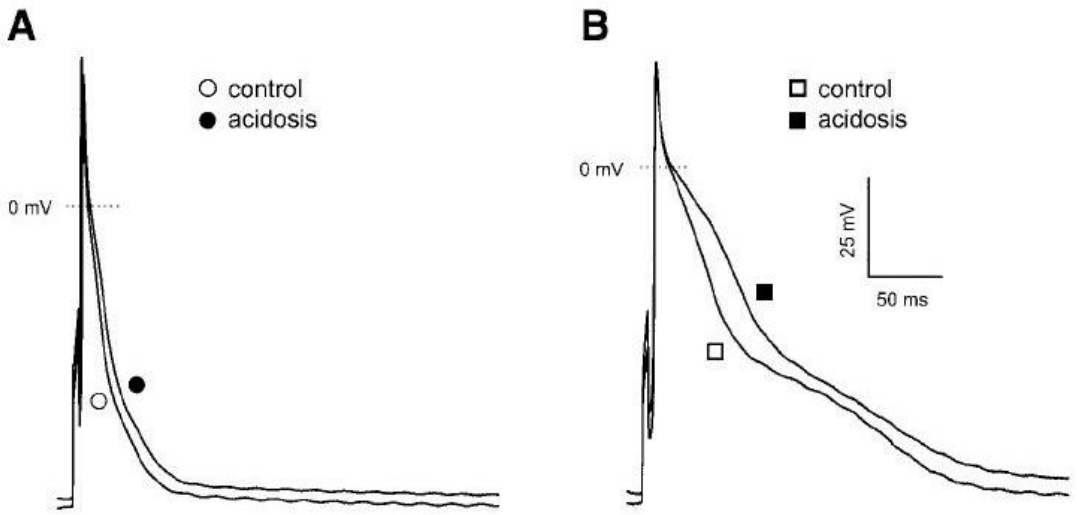

Figure 6-2 – Action potential of epicardial (A) and endocardial (B) rat ventricular myocytes at control pH and during acidosis. (Adapted from (178)).

6.1.5 Effect of acidosis on the ECG

To further study the heterogeneity of the effect of acidosis on cardiac cells, Aberra *et al* (181) investigated the effect of acidosis on the ECG of the isolated rat heart. Perfusion with acidotic solution (pH 6.5) markedly slowed the heart rate and prolonged the PR interval of the ECG of the isolated rat heart (Figure 6-3). The effect of acidosis was rapid and reversible. There was no apparent effect on the duration of the QRS complex. The absence of any effect of acidosis on the duration of the QRS complex suggests that the prolongation of the PR interval was a consequence of conduction slowing through the AV node.

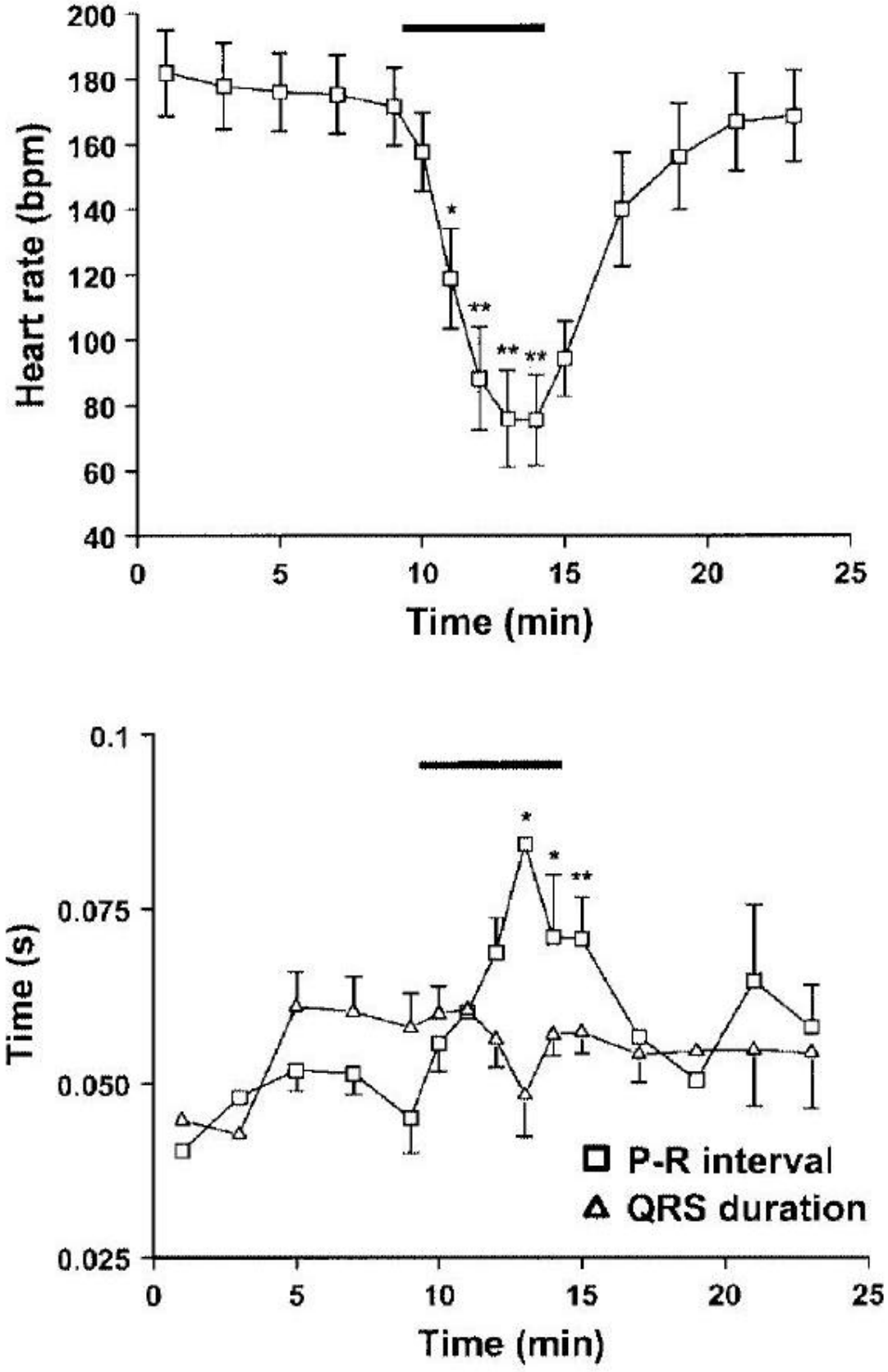

Figure 6-3 – Effect of acidosis on heart rate (top panel) and on PR interval and QRS duration (bottom panel). The horizontal bar denotes perfusion with solution at pH 6.5. (Adapted from (181)).

To date, no literature has been published on the response of isolated AV nodal tissue or AV nodal cells to acidosis. The present study was designed to investigate the effect of acidosis on the electrophysiology of the SA and AV nodes, determined by surface electrogram recordings from an isolated AV node tissue preparation.

6.2 Methods

Under terminal anaesthesia with sodium pentobarbitone 200mg/kg (Rhone Merieux) mixed with 500IU of heparin, hearts from adult male New Zealand White rabbits were rapidly excised and placed in ice cold Tyrode's solution, of the following composition (mmol/L): Na^+ 134.5, Mg^{2+} 1.0, K^+ 5.0, Ca^{2+} 1.9, Cl^- 101.8, SO_4 1.0, H_2PO_4 0.7, Hepes 20, acetate 20 and glucose 50. The pH of aliquots of the solution was adjusted to 7.4, 6.8 and 6.3 by the addition of NaOH and HCl. Final solutions were oxygenated with 100% O_2. The isolated AV node preparation was created as outlined in Chapter 2. This tissue was pinned onto a Sylgard plate and superfused with oxygenated Tyrode's solution at pH 7.4. A constant superfusion rate of 40ml/min was maintained using a Gilson Minipuls 3 peristaltic pump. Temperature was maintained at 37ºC. Baseline data was obtained at pH 7.4. The preparation was then superfused with solution at pH 6.8 and data recorded after 10 minutes. Following this, the preparation was superfused with solution at pH 6.3 and again data recorded after 10 minutes. To determine reversibility of the effects of acidosis, the solution was returned to pH 7.4 and data recorded after 10 minutes.

6.2.1 Surface electrogram recording

Electrograms recorded from the surface of the isolated atrioventricular node preparation were recorded using locally developed ECG acquisition software (NMap, Dr FL Burton, University of Glasgow). The spontaneous sinus cycle length was recorded in every experiment. The basic stimulus cycle length was 300ms. Atrio-Hisian (AH) intervals, Wenckebach cycle length, functional and effective refractory periods of the AV node and the atrial effective refractory periods were derived using standard pacing protocols as described earlier.

6.2.2 Optical mapping of activation

The pattern of activation through the right atrial/AV node preparation during normal pH and acid pH was studied in a further series of 3 controls using the optical mapping methodology described earlier (see chapter 2, General Methods). Hearts

excised under terminal anaesthesia were loaded with RH237 via the coronary circulation via Langendorff perfusion. Thereafter the isolated right atrial preparation was prepared as previously described and mounted in a custom made chamber to allow superfusion with Tyrode's solution of the above composition at pH 7.4. The preparation was paced using protocols previously described to derive AH intervals and WCL at pH 7.4, 6.8 and 6.3. Surface electrograms and optically derived action potentials were recorded simultaneously.

6.2.3 Statistical analysis

At pH 7.4, n=11. In some cases, acidosis resulted in conduction block at the level of the AV node, precluding derivation of the AH interval, FRP or ERP. More details are given in the results section. Results are expressed as mean ± standard error of the mean unless otherwise stated. Comparisons between two groups of data were made using a paired Student's *t*-test. A two-tailed p-value of less than 0.05 was considered statistically significant.

6.3 Results

6.3.1 Effect of acidosis on spontaneous sinus cycle length

Figure 6-4 shows the effect of reducing the pH of the superfusate on the spontaneous sinus cycle length of the isolated atrioventricular node preparation. There is significant prolongation of the spontaneous sinus cycle length at pH 6.8 compared to normal pH conditions (pH 7.4: 420.5 ± 24.5; pH 6.8: 572.7 ± 56.8, $p<0.05$). There was further significant prolongation of the spontaneous sinus cycle length at pH 6.3 (pH 6.8: 572.7 ± 56.8; pH 6.3: 720.2 ± 59.6, $p<0.05$). The effects of lowering pH on the spontaneous sinus cycle length were reversible at 10 minutes (pH 7.4 return: 493.7 ± 29.9).

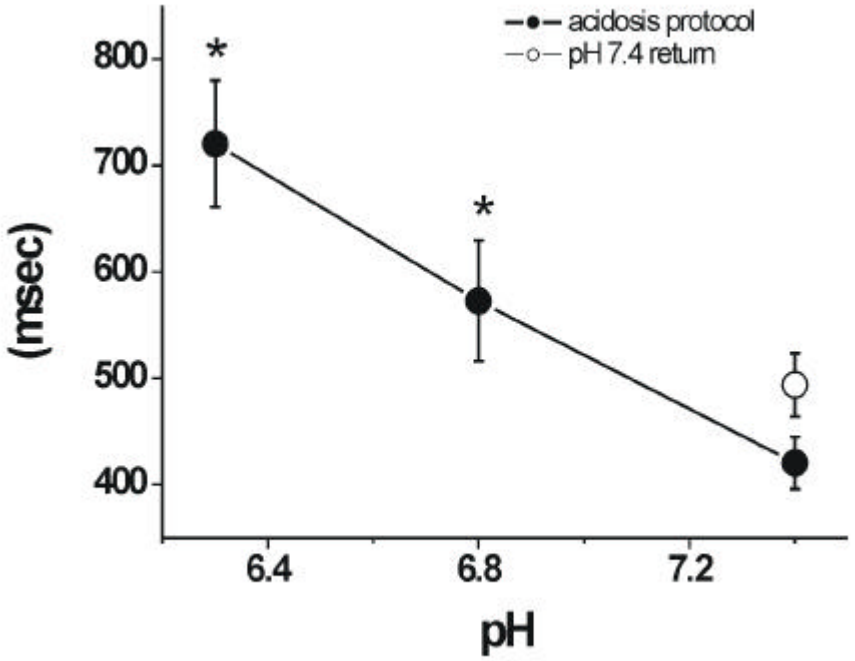

Figure 6-4 - Effect of pH on spontaneous sinus cycle length. Significant, reversible prolongation of the spontaneous sinus cycle length occurred in the presence of an acidic pH. *p<0.05. N=11 at all 3 pHs.

6.3.2 Effect of acidosis on AV node conduction characteristics

There was significant, reversible prolongation of the WCL with reduction in pH (Figure 6-5). Furthermore, the AH intervals progressively prolonged with reduction in pH (Figures 6-6 and 6-7). Table 6-1 summarises the effects of acidosis on WCL and

AH intervals at PCL 300ms and 200ms. In 4 of 11 samples, complete heart block occurred at PCL 300ms in pH 6.3. In 9 of 11 samples complete heart block occurred at a PCL 200ms in pH 6.3, therefore these values were excluded from the analysis. However, figure 6-7 documents progressive prolongation of the AH interval at PCL 200ms in pH 6.3 of the two samples which did conduct through the AV node at this pH.

	pH 7.4	pH 6.8	pH 6.3	pH 7.4 return
WCL	198.2 ± 21.5	268.3 ± 29.4	296.0 ± 46.8	262.0 ± 32.8
AH300	45.8 ± 3.1	54.2 ± 3.5	68.5 ± 7.4	68.5 ± 7.4
AH200	76.0 ± 26.2	90.9 ± 24.6	-	85.3 ± 24.2

Table 6-1- Effect of pH on AV node conduction characteristics. WCL - Wenckebach cycle length; AH300 - AH interval at PCL 300ms; AH200 - AH interval at PCL 200ms. N=11 except at pH 6.3 (PCL 300ms) where N=7 and at pH 6.3 (PCL 200ms) where N=2.

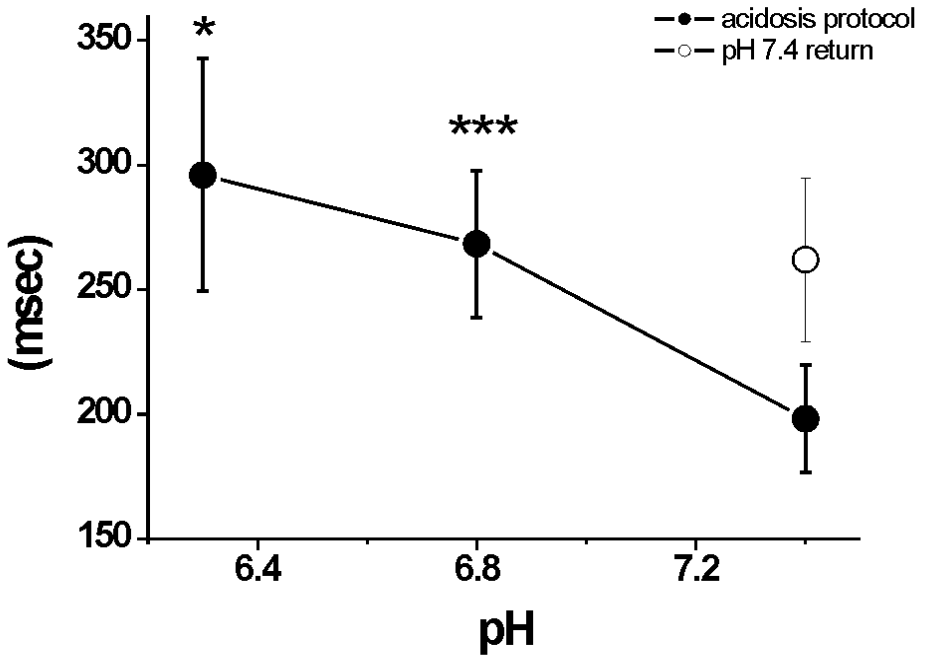

Figure 6-5- Effect of pH on Wenckebach cycle length. Significant, reversible prolongation of the WCL occurred in the presence of an acidic pH. *p<0.05; ***p<0.001.

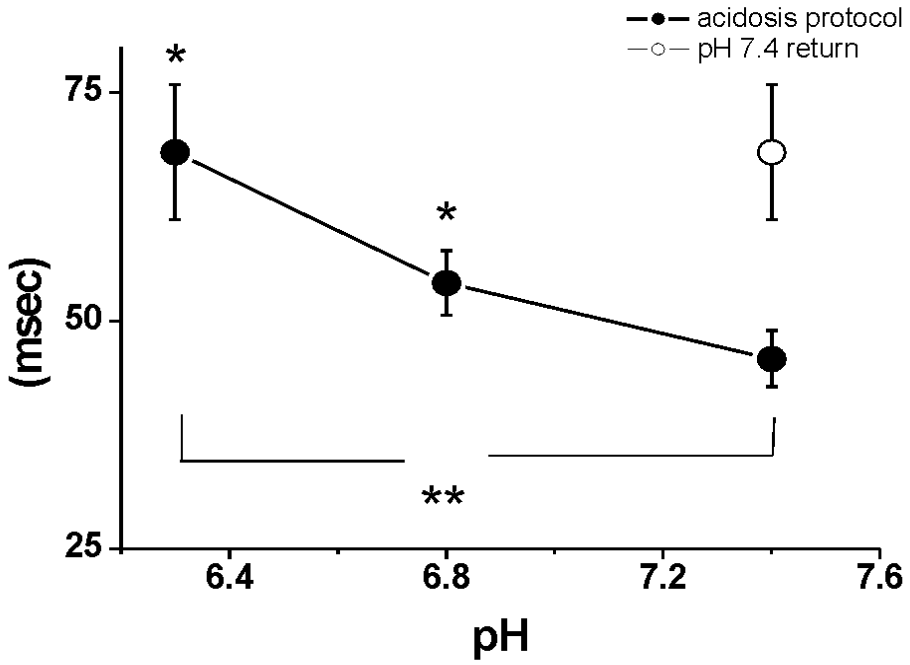

Figure 6-6 - Effect of pH on AH interval at PCL 300ms. *p<0.05; **p<0.01.

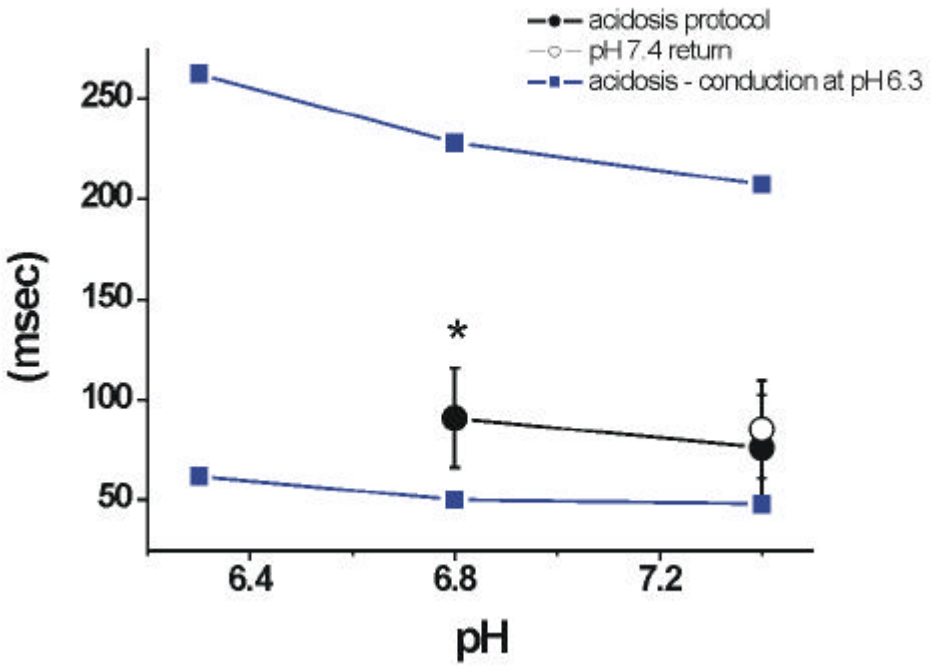

Figure 6-7 - Effect of pH on AH interval at PCL 200ms. In 9 of 11 samples, complete heart block occurred at pH 6.3 therefore were excluded from analysis. In two samples, as shown in blue, conduction through the AV node persisted despite pH 6.3. *p<0.05; *p<0.01.

6.3.3 Effect of acidosis on refractory characteristics of the atrium and AV node

Progressive prolongation of the AV nodal functional and effective refractory periods occurred in the presence of acidosis. Refractory periods were derived at PCL of 300ms. Figure 6-8 shows examples of the AV nodal refractory curves derived from one sample, demonstrating the effect of acidosis, namely upward shift in the curves due to an increase in the ERP and FRP with reduction in pH. This effect was consistent throughout all experiments.The cumulative results are expressed as mean ± SEM. H1H2 values for each A1A2 shown in figure 6-9. At pH 6.3, in all but three samples premature stimulation, decrementing from PCL 300ms to only 295ms, resulted in conduction block immediately such that it was not possible to derive the FRP or ERP. These samples were therefore excluded from the analysis. In samples with persistent conduction allowing FRP and ERP to be derived, the FRP and ERP further prolonged at pH 6.3 compared to pH 6.8, as shown in figures 6-11 and 6-13. Table 6-2 documents the effect of pH on atrial and AV nodal refractory characteristics.

	pH 7.4	**pH 6.8**	**pH 6.3**	**pH 7.4 return**
AVN FRP	205.1±21.7	237.6±18.4	220.7±27.4	246.3±33.4
AVN ERP	176.8±22.0	210.7±16.9	209.3±30.6	220.4±27.7
Atrial ERP	120±22.3	153.3±19.3	187.5±27.7	139.2±14.8

Table 7-2 - Effect of pH on atrial and AV nodal refractory characteristics. AVNFRP - AV nodal functional refractory period; ERP - effective refractory period. N=11 except at pH 6.3 where N=3.

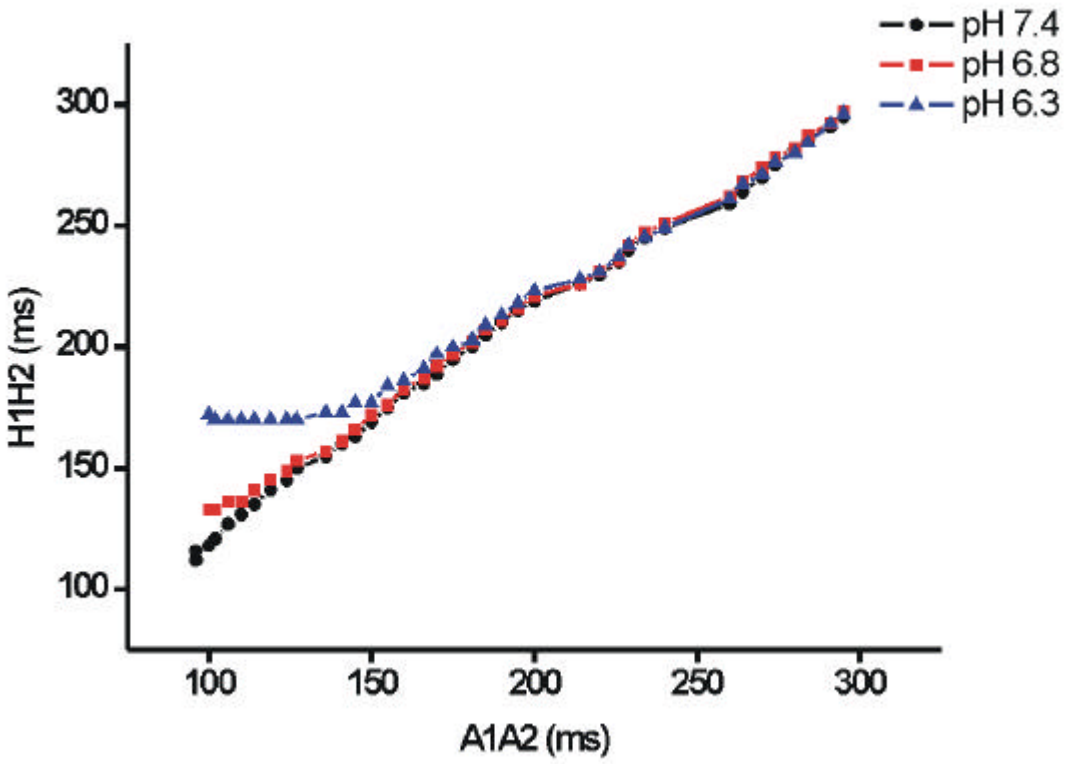

Figure 6-8 - Effect of pH on AV node refractory curve.

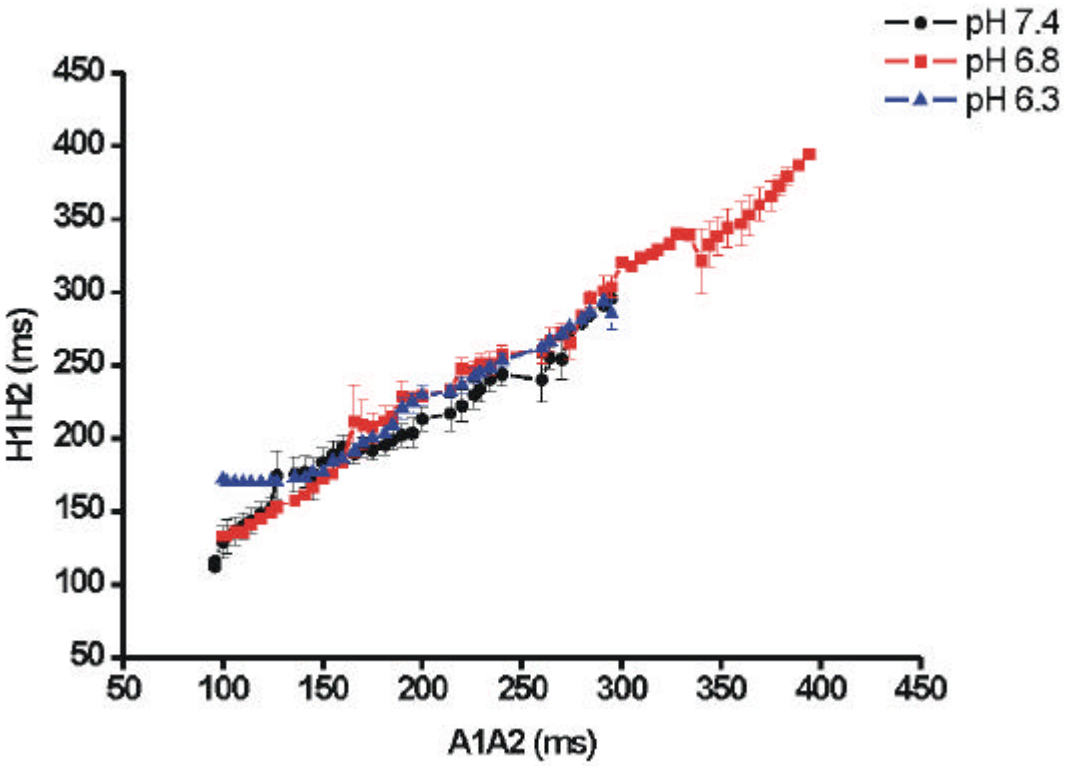

Figure 6-9 - Effect of pH on AV node refractory curves - cumulative (mean) results.

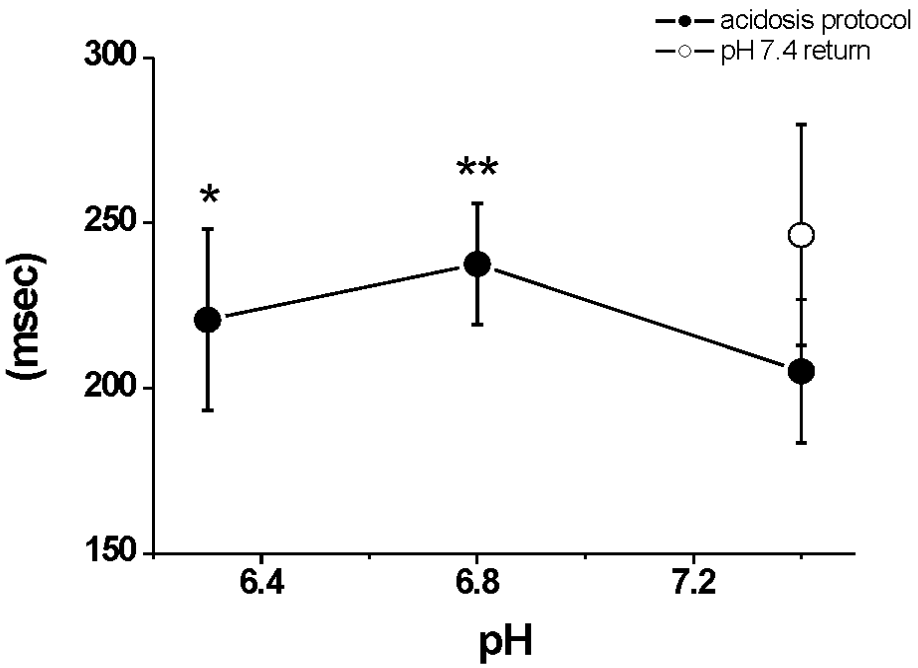

Figure 6-10 - Effect of pH on AVN FRP. FRP determined at a basic PCL of 300ms. This figure shows the overall mean changes in FRP. At pH 7.4 and 6.8, n=11. At pH 6.3, n=3 due to conduction block in the remainder.

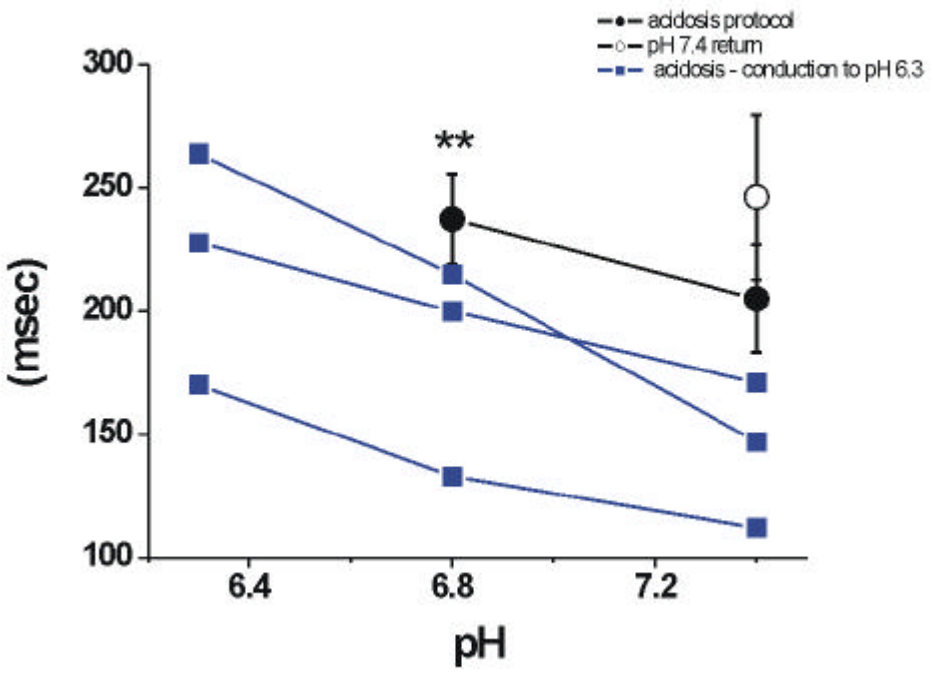

Figure 6-11 - Effect of pH on AVN FRP. In blue, the three samples in which FRP could be determined at pH 6.3. This confirms that the FRP further prolongs at pH 6.3 compared to pH 6.8.

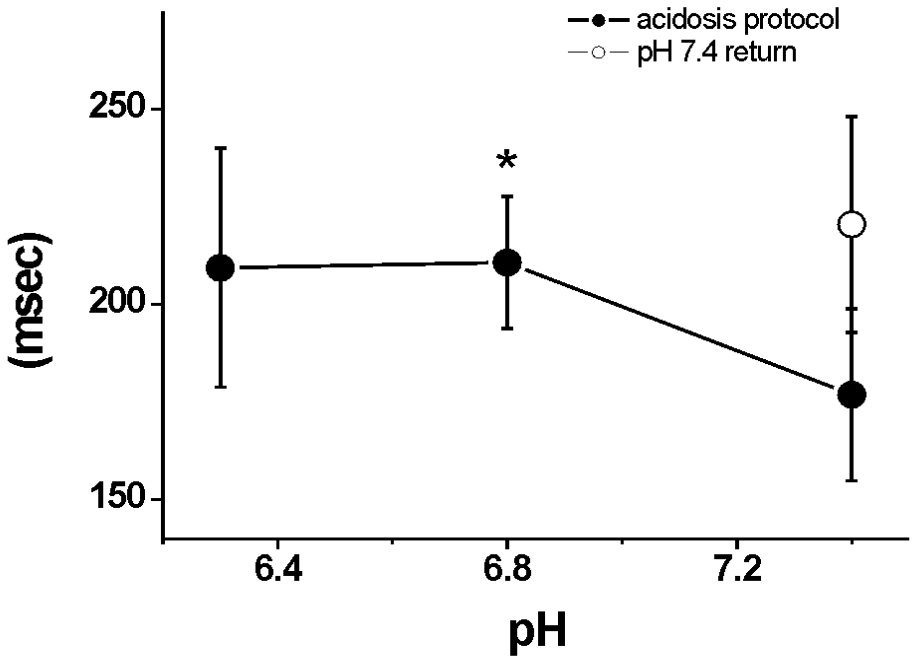

Figure 6-12 - Effect of pH on AVN ERP. ERP determined at basic PCL of 300ms. This figure shows the overall mean changes in AVN ERP. At pH 7.4 and 6.8, n=11. At pH 6.3, n=3 due to conduction block in the remainder.

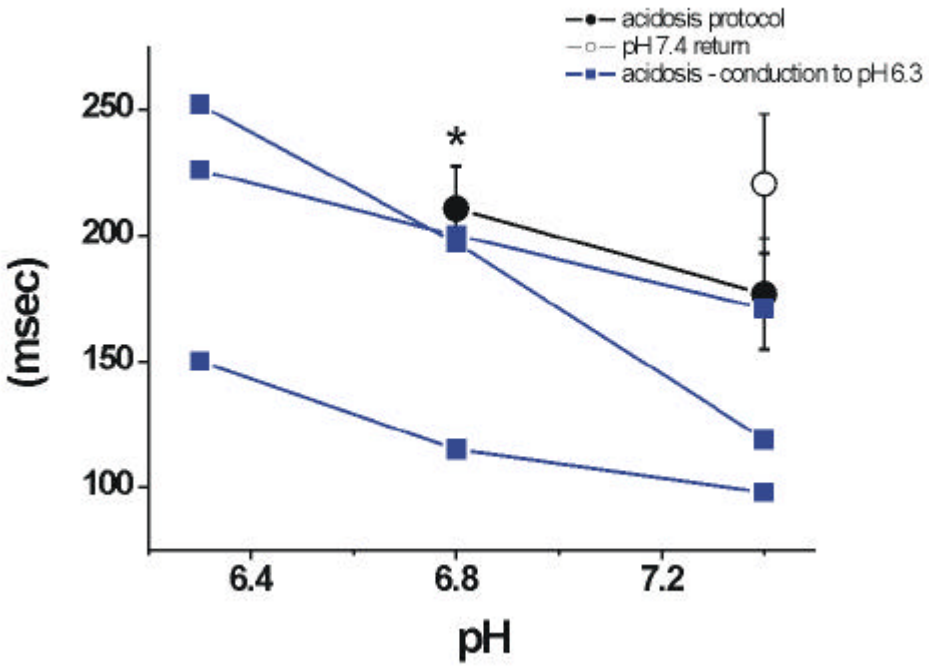

Figure 6-13 - Effect of pH on AVN ERP. In blue, the three samples in ERP could be determined at pH 6.3. This confirms that the ERP further prolongs at pH 6.3 compared to pH 6.8.

6.3.4 Effect of acidosis on optically derived activation times

Typical optically derived action potentials are shown in Figure 6-14. Figures 6-15A and 6-16A illustrate the effect of pH on activation time of the optically derived action potential (T_{act}) during both spontaneous activation and right atrial pacing. On decreasing the pH from 7.4 to 6.3, there is a consistent increase in the activation time most marked at the compact node and His bundle regions (ANOVA $P<0.001$). The effect is less pronounced at the atrial and AVN input regions. The conduction times between regions ($?T_{act}$) are shown in figures 6-15B and 6-16B, where 1 = conduction time between the atrium and the AVN input, 2 = conduction time between the AVN input and the compact node and 3 = conduction time between the compact node and the His bundle. There is considerable slowing of the impulse conduction at region 2 (AVN input to compact AVN) with reducing pH from 7.4 to 6.8 and 6.3. Statistical significance was not reached due to the small sample size (n=3). During right atrial pacing at PCL 250ms, at pH 6.3 there was no conduction of the atrial impulse in 2 of 3 samples, therefore data for pH 6.3 are not shown in Figure 6-16B.

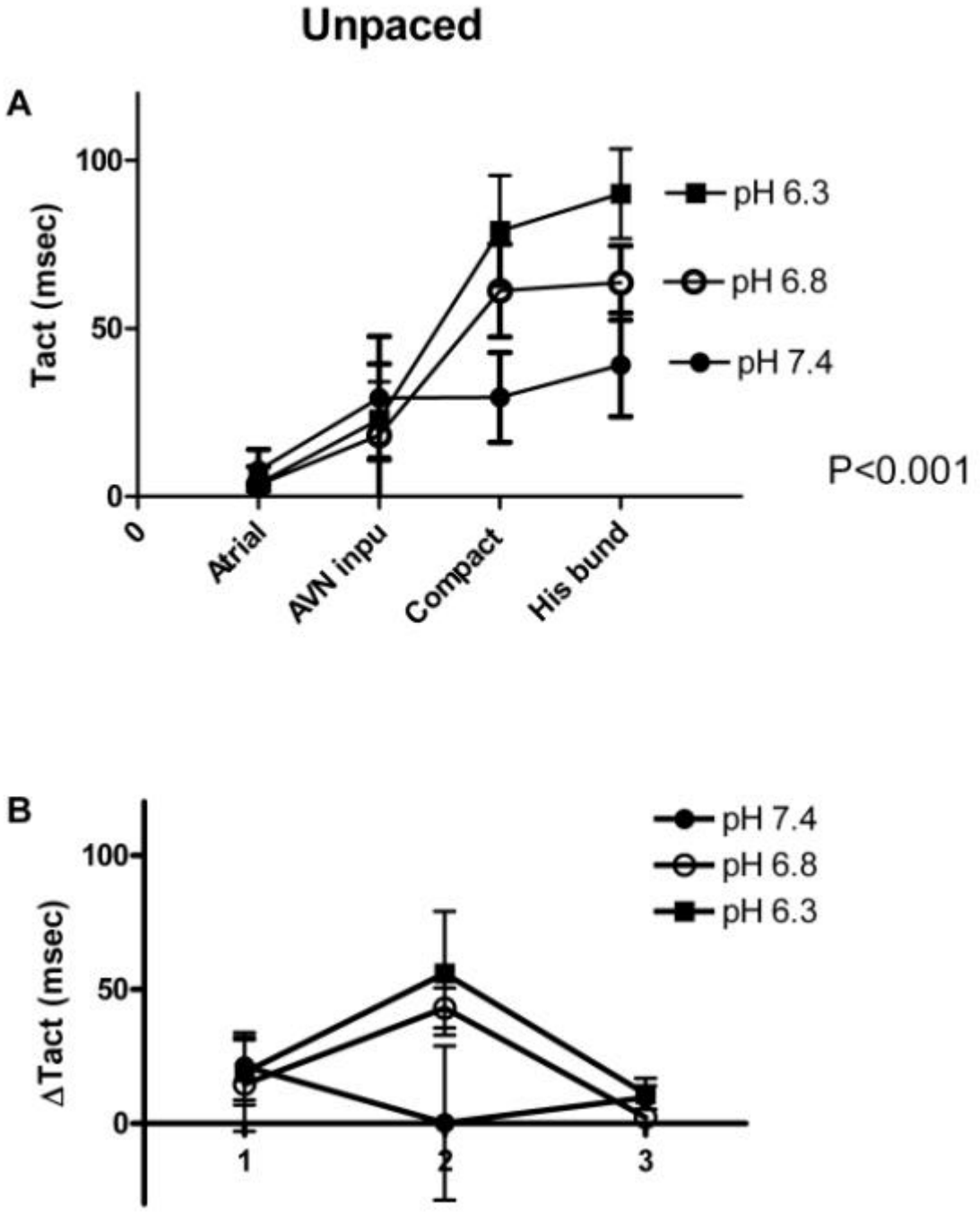

Figure 6-14 – A – Activation time (Tact, mean ± SEM ms) at designated regions at pH 7.4, 6.8 and 6.3. B – Change in activation time (?Tact, mean ± SEM ms) between regions (1=atrial to AVN input; 2=AVN input to compact node; 3=compact node to His bundle). N=3 at each pH. Preparations unpaced.

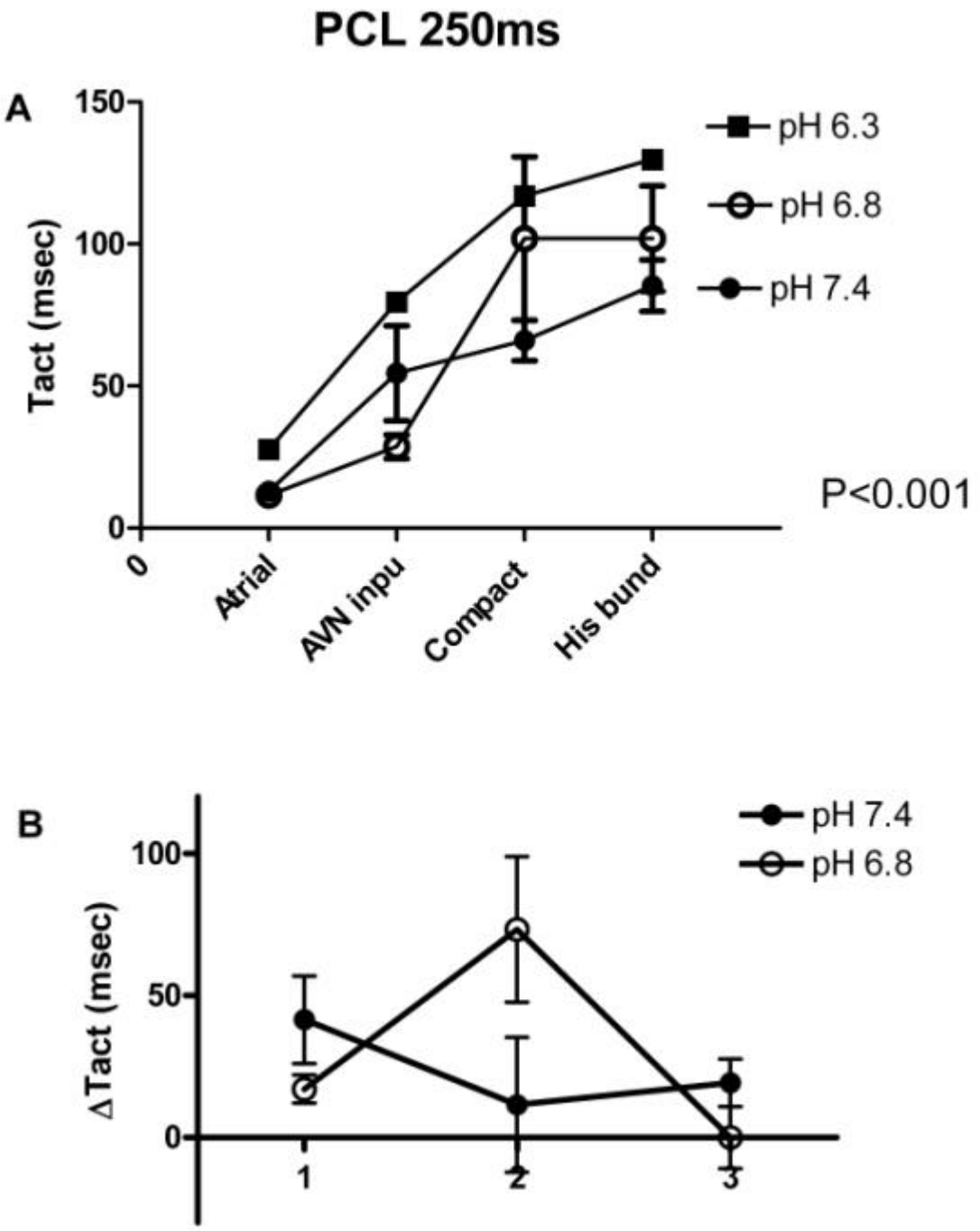

Figure 6-15 - A – Activation time (Tact, mean ± SEM ms) at designated regions at pH 7.4, 6.8 and 6.3. B – Change in activation time (?Tact, mean ± SEM ms) between regions (1=atrial to AVN input; 2=AVN input to compact node; 3=compact node to His bundle). N=3 at pH 7.4 and 6.8 but n=1 at pH 6.3 due to failure of conduction of the atrial impulse in 2 preparations. Preparations paced at cycle length 250ms. .

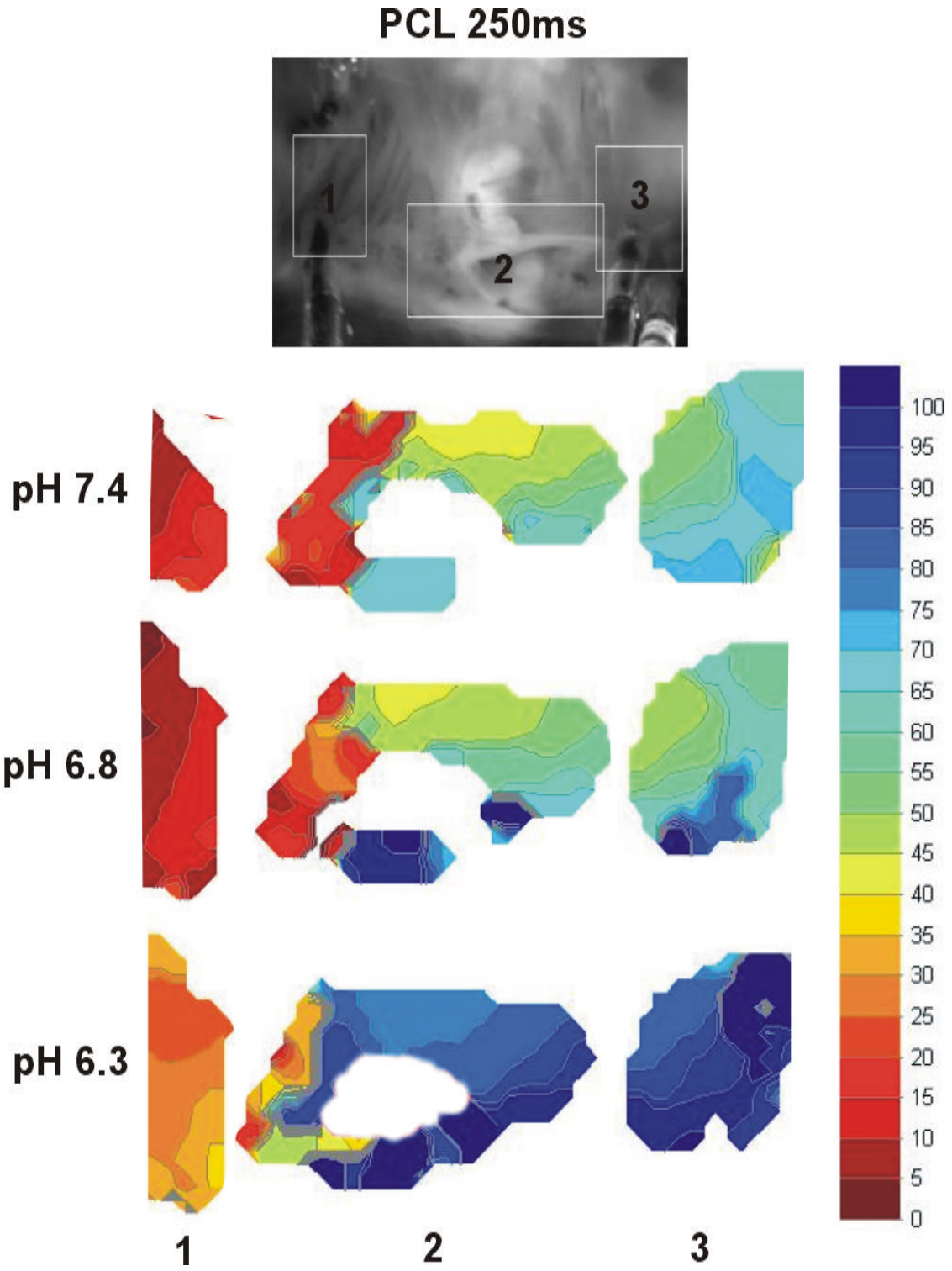

Figure 6-16 – Isochronal maps of activation showing conduction delay with reducing pH. Region 1 = atrial to proximal AVN; 2 = proximal to compact nodal AVN; 3 = compact AVN to His bundle. The key on the right is in milliseconds. Activation times are relative to the onset of the atrial electrogram.

Figure 6-17 shows isochronal maps of activation derived from the optically derived action potentials at pH 7.4, 6.8 and 6.3. Measurements are in milliseconds relative to the onset of the atrial action potential. At every pH there is an area of conduction delay between the proximal and compact AV node (Region 2). The

magnitude of delay is increased with reducing pH. In the above example there is also evidence of conduction delay between the atrial stimulus and the proximal AV node (region 1) at pH 6.3 that is not apparent at pH 6.8 or 7.4. It is also interesting to observe that in region 2, corresponding to the area surrounding the coronary sinus, there is an increase in conduction time along the floor of the coronary sinus compared to the superior aspect of this region. This area is anatomically and functionally considered the "slow pathway" of the AV node and these results confirm dual pathway AV nodal conduction in this sample. Furthermore, the magnitude of conduction delay occurring at pH 6.8 in region 2 is much greater at the area corresponding to the slow pathway than superiorly.

6.4 Discussion

The present study confirms that in an isolated AV node preparation, acidosis has significant effects on the electrical activity of the sinoatrial node and on the conduction and refractory characteristics of the AV node. The results and possible mechanisms are discussed in detail below.

6.4.1 Physiological significance of experimental conditions

Assuming an extracellular pH (pH_o) of 7.4, the intracellular pH (pH_i) of most cell types is maintained between 6.8 and 7.2. Myocardial ischaemia is characterised by hypoxia, hyperkalaemia and profound acidosis in the extracellular space. Consequently, pH_i is also markedly reduced in ischaemia, with reductions of 0.5 pH units being observed in some studies (170). The presence of modest acidosis (pH 6.8) has previously been associated with changes in the electrophysiological characteristics of sinoatrial nodal cells (182). Furthermore, reducing the pH of the perfusate to pH 6.5 has also been shown to both slow the heart rate and prolong the PR interval in isolated rat hearts (181). In myocardial ischaemia, values of pH_i as low as 6.2 have been recorded (183). In studies measuring the pH_i using the fluorescent dye 2',7'-bis(2-carboxyethyl)-5(6)-carboxyfluorescein, the pH_i decreases by approximately 0.5 pH units in response to a reduction in the pH_o from 7.4 to 6.5 (184). The pH_i reaches steady state within 3 minutes (170). The present study investigates the effect of both modest and severe acidosis using superfusate at pH 6.8 and 6.3. These values are within the range observed pathophysiologically. Data were acquired at 10 minutes after each exchange of solution, allowing adequate time for washout of the previous solution and time for the effects of the acid solution to reach steady state.

6.4.2 Effect of acidosis on sinus node automaticity

Reducing the pH of the superfusate from pH 7.4 to 6.8 caused a significant reduction in the spontaneous sinus rate, an effect which was enhanced by reducing the pH further to 6.3. This result is in keeping with observations made by other groups. Acidosis has previously been reported to alter the rate of contraction of isolated atria, whether induced by HCl (mimicking metabolic acidosis) or CO_2 (mimicking respiratory acidosis) (185). Furthermore, Aberra *et al* observed

significant reduction in heart rate in isolated Langendorff perfused rat hearts in the presence of acidic pH (181).

The mechanism whereby acidosis inhibits the sinus node is unclear. Aberra *et al* hypothesised that the inhibition of the sinus node in acidosis was mediated by an increase in I_{to}, in keeping with observations that in ventricular myocytes I_{to} becomes larger in acidosis and when the diastolic membrane potential is depolarised (186). However, in the isolated rat heart, blocking I_{to} by adding 4-Aminopyridine (4-AP) had no effect on the changes in heart rate observed in the presence of acidosis (181), making I_{to} mediated inhibition of the sinus node unlikely.

Inhibition of heart rate in the presence of acidosis may be a consequence of alteration in the pacemaker currents in the sinus node. The SA node contains specialised cells that generate action potentials that are different to ventricular myocyte action potentials (187). Sinoatrial nodal cells do not have a true resting membrane potential. Action potentials are characterised by the presence of a "pacemaker potential", which is a slow diastolic depolarisation phase (Phase 4) of the action potential. This renders these cells spontaneously active. Heart rate is determined by the rate of action potential firing, which is determined by the slope of the phase 4 depolarisation (188). The generation and control of the diastolic depolarisation in SAN cells is predominantly due to the pacemaker "funny" current, I_f, first described in detail in 1979 (189). Typical features of this current include hyperpolarisation-induced activation, slow kinetics of activation and deactivation, mixed Na^+ and K^+ ionic permeability, and modulation by cAMP (190). Inhibition of I_f occurs in the presence of acetylcholine, suggesting that autonomic modulation of heart rate is I_f mediated. However, Aberra *et al* excluded the possibility that reduction in sinus rate in acidosis was due to acidosis-induced changes in neurotransmitter release from severed autonomic nerve terminals within the heart, because the changes persisted in the presence of antagonists atropine and propranolol (181). Extrapolating this observation to the present study, slowing of the sinus rate in the presence of acidosis is not due to muscarinic modulation of I_f, but may be due to direct inhibition of I_f. Further study into the effect of acidosis on the pacemaker potential of isolated SAN cells is required to clarify the mechanism.

6.4.3 Effect of acidosis on parameters of AV nodal function

6.4.3.1 Effect of acidosis on conduction time (AH interval and WCL)

In the present study, we observed significant prolongation of the AV conduction time with reduction of the pH of the superfusate. This was manifest by significant prolongation of the AH intervals at baseline and at all pacing cycle lengths. The AH intervals shifted to the right in the presence of acidosis. The pacing rate at which AV nodal block was observed (Wenckebach phenomenon) was significantly slower at pH 6.8 than at 7.4, and yet slower at pH 6.3. In the presence of severe acidosis, profound AV nodal block was observed, most marked at faster pacing rates. In 4 of 11 samples, complete AV block occurred at PCL 300ms at pH 6.3. In 9 of 11 samples complete AV block occurred at a PCL 200ms at pH 6.3. The effect of acidosis on AH interval and Wenckebach cycle length appear to be partially reversible at 10 minutes of washout with superfusate at pH 7.4. Further confirmation was gained from the optical mapping experiments, in which slowing of conduction between the AVN inputs and the compact node appeared to be the major contributor to the acidosis induced prolongation of the AH interval. Furthermore, conduction block as proximal as the inputs of the AV node at pH 6.3 during right atrial pacing limited the analysis of 2 of 3 samples studied.

Aberra *et al* observed prolongation of the PR interval with no change in the QRS duration in the ECG of the rat heart in the presence of acidosis (181). They postulated that the absence of effect of acidosis on the QRS duration suggested that the prolonged AV delay was due to conduction delay at the level of the AV node with no effect on intra-ventricular conduction. The results of the present study are in keeping with this hypothesis. However, in the isolated AV node preparation the ventricular tissue is removed therefore it is not possible to extrapolate the results to comment on the effect of acidosis on intra-ventricular conduction.

The mechanism whereby acidosis prolongs conduction through AV nodal tissue was not explored in the present study. Heterogeneity of ion channel and gap junction expression exists within the AV nodal architecture (46;47). Transitional cells of the AV node (AN and NH cells) have relatively abundant sodium current (I_{Na}). There is a relative lack of expression of sodium channels in the ovoid type compact nodal cells (N cells), in which the main depolarising current is the L-type calcium current ($I_{Ca,L}$). This results in a relatively slow Phase 0 and therefore a slow speed of conduction. Acidosis has been shown to inhibit $I_{Ca,L}$ in rat ventricular myocytes (180). Inhibition

of $I_{Ca,L}$ by acidosis in AV nodal cells would slow the speed of the upstroke of the action potential and subsequently slow conduction. The main repolarising currents of the AV node are the transient outward K^+ current (I_{to}) and the delayed rectifier K^+ current (I_{Kr}). Aberra *et al* explored the possibility of inhibition of I_{to}, by the addition of 4-AP to the perfusion fluid (181). Similar to their observations on the effects on heart rate, 4-AP did not alter the effects of acidosis on PR interval. It is therefore unlikely that I_{to} is implicated in the observed AV nodal delay in acidosis.

Acidosis increases gap junctional resistance, which slows the transmission of action potentials from cell to cell (175). This is likely to be a significant contributor to the observed conduction delay in the AV node in the presence of acidosis.

6.4.3.2 Effect of acidosis on atrial and AV nodal refractory characteristics

In addition to the observed prolongation of AV nodal conduction, acidosis alters the refractory characteristics of the atrium and AV node in this preparation. There was significant prolongation of both the effective and functional refractory period of the AV node at pH 6.8 compared to pH 7.4. This resulted in upward shift of the refractory curves at pH 6.8, and further upward shift at pH 6.3. However, due to conduction block, it was only possible to generate refractory curves in 3 samples at pH 6.3. However, despite this, the overall effect of further prolongation of the ERP and FRP in the presence of severe acidosis (as compared to moderate acidosis) is confirmed as shown in Figures 6-11 and 6-13. It is interesting to note that in contrast to measures of conduction delay, the effect of acidosis on AV nodal refractoriness do not appear to reverse at 10 minutes of washout with superfusate at pH 7.4.

Atrial effective refractory period is also significantly prolonged by acidosis. The magnitude of the effect is inversely proportional to the pH of the superfusate. The effect appears to be reversible.

AV nodal refractory periods represent a composite of the effective refractory periods of a number of different cell types within the heterogeneous structure that is the AV node. There is evidence that different cell types (from different regions) within AV nodal tissue contribute to a varying extent to nodal refractoriness (49). This may yield some clues to the mechanisms by which acidosis exerts its effects on AV nodal function. The functional refractory period of the AV node is by definition the minimum H1H2 that can be propagated to the ventricle from the atria, and as

such is an important determinant of the ventricular response to fast atrial rates. When heart rate increases, a change in the conduction time of the regular beats causes a decrease in the functional refractory period (56). Thus it can be deduced that the increase in the functional refractory period of the AV node in response to acidosis is a function of the increase in conduction time through the AV node at the predefined pacing cycle lengths. The effective refractory period of the AV node may also to some extent be influenced by conduction time, but is more importantly influenced by the longest ERP of the components of the conduction pathway (58). Workman *et al* postulated that mid-nodal cells may have the greatest influence on the ERP of the intact AV node based on observations that the mid-nodal cells had a longer ERP compared to cells from the proximal, transitional nodal region (59). Furthermore, Workman *et al* showed that I_{to} does not contribute to ERP in isolated AV nodal cells (58). This is in keeping with the hypothesis that the observed changes in AV nodal conduction time are not due to changes in I_{to} in response to acidosis. It follows therefore that prolonged ERP (and FRP) is not due to inhibition of I_{to} in acidosis. The kinetics of $I_{Ca,L}$ may account for both conduction slowing and prolonged ERP of the AV node in this preparation.

6.4.4 Conclusion

This study has shown that significant prolongation of AV nodal conduction time occurs in the presence of acidosis, as evidenced by prolongation of the AH interval and Wenckebach cycle length, proportional to the severity of acidosis. This confirms that the origin of prolongation of the PR interval of the ECG in the presence of acidosis is due to intrinsic conduction delay at the level of the AV node. The optical mapping data have indicated that conduction delay between the AV nodal inputs and the compact AV node regions is the major contributor to prolongation of the AH interval, which translates as prolongation of the PR interval of the surface ECG. This study has also demonstrated prolongation of AV nodal functional and effective refractory periods in the presence of acidosis. The mechanisms underlying these observations are likely to be complex and multiple. It is likely that acidosis induced inhibition of $I_{Ca,L}$ plays a role in both conduction delay and prolongation of the ERP. In addition, the effect of acidosis on the electrotonic interaction between AV nodal cells is a likely contributor. Further investigation is ongoing into the effect of acidosis on the ion currents in isolated AV nodal cells to clarify the mechanisms involved.

Chapter 7 - Synopsis

7 Synopsis

7.1 Summary of aims and key findings

The main aim of this thesis was to confirm the presence of abnormal conduction delay at the level of the AV node in the rabbit model of LVD due to apical myocardial infarction. Further investigations aimed to determine the spatiotemporal pattern of the delay within the AV node and then to determine the underlying mechanism. These investigations were carried out on an isolated tissue preparation comprising right atrial and AV nodal tissue using a combination of surface electrogram recordings and optical mapping of electrical activation using voltage sensitive dye. The key findings of the investigations were:

1. There is abnormal prolongation of AV delay in the rabbit model of LVD due to apical myocardial infarction, confirmed by prolongation of the AH interval and Wenckebach cycle length in LVD preparations compared to control animals.

2. The prolongation of the AH interval is predominantly a consequence of conduction delay between the AV nodal input and the compact nodal regions of the preparation.

3. There was no evidence of ß-adrenoceptor downregulation in the AV node in LVD compared to control to account for the abnormal conduction delay.

4. There was no evidence of an increase in the action of endogenous adenosine in the AV node of LVD animals, but there was an increased sensitivity to exogenous adenosine in these samples, and

5. Acidosis caused similar prolongation of AV nodal delay with a similar spatiotemporal pattern to the effects observed in LVD.

These findings are summarised in detail below.

7.1.1 Abnormal AV nodal conduction delay in the rabbit model of LVD due to apical myocardial infarction

Previous research has suggested that there may be abnormal AV nodal conduction delay in the rabbit model of LVD due to apical myocardial infarction despite absence of any direct ischaemic insult to the base of the heart (81). This thesis has confirmed that the observed AV delay in the whole heart model studied by NL Walker is due to delay originating in AV nodal tissue. At both 8 and 32 weeks post coronary ligation, LVD animals exhibited significant prolongation of AH interval and Wenckebach cycle length compared to controls. The overall AV nodal recovery curve was shifted upwards and to the right in LVD at 8 weeks and further at 32 weeks post infarct. This was in the absence of any significant increase in AV nodal refractory periods at 8 weeks, but a modest increase in AV nodal FRP at 32 weeks. Sinus node automaticity was not affected.

7.1.2 Spatiotemporal pattern of AV nodal delay

Using optical mapping of electrical activation, I was able to confirm that the prolongation of AH interval occurred as a consequence of abnormally delayed conduction between the AV nodal inputs and the His bundle region. There was an almost 4-fold increase in the mean conduction time between the AV nodal inputs and the compact node and a 3-fold increase in mean conduction time between the compact AV node and the His bundle region in LVD compared to controls (Figure 3-13). A characteristic of the LVD model used is an increase in the left atrial diameter (Table 2-1). I ensured that the distance between the electrodes recording the surface electrograms from the isolated AV node preparation was consistent during optical mapping experiments to exclude left atrial enlargement as a contributor to the observed increase in AH interval. Furthermore, on optical imaging there was no evidence of delayed conduction through atrial myocardium, strengthening the conclusion that the delay is due to remodelling of AV nodal conduction.

7.1.3 Mechanism of prolonged AV nodal delay in LVD

Four theoretical mechanisms were identified and investigated as potential causes of the abnormal AV nodal conduction delay observed in LVD. These are outlined below:

7.1.3.1 Age-related degenerative changes in AV nodal conduction

Age-related AV nodal conduction disturbances are recognised to occur frequently in human (111-113) and animal studies (115;132). Although not statistically significant, there appeared to be progressive prolongation of AH intervals and further increase in Wenckebach cycle length at 32 weeks compared to 8 weeks post infarct. To investigate the possibility that there is an age related phenomenon rather than progression of the effect of the LVD condition a series of sham operated animals were studied at 32 weeks post sham ligation procedure to age match for the 32 week LVD samples. There was evidence of modest but not statistically significant prolongation of the AH intervals and significant prolongation of WCL in the 32 week sham operated animals compared to younger controls (aged 12-20 weeks). AV nodal refractory periods were not affected by age in this study. When the 32 week sham operated animals were compared to the 32 week infarct, the magnitude of the increase in AH interval was much less marked in the sham compared to the infarct group. Overall, one may conclude that age may indeed contribute to the progressive prolongation of AV nodal delay in the LVD model but age cannot be considered to be a major factor resulting in this phenomenon.

7.1.3.2 Beta-adrenergic sensitivity of the AV node in the rabbit model of LVD

The negative inotropic effect of chronic catecholamine excess and subsequent ß-adrenoceptor downregulation in the left ventricle has been demonstrated in both human (74-76) and animal studies (77-79). This pathophysiological phenomenon is the target of prognostically beneficial ß-blocker therapy in chronic heart failure in humans (191-194). I postulated that global ß-adrenoceptor downregulation may occur in the failing heart resulting in a negative dromotropic effect through the AV node in LVD. This did not appear to be the case, with no difference observed in the EC_{50} for isoproterenol between control and LVD samples (Table 4-1). In contrast to expected findings, there was an increase in the maximal reduction of the AH interval and WCL in LVD compared to controls, suggesting enhanced effect of isoproterenol in LVD in the AV node of LVD samples compared to controls. This "up-regulation" of AV nodal ß-adrenoceptors may have a protective role to play, helping to prevent high degree AV block in vivo, which is known to be associated with a poorer prognosis in chronic heart failure.

7.1.3.3 Endogenous and exogenous adenosine and AV nodal delay in LVD

In the absence of evidence of chronic ß-adrenoceptor downregulation as a mechanism underlying the abnormal prolongation of AV nodal delay, I looked to another neuro-humoral factor known to have profound effects on AV nodal conduction: adenosine. I postulated that tonic depression of AV nodal conduction may occur in LVD, which appeared to be overcome by ß-adrenergic stimulation, for example as a result of excess endogenous adenosine production. In a series of experiments examining the differential effects of exogenously applied adenosine A_1 receptor antagonist (CPX) there was no evidence of an excess of endogenous adenosine in the isolated AV node preparations from LVD samples compared to controls (Figures 5-1 – 5-3).

In contrast, there was a marked increase in the sensitivity of the LVD samples to exogenous adenosine compared to controls, with a significant increase in the AH interval and WCL with increasing adenosine concentrations (Figure 5-4). The effects of exogenous adenosine were reversible with CPX in both controls and LVD. This increased sensitivity to adenosine in LVD may potentially be protective to the impaired ventricle from the increased oxygen demand that ensues from rapid atrial rates, as may be caused by atrial fibrillation, which occurs in up to 50% of individuals with chronic heart failure (195;196). However, it may also be detrimental to the already failing heart as adenosine released in response to a hypoxic insult may have a direct effect on conduction at the level of the AV node, resulting in degrees of AV block that further impair cardiac function.

7.1.3.4 Slowed AV nodal conduction as a consequence of changes in gap junction expression/conductance

In this thesis, functional studies of AV nodal conduction in LVD have shown significant conduction delay originating within the AV node, extending to the His bundle region, with little effect on AV nodal refractory periods. This indicates a disturbance of the electrotonic interaction of cells comprising the AV junction as a mechanism underlying the delay. There is considerable diversity in connexin expression patterns within the architecture of the AV junction, which is thought to be relevant to its complex conduction characteristics (197;198). Studies of connexin 40 deficient mice have shown evidence of abnormal AV nodal conduction (199;200). As part of this investigation AV node preparation samples were sent to colleagues in the University of Oxford with expertise in the histological analysis and

immunohistochemistry of the AV junction. The preliminary results are summarised in Appendix 1. Control data was acquired from 2 samples, 8 week infarct data from 1 sample and 32 week infarct data from 2 samples. The key findings from this preliminary analysis are:

(i). Within the AV node, there is a statistically significant increase in the area of Cx 40 expressed by myocytes and fibroblasts at 8 weeks post infarct compared to control (Table 2). This effect is not seen at 32 weeks in the samples analysed thus far.

(ii). At the fibroblast rich interface between the AV node and the ventricle (understood to be anatomically consistent with the His bundle region) there is a reduction in Cx 43 and an increase in the density of Cx 40 expression by fibroblasts at 8 and 32 weeks post infarct (Table 3).

This relative abundance of Cx40 within the AV node and the His bundle region in the LVD samples may account for the reduction in conduction velocity observed.

Overall the distribution of gap junctions within the AV node is unchanged in the LVD samples compared to control. Further work is ongoing with additional samples. It remains unclear if these changes in connexin expression, although statistically significant, are of a magnitude sufficient to see functional changes in AV nodal conduction. It does appear, however, that AV nodal conduction delay in LVD may be caused at least in part by disturbance in the electrotonic interactions between cells at the AV junction.

7.1.4 Acidosis slows sinus node automaticity and AV nodal conduction

Myocardial hypoperfusion can result in global myocardial acidosis. Regional hypoperfusion, for example as a result of coronary arterial occlusion, reduces extra-cellular and intra-cellular pH and has a negatively inotropic and potentially arrhythmogenic effect on the myocardium (170;171). Previous investigators have demonstrated evidence of reduced sinus node firing rate and prolonged AV conduction in whole hearts subjected to acidosis (181). I investigated the effects of acidosis on atrial-AV nodal conduction. I demonstrated significant prolongation of the spontaneous sinus cycle length, AH interval, WCL and AV nodal FRP and ERP proportional to the degree of acidosis in the isolated rabbit AV node preparation

(Figures 6-4 – 6-13). These effects were reversible. Optical mapping studies showed that the spatiotemporal pattern of AV delay during acidosis was similar to that observed in LVD samples, with the predominant delay in conduction occurring between the AV nodal input and the compact AV node (Figures 6-15 – 6-16).

The acute, reversible changes in AV nodal conduction characteristics during acidosis point to changes in ion channel function/kinetics rather than changes in gap junctional expression at the AV junction, although gap junctional conductance is likely to be reduced. I hypothesised that acidosis alters the kinetics of $I_{Ca,L}$, I_{Na} and $I_{K,r}$, as well as reduced cell-cell coupling, resulting in conduction slowing and prolongation of refractory periods of the AV node in this preparation. Appendix 2 shows the results of preliminary mathematical modelling studies carried out Drs Boyett and Inada in the University of Manchester. To simulate the effect of acidosis, they reduced the L-type Ca^{2+} current ($I_{Ca,L}$), rapid delayed K^+ current ($I_{K,r}$), Na^+ current (I_{Na}) and cell-to-cell coupling (gj). Assuming that acidosis reduced L-type Ca^{2+} current, rapid delayed outward K^+ current, Na^+ current and cell-to-cell communication (i.e. the coupling conductance, g_j), they investigated these changes in the string model. The simulation results showed a prolongation of the effective refractory period and functional refractory period as well as increase in the AV node conduction time. These results are comparable to experimental results. Further work is ongoing to investigate the effects of acidosis in isolated atrial and AV nodal cells and confirm the results of the current experiments and mathematical modelling studies.

7.2 Clinical relevance and conclusion

Conduction abnormalities are common in chronic heart failure and are associated with an adverse prognosis. The resultant detrimental effect on LV haemodynamics is the target of cardiac resynchronisation therapy, which aims to optimise ventricular preload by shortening AV delay to minimise pre-systolic mitral regurgitation, and resynchronise right and left ventricular activation/relaxation sequence.

This thesis has confirmed that even in the absence of direct ischaemia to the AV junction, conduction abnormalities may occur as a pathophysiological response to a myocardial infarction resulting in left ventricular dysfunction. The mechanisms underlying this response are likely to be complex and multiple, and are not yet clear. In the acute setting, hypoxia resulting in regional and/or global myocardial

acidosis results in conduction delay as a consequence of reduced ion channel conductance as well as slowed conduction through disturbance of cell-cell coupling. This appears to be reversible in the short term, however the longer term effects are not clear. It may be that chronic hypoperfusion, hypoxia and lactic acidosis due to tissue hypoperfusion as a consequence of the infarction result in irreversible global detrimental effects affecting both ventricular systolic function and the conducting system. While adaptive, and potentially protective responses may occur as demonstrated in this thesis (increase in the maximal reduction of the AH interval in response to beta-adrenergic stimulation in LVD, and increased sensitivity of the AV node to adenosine in LVD) these do not effectively reverse the global negative inotropic and negative dromotropic effect of ischaemic myocardial disease. Cardiac resynchronisation therapy effectively improves haemodynamics when the pathological state is established, however the aim remains the prompt restoration of myocardial oxygen supply to minimise the effects of the ischaemic insult. Further work is required to establish the electrophysiological basis for conduction abnormalities in CHF, which may lead to the development of targeted therapeutic strategies to improve symptom control and overall survival for patients.

Appendix 1

Table 1 - Area of myocytes (M) and fibroblasts (F) in AVN, and Ventricle and Atrium surrounding the AVN.

	Ventricle			Atrium			AVN		
	Control n=39	*8 weeks* n=52	*32 weeks* n=74	*Control* n=53	*8 weeks* n=56	*32 weeks* n=46	*Control* n=35	*8 weeks* n=37	*32 weeks* n=75
% M Area	72.62±1.64	75.57±1.08	82.07±0.89**	67.39±1.36	76.08±1.12**	67.77±1.13	39.94±2.00	61.25±1.37**	34.47±1.00*
% F Area	12.76±0.43	14.5±0.62	8.918±0.57**	13.33±0.5	20.54±0.68**	9.40±0.30**	22.65±1.04	25.96±0.92*	15.93±0.54**

Data obtained at control and different post-infarction time points were compared using ANOVA. Data are presented as mean ± S.E.M. $^{*}P < 0.05$ and $^{**}P < 0.001$ *vs.* control (statistically significant differences)

Table 2 - Gap junction density (Cx43 and Cx40) in AVN, and Ventricle and Atrium surrounding the AVN.

M= Area of gap junction expressed by myocytes (M)
F= Area of gap junction expressed by fibroblasts (F)
M/F = ratio of area of gap junction expressed by myocyte/ area of gap junction expressed by fibroblasts
F/M = ratio of area of gap junction expressed by fibroblasts / area of gap junction expressed by myocyte
% GJ on M= % of gap junctions expressed by myocytes
% GJ on F= % of gap junctions expressed by fibroblasts
% GJ on MF= % of gap junctions expressed by both myocytes and fibroblasts
There is no Cx43 in AVN and Cx40 in Ventricle is only present in blood vessels.

	Cx43						**Cx40**					
	Ventricle			**Atrium**			**Atrium**			**AVN**		
	Control n=20	*8 weeks infarct* n=29	*32 weeks infarct* n=51	*Control* n=23	*8 week* n=30	*32 weeks* n=26	*Control* n=30	*8 weeks* n=26	*32 weeks* n=20	*Control* n=35	*8 weeks* n=37	*32 weeks* n=75
M	2.50±0.23	3.00±0.24	2.94±0.16	1.73±0.14†	1.75±0.07††	1.68±0.09††	10.61±0.84‡‡	5.71±0.49**‡‡	5.28±0.36**‡‡	18.92±1.53$^{?\,?}$	25.32±0.78$^{**?\,?}$	7.38±0.54**
F	1.16±0.12	3.89±0.30**	1.36±0.08	0.58±0.07†	1.54±0.18**††	0.72±0.06††	4.32±0.44‡‡	2.12±0.18**‡	3.60±0.33‡‡	4.05±0.57	7.38±0.40$^{**?\,?}$	1.47±0.07$^{**?\,?}$
M/F	2.19±0.11	0.77±0.02**	2.36±0.11	3.55±0.28†	1.45±0.11**††	2.74±0.27*	2.65±0.09‡	2.77±0.10‡‡	1.78±0.21**‡	6.95±0.77$^{?\,?}$	3.67±0.16$^{**?\,?}$	5.44±0.34$^{*?\,?}$
F/M	0.48±0.03	1.33±0.04*	0.468±0.02	0.33±0.03†	0.87±0.09**††	0.44±0.04	0.39±0.013	0.37±0.01‡‡	0.71±0.07**‡	0.21±0.02$^{?\,?}$	0.286±0.01$^{*?\,?}$	0.261±0.02$^{?\,?}$
GJ on M	95.8±0.5	90.7±0.46**	97.8±0.24*	95.4±0.46	93.7±0.75†	96.1±0.51†	96.6±0.4‡	97.3±0.28‡	95.3±0.47	98.1±0.18$^{?}$	96.3±0.20$^{**?}$	98.25±0.20$^{?\,?}$
GJ on F	7.4±0.43	28.6±1.80**	4.55±0.25	7.20±0.62	19.3±1.15**††	6.84±0.48††	6.86±0.50	9.81±0.38**‡‡	7.40±0.63	11.19±0.87$^{?}$	11.64±0.51$^{?}$	10.7±0.53$^{?}$
GJ on MF	3.23±0.54	19.3±1.60**	2.35±0.21	2.57±0.53	13±0.90**†	2.95±0.35	3.49±0.51	7.09±0.52**‡‡	2.75±0.44	9.62±0.83$^{?\,?}$	8.12±0.56	8.95±0.63$^{?\,?}$

Data obtained at control and different post-infarction time points were compared using ANOVA. Gap junction density is expressed as area of connexin related fluorescence per cell type tissue area (?m²??m⁻²), and as the ratio of M/F or F/M. Data are presented as mean ± S.E.M. $^{*}P < 0.05$ and $^{**}P < 0.001$ *vs.* control (statistically significant differences).

Cx43 in ventricle *vs.* atrium, Cx40 in ventricle *vs.* AVN and atrial levels of Cx43 *vs.* Cx40 were compared using unpaired t-test. †$P < 0.01$ and ††$P < 0.001$ *vs.* Cx43 in ventricle at same time point. ‡$P < 0.05$ and ‡‡$P < 0.0001$ *vs.* Cx43 in atrium at same time point. ?$P < 0.05$ and ??$P < 0.0001$ *vs.* Cx40 in atrium at same time point.

Table 3 - Gap junctions expressed by fibroblasts in fibroblast-rich areas at the interface between ventricle and AVN

	Cx43			Cx40		
	Control n=25	*8 weeks* n=55	*32 weeks* n=52	*Control* n=43	*8 weeks* n=46	*32 weeks* n=68
Area?10^{-2} ? m^2?? m^{-2}	7.11±0.96	3.12±0.21**	4.42±0.28**	0.85±0.18	2.60±0.46**	1.94±0.13*

Data obtained at control and different post-infarction time points were compared using ANOVA.
Gap junction density is expressed as area of connexin related fluorescence per fibroblast area (?m^2??m^{-2}).
Data are presented as mean ± S.E.M. $^{*}P < 0.05$ and $^{**}P < 0.001$ *vs.* control (statistically significant differences).

Appendix 2

Effect of Acidosis (simulation study)

(Courtesy of Shin Inada and Mark Boyett, University of Manchester)

Recently, this group developed action potential models for AN, N and NH cells of the rabbit atrioventricular (AV) node. From these models, they constructed a 1D string model. This model has atrial cells (AM), a slow pathway (SP) made up of N cells, a fast pathway made up of AN cells, and transitional NH cells. The model is composed of 500 elements (150 AM elements, 150 N elements, 150 AN elements and 50 NH elements). This represents the conduction pathway from the atrial muscle, through the AV node to the His bundle (Figure 1A).

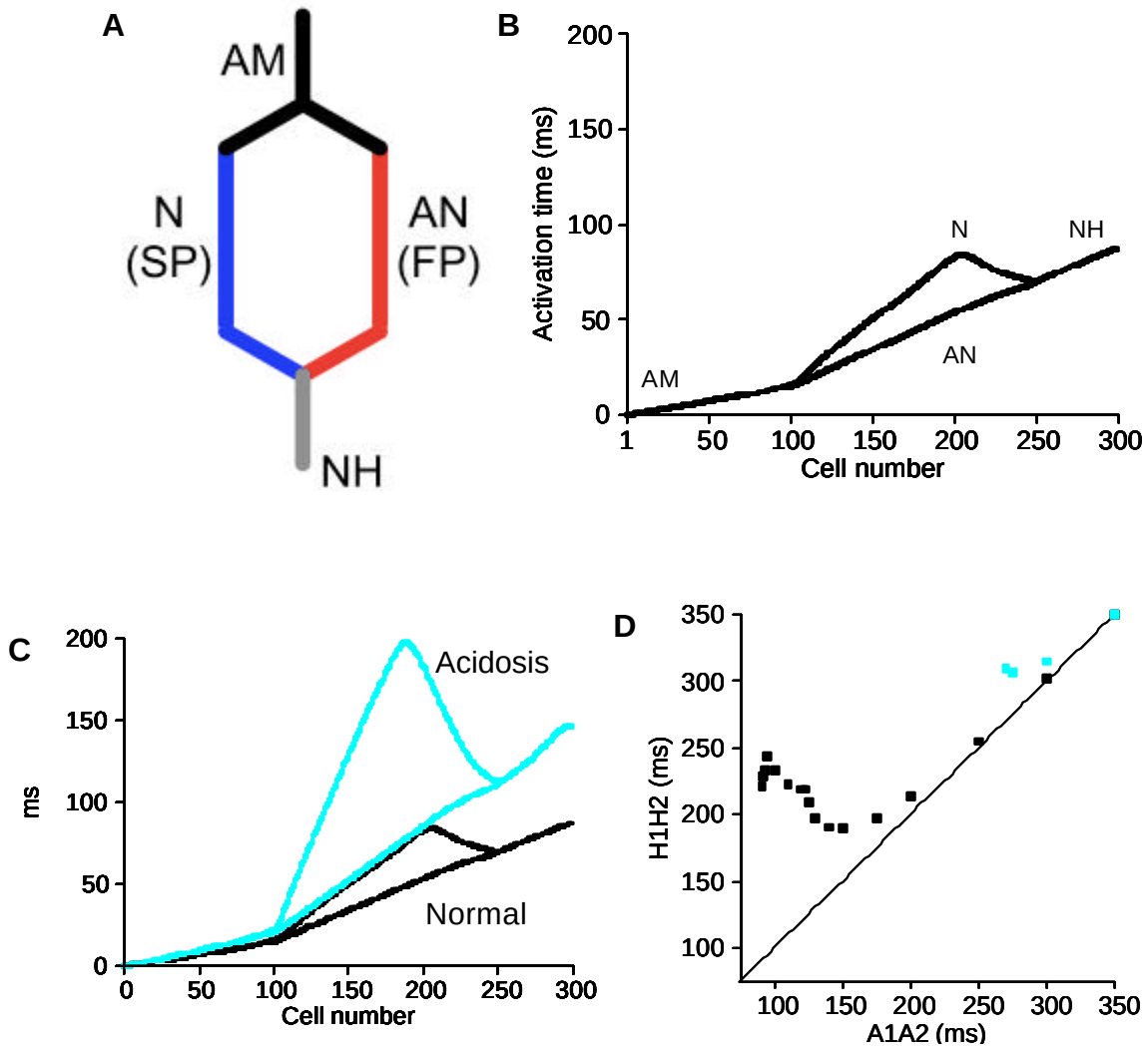

Figure 1 – Effect of acidosis simulation study. (Courtesy of Dr Inada and Dr Boyett, University of Manchester) A - 1D string model. This model has atrial cells (AM), a slow pathway (SP) made up of N cells, a fast pathway made up of AN cells, and transitional NH cells. The model is composed of 500 elements (150 AM elements, 150 N elements, 150 AN elements and 50 NH elements). This represents the conduction pathway from the atrial muscle, through the AV node to the His bundle. B - relationship between activation time (in ms) and cell number (distance from atrium). In this simulation, the conduction time from atrial muscle to the His bundle (AH interval) was 88 ms. C and D – effect of acidosis on activation sequence and refractory curve.

Action potential propagation in 1D model (normal conditions) are illustrated below. Figure 2 shows calculated action potentials and action potential propagation in normal conditions. In this simulation, the atrial cells (top of the figure) were stimulated. The action potential propagated from the atrial muscle to the His bundle. In this simulation A1A1 interval was 350 ms.

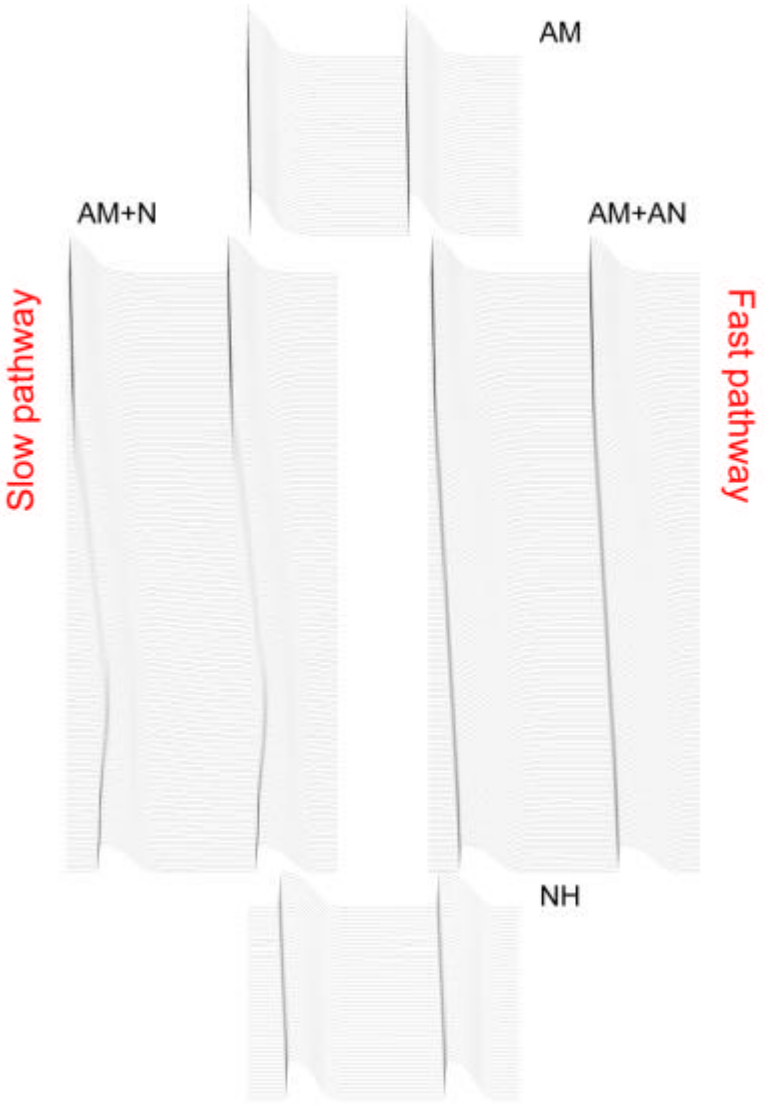

Figure 2 - Calculated action potentials and action potential propagation in normal conditions. AM – atrial cells; N – AV nodal cells; NH – nodal-His cells.

Figure 1B shows the relationship between activation time (in ms) and cell number (distance from atrium). In this simulation, the conduction time from atrial muscle to the His bundle (AH interval) was 88 ms. Figure 3 shows refractory curves. The simulation results (in red) are comparable to experimental data (in black).

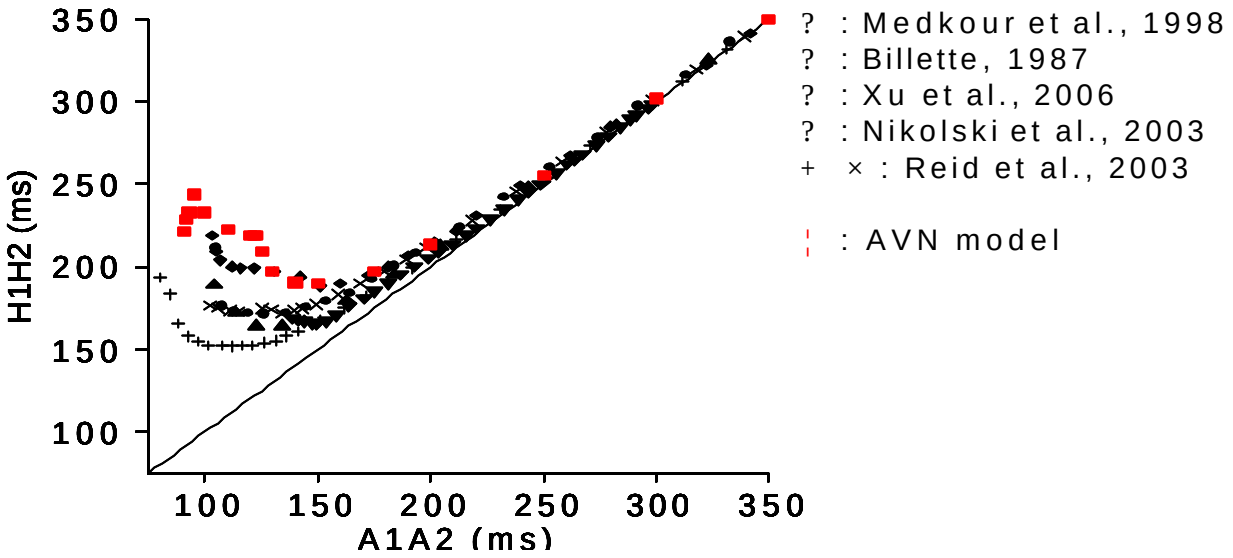

Figure 3 – Refractory curves of experimental data (black) and simulation data (red).

To simulate the effect of acidosis, they reduced the L-type Ca^{2+} current ($I_{Ca,L}$), rapid delayed K^+ current ($I_{K,r}$), Na^+ current (I_{Na}) and cell-to-cell coupling (g_j). When $g_{Ca,L}$ was set to 66 %, $g_{K,r}$ was set to 58 %, g_{Na} was set to 75 %, g_j was set to 69 % in the atrial muscle and AN and NH regions, and g was set to 21 % in the N region, action potential propagation was slowed and the effective refractory period (ERP) and functional refractory period (FRP) were prolonged. Note the decrease in I_{Na} and g_j is based on reported changes in the literature. Acidosis has a greater effect on Cx45 than Cx43; this is why we assumed a greater decrease in g_j in N cells. The effect of acidosis on g_j is mediated by the intracellular pH; they estimated changes in intracellular pH from the literature. Table 1 documents the changes in conduction time, ERP and FRP with acidosis both in published experimental work and in this simulation study.

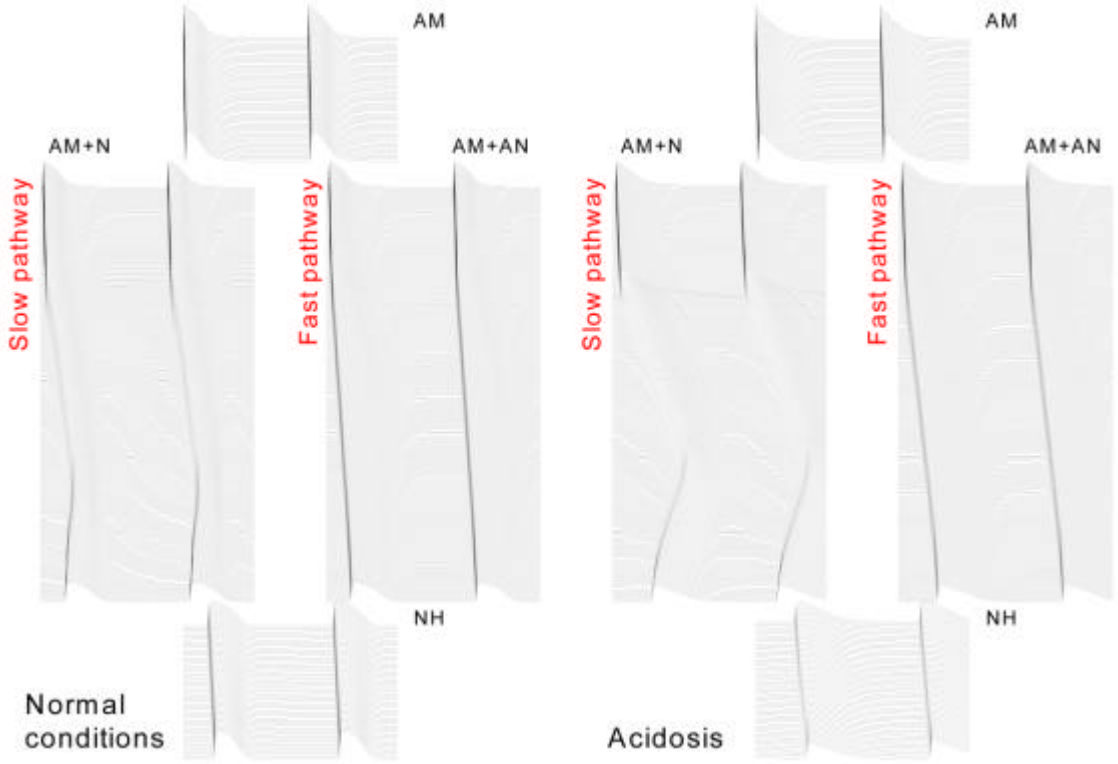

Figure 4 - Calculated action potentials and action potential propagation in normal and acidosis conditions. Note the marked slowing of conduction at the slow pathway of the the AV node. AM – atrial cells; N – AV nodal cells; NH – nodal-His cells.

In summary, the simulation results showed a prolongation of the effective refractory period and functional refractory period as well as increase in the AV node conduction time. These results are comparable to experimental results. Furthermore, the simulation results suggest a significantly greater delay in conduction in the slow pathway consistent with optical mapping data shown earlier in this thesis.

	CT (ms)	ERP (ms)	FRP (ms)
Control	87	90	190
$\times 0.66 g_{Ca,L}$	91	125	197
$\times 0.58 g_{K,r}$	88	125	204
$\times 0.75 g_{Na}$	106	105	197
Reduce g_j	106	105	197
Acidosis	146	270	367
Billette, 1987	48 ± 1.5	116 ± 2.7	167 ± 1.4
Medkour et al., 1998	64	105	171
Nikolski et al., 2003	43 – 88	99	165 – 203
Reid et al., 2003	43 ± 5 (min) 150 ± 10 (max)	91 ± 10	171 ± 11
Xu et al., 2006	58	103	188
Smith, 2007 (pH 7.4)	45.8 ± 3.1	176.8 ± 22.0	205 ± 21.7
Smith, 2007 (pH 6.3)	54.2 ± 3.5	209.3 ± 30.6	220.7 ± 27.4

ERP: minimum S1S2 interval conducted to His bundle

FRP: minimum H1H2 interval

Table 1 – Acidosis simulation data (top section) compared with experimental data (bottom section). CT – conduction time. To simulate the effect of acidosis, they reduced the L-type Ca^{2+} current ($I_{Ca,L}$), rapid delayed K^+ current ($I_{K,r}$), Na^+ current (I_{Na}) and cell-to-cell coupling (g_j). When $g_{Ca,L}$ was set to 66 %, $g_{K,r}$ was set to 58 %, g_{Na} was set to 75 %, g_j was set to 69 % in the atrial muscle and AN and NH regions, and g_j was set to 21 % in the N region, action potential propagation was slowed and the effective refractory period (ERP) and functional refractory period (FRP) were prolonged. Note the decrease in I_{Na} and g_j is based on reported changes in the literature. Acidosis has a greater effect on Cx45 than Cx43; this is why they assumed a greater decrease in g_j in N cells. The effect of acidosis on g_j is mediated by the intracellular pH; they estimated changes in intracellular pH from the literature.

Reference List

(1) Ho KK, Pinsky JL, Kannel WB, Levy D. The epidemiology of heart failure: the Framingham Study. J Am Coll Cardiol 1993; 22(4 Suppl A):6A-13A.

(2) Cleland JGF, McGowan J. Heart failure due to iscahemic heart disease: epidemiology, pathophysiology and progression. J Cardiovasc Pharmacol 1999; 33 (3): S17-S29. .

(3) Davis RC, Hobbs FDR, Lip GYH. History and epidemiology (clinical review: ABC of Heart Failure). BMJ 2000; 320(7226):39-42.

(4) Xiao HB, Roy C, Fujimoto S, Gibson DG. Natural history of abnormal conduction and its relation to prognosis in patients with dilated cardiomyopathy. Int J Cardiol 1996; 53(2):163-170.

(5) Schoeller R, Andresen D, Buttner P, Oezcelik K, Vey G, Schroder R. First or second degree atrioventricular block as a risk factor in idiopathic dilated cardiomyopathy. American Journal of Cardiology 1993; 71(8):720-726.

(6) Shamim W. Intraventricular conduction delay: a prognostic marker in chronic heart failre. International Journal of Cardiology 1999; 70:171-178.

(7) Shamim W, Yousufuddin M, Cicoria M, Gibson DG, Coats AJS, Henein MY. Incremental changes in QRS duration in serial ECGs over time identify high risk elderly patients with heart failure. Heart 2002; 88(1):47-51.

(8) Ganong WF. Origin of the heartbeat and the electrical activity of the heart. In: Ganong WF, editor. Review of medical physiology. Norwalk: Appleton & Lange, 1991: 504-520.

(9) Alonso C, Leclercq C, Victor F, Mansour H, de Place C, Pavin D et al. Electrocardiographic predictive factors of long-term clinical improvement with multisite biventricular pacing in advanced heart failure. American Journal of Cardiology 1999; 84(12):1417-1421.

(10) Meisner JS, McQueen DM, Ishida Y, Vetter HO, Bortolotti U, Strom JA et al. Effects of timing of atrial systole on LV filling and mitral valve closure: computer and dog studies. Am J Physiol Heart Circ Physiol 1985; 249(3):H604-H619.

(11) Bradley DJ, Bradley EA, Baughman KL, Berger RD, Calkins H, Goodman SN et al. Cardiac resynchronization and death from progressive heart failure: a meta-analysis of randomized controlled trials. JAMA 2003; 289(6):730-740.

(12) Abraham WT, Fisher WG, Smith AL, Delurgio DB, Leon AR, Loh E et al. Cardiac resynchronization in chronic heart failure. N Engl J Med 2002; 346(24):1845-1853.

(13) Abraham W. Rationale and design of a Randomised clinical trial to assess the safety and efficacy of cardiac resynchronisation therapy in patients with advanced heart failure: The Multicenter InSync Randomised Clinical Evaluation (MIRACLE). Journal of Cardiac Failure 2000; 6(4):369-380.

(14) Bax JJ, Abraham T, Barold SS, Breithardt OA, Fung JW, Garrigue S et al. Cardiac resynchronization therapy: Part 1--issues before device implantation. J Am Coll Cardiol 2005; 46(12):2153-2167.

(15) Cowie MR, Zaphiriou A. Recent developments: Management of chronic heart failure. BMJ 2002; 325(7361):422-425.

(16) Linde C, Leclercq C, Rex S, Garrigue S, Lavergne T, Cazeau S et al. Long-term benefits of biventricular pacing in congestive heart failure: results from the MUltisite STimulation in cardiomyopathy (MUSTIC) study*1. Journal of the American College of Cardiology 2002; 40(1):111-118.

(17) Gilligan DM, Sargent D, Ponnathpur V, Dan D, Zakaib JS, Ellenbogen KA. Echocardiographic atrioventricular interval optimisation in patients with dual chamber pacemakers and symptomatic left ventricular systolic dysfunction. American Journal of Cardiology 2003; 91:629-631.

(18) Gasparini M, Mantica M, Galimberti P, La Marchesina U, Manglavacchi M, Faletra F et al. Optimization of cardiac resynchronization therapy: technical aspects. Eur Heart J Suppl 2002; 4(suppl_D):D82-D87.

(19) Whinnett ZI, Davies JER, Willson K, Manisty CH, Chow AW, Foale RA et al. Haemodynamic effects of changes in atrioventricular and interventricular delay in cardiac resynchronisation therapy show a consistent pattern: analysis of shape, magnitude and relative importance of atrioventricular and interventricular delay. Heart 2006; 92(11):1628-1634.

(20) Bax JJ, Abraham T, Barold SS, Breithardt OA, Fung JW, Garrigue S et al. Cardiac resynchronization therapy: Part 2--issues during and after device implantation and unresolved questions. J Am Coll Cardiol 2005; 46(12):2168-2182.

(21) Jansen AHM, Bracke FA, van Dantzig JM, Meijer A, van der Voort PH, Aarnoudse W et al. Correlation of Echo-Doppler Optimization of Atrioventricular Delay in Cardiac Resynchronization Therapy With Invasive Hemodynamics in Patients With Heart Failure Secondary to Ischemic or Idiopathic Dilated Cardiomyopathy. The American Journal of Cardiology 2006; 97(4):552-557.

(22) St John Sutton MG, Plappert T, Abraham WT, Smith AL, DeLurgio DB, Leon AR et al. Effect of Cardiac Resynchronization Therapy on Left Ventricular Size and Function in Chronic Heart Failure. Circulation 2003; 107(15):1985-1990.

(23) Breithardt OA, Stellbrink C, Franke A, Balta O, et al. Acute effects of cardiac resynchronisation therapy on left ventricular Doppler indices in patients with congestive heart failure. American Heart Journal 2002; 143:34-44.

(24) Auricchio A, Stellbrink C, Block M, Sack S, Vogt J, Bakker P et al. Effect of Pacing Chamber and Atrioventricular Delay on Acute Systolic Function of Paced Patients With Congestive Heart Failure. Circulation 1999; 99(23):2993-3001.

(25) Auricchio A, Ding J, Spinelli JC, Kramer AP, Salo RW, Hoersch W et al. Cardiac resynchronization therapy restores optimal atrioventricular mechanical timing in heart failure patients with ventricular conduction delay. Journal of the American College of Cardiology 2002; 39(7):1163-1169.

(26) Bristow MR, Saxon LA, Boehmer J, Krueger S, Kass DA, De Marco T et al. Cardiac-Resynchronization Therapy with or without an Implantable Defibrillator in Advanced Chronic Heart Failure. N Engl J Med 2004; 350(21):2140-2150.

(27) McAlister FA, Ezekowitz JA, Wiebe N, Rowe B, Spooner C, Crumley E et al. Systematic review: cardiac resynchronization in patients with symptomatic heart failure. Ann Intern Med 2004; 141(5):381-390.

(28) Zipes DP. Introduction. The atrioventricular node. In: Mazgalev TN, Tchou PJ, editors. Atrial-AV Nodal Electrophysiology: A View from the Millenium. New York: Futura Publishing Group, 2000: xi-xiv.

(29) Siegel RE. Galen's system of Physiology and Medicine. New York: S. Karger, 1968.

(30) Silverman ME, Grove D, Upshaw CB, Jr. Why Does the Heart Beat?: The Discovery of the Electrical System of the Heart. Circulation 2006; 113(23):2775-2781.

(31) Roguin A. Wilhelm His Jr. (1863-1934)-The man behind the bundle. Heart Rhythm 2006; 3(4):480-483.

(32) Tawara S. The conduction system of the mammalian heart. An anatomico-histological study of the atrioventricular bundle and the Purkinje fibers. London: Imperial College Press, 2007.

(33) Anderson RH, Ho SY, Becker AE. Anatomy of the human atrioventricular junctions revisited. Anat Rec 2000; 260(1):81-91.

(34) James TN. Structure and function of the sinus node, AV node and His Bundle of the human heart: Part II - Function. Progress in Cardiovascular Diseases 46[1], 327-360. 2003.

(35) Racker DK. The AV junction region of the heart: a comprehensive study correlating gross anatomy and direct three-dimensional analysis. Part I. Architecture and topography. Anat Rec 1999; 256(1):49-63.

(36) Racker DK, Kadish AH. Proximal Atrioventricular Bundle, Atrioventricular Node, and Distal Atrioventricular Bundle Are Distinct Anatomic Structures With Unique Histological Characteristics and Innervation. Circulation 2000; 101(9):1049-1059.

(37) Moe GK, Preston JB, Burlington H. Physiologic evidence for a dual A-V transmission system. Circ Res 1956; 4(4):357-375.

(38) Kistin AD. Multiple pathways of conduction and reciprocal rhythm with interpolated ventricular premature systoles. Am Heart J 1963; 65:162-179.

(39) Schuilenburg RM, Durrer D. Ventricular echo beats in the human heart elicited by induced ventricular premature beats. Circulation 1969; 40(3):337-347.

(40) Amellal F, Billette J. Selective functional properties of dual atrioventricular nodal inputs. Role in nodal conduction, refractoriness, summation, and rate-dependent function in rabbit heart. Circulation 1996; 94(4):824-832.

(41) Mazgalev TN, Tchou PJ. Surface Potentials From the Region of the Atrioventricular Node and Their Relation to Dual Pathway Electrophysiology. Circulation 2000; 101(17):2110-2117.

(42) Mendez C, Moe GK. Demonstration of a Dual A-V Nodal Conduction System in the Isolated Rabbit Heart. Circ Res 1966; 19(2):378-393.

(43) Nikolski V, Efimov I. Fluorescent imaging of a dual-pathway atrioventricular-nodal conduction system. Circ Res 2001; 88(3):E23-E30.

(44) Nikolski VP, Jones SA, Lancaster MK, Boyett MR, Efimov IR. Cx43 and dual-pathway electrophysiology of the atrioventricular node and atrioventricular nodal reentry. Circ Res 2003; 92(4):469-475.

(45) Scheinmann MM, Gonzalez R, Thomas A, Ullyot D, Bharati S, Lev M. Reentry confined to the atrioventricular node: electrophysiologic and anatomic findings. Am J Cardiol 1982; 49(7):1814-1818.

(46) Meijler FL, Janse MJ. Morphology and electrophysiology of the mammalian atrioventricular node. Physiol Rev 1988; 68(2):608-647.

(47) Mazgalev TN, Van Wagoner D, Efimov I. Mechanisms of AV Nodal Excitability and Propagation. Cellular Electrophysiology. 2004: 196-205.

(48) Merideth J, Mendez C, Mueller WJ, Moe GK. Electrical Excitability of Atrioventricular Nodal Cells. Circ Res 1968; 23(1):69-85.

(49) Billette J, Nattel S. Dynamic behavior of the atrioventricular node: a functional model of interaction between recovery, facilitation, and fatigue. [Review] [86 refs]. Journal of Cardiovascular Electrophysiology 1994; 5(1):90-102.

(50) Fahy GJ, Efimov I, Cheng Y, Kidwell GA, Van Wagoner D, Tchou PJ et al. Mechanism of atrioventricular nodal facilitation in the rabbit heart: role of the distal AV node. Am J Physiol 1997; 272(6 Pt 2):H2815-H2825.

(51) Levy MN, Martin PJ, Iano T, Zieske H. Effects of single vagal stimuli on heart rate and atrioventricular conduction. Am J Physiol 1970; 218(5):1256-1262.

(52) Mazgalev T, Mowrey K, Efimov I, Fahy GJ, Van Wagoner D, Cheng Y et al. Mechanism of atrioventricular nodal facilitation in rabbit heart: role of proximal AV node. Am J Physiol Heart Circ Physiol 1997; 273(4):H1658-H1668.

(53) Wenckebach KF. Analyse des unregelmassigen Pulses. II. Ueber den regelmassig intermittirenden Puls. Zeitschr Klin Med 1899; 37:475-488.

(54) Billette J, Amellal F, Zhao J, Shrier A. Relationship between different recovery curves representing rate-dependent AV nodal function in rabbit heart. Journal of Cardiovascular Electrophysiology 1994; 5(1):63-75.

(55) Billette J, Zhao J, Shrier A. Mechanisms of conduction time hysteresis in rabbit atrioventricular node. American Journal of Physiology 1995; 269(4 Pt 2):H1258-H1267.

(56) Ferrier GL, Dresel PE. Relationship of the functional refractory period to conduction in the atrioventricular node. Circ Res 1974; 35:204-214.

(57) Hoshino K, Anumonwo J, Delmar J, Jalife J. Wenckebach periodicity in single atrioventricular nodal cells from the rabbit heart. Circulation 1990; 82:2201-2216.

(58) Workman AJ, Kane KA, Rankin AC. Rate-dependency of action potential duration and refractoriness in isolated myocytes from the rabbit AV node and atrium. Journal of Molecular and Cellular Cardiology 32, 1525-1537. 2000.

(59) Workman AJ, Kane KA, Rankin AC. Ionic basis of a differential effect of adenosine on refractoriness in rabbit AV nodal and atrial isolated myocytes. Cardiovascular Research 43, 974-984. 1999.

(60) Rudy Y. The ionic mechanisms of conduction in cardiac tissue. J Electrocardiol 2001; 34 Suppl:65-68.

(61) Greener ID, Tellez JO, Dobrzynski H, Yamamoto M, Billeter-Clark R, Boyett MR. Distribution of ion channel transcripts in the rabbit atrioventricular node as studied using in situ hybridisation and quantitative PCR. Journal of Molecular and Cellular Cardiology 2006; 40(6):982-983.

(62) Gourdie RG, Severs NJ, Green CR, Rothery S, Germroth P, Thompson RP. The spatial distribution and relative abundance of gap-junctional connexin40 and connexin43 correlate to functional properties of components of the cardiac atrioventricular conduction system. J Cell Sci 1993; 105(4):985-991.

(63) Schram G, Pourrier M, Melnyk P, Nattel S. Differential distribution of cardiac ion channel expression as a basis for regional specialization in electrical function. Circ Res 2002; 90(9):939-950.

(64) Kyndt F, Probst V, Potet F, Demolombe S, Chevallier JC, Baro I et al. Novel SCN5A mutation leading either to isolated cardiac conduction defect or Brugada syndrome in a large French family. Circulation 2001; 104(25):3081-3086.

(65) Lupoglazoff JM, Cheav T, Baroudi G, Berthet M, Denjoy I, Cauchemez B et al. Homozygous SCN5A mutation in long-QT syndrome with functional two-to-one atrioventricular block. Circ Res 2001; 89(2):E16-E21.

(66) Papadatos GA, Wallerstein PM, Head CE, Ratcliff R, Brady PA, Benndorf K et al. Slowed conduction and ventricular tachycardia after targeted disruption of the cardiac sodium channel gene Scn5a. Proc Natl Acad Sci U S A 2002; 99(9):6210-6215.

(67) Schott JJ, Alshinawi C, Kyndt F, Probst V, Hoorntje TM, Hulsbeek M et al. Cardiac conduction defects associate with mutations in SCN5A. Nat Genet 1999; 23(1):20-21.

(68) Yoo S, Dobrzynski H, Fedorov VV, Xu SZ, Yamanushi TT, Jones SA et al. Localization of Na+ Channel Isoforms at the Atrioventricular Junction and Atrioventricular Node in the Rat. Circulation 2006; 114(13):1360-1371.

(69) Kucera JP, Kleber AG, Rohr S. Slow conduction in cardiac tissue: insights from optical mapping at the cellular level. J Electrocardiol 2001; 34 Suppl:57-64.

(70) Spach MS, Dolber PC. Relating extracellular potentials and their derivatives to anisotropic propagation at a microscopic level in human cardiac muscle. Evidence for electrical uncoupling of side-to-side fiber connections with increasing age. Circ Res 1986; 58(3):356-371.

(71) Martin P. The influence of the parasympathetic nervous system on atrioventricular conduction. Circ Res 1977; 41(5):593-599.

(72) Kobayashi M, Furukawa Y, Chiba S. Positive chronotropic and inotropic effects of angiotensin II in the dog heart. Eur J Pharmacol 1978; 50(1):17-25.

(73) Bastien NR, Ciuffo GM, Saavedra JM, Lambert C. Angiotensin II receptor expression in the conduction system and arterial duct of neonatal and adult rat hearts. Regul Pept 1996; 63(1):9-16.

(74) Bristow MR, Ginsburg R, Minobe W, Cubicciotti RS, Sageman WS, Lurie K et al. Decreased catecholamine sensitivity and beta-adrenergic-receptor density in failing human hearts. N Engl J Med 1982; 307(4):205-211.

(75) Harding SE, Jones SM, O'Gara P, Vescovo G, Poole-Wilson PA. Reduced beta-agonist sensitivity in single atrial cells from failing human hearts. Am J Physiol 1990; 259(4 Pt 2):H1009-H1014.

(76) Harding SE, Brown LA, Wynne DG, Davies CH, Poole-Wilson PA. Mechanisms of beta adrenoceptor desensitisation in the failing human heart. Cardiovasc Res 1994; 28(10):1451-1460.

(77) Denvir MA, MacFarlane NG, Miller DJ, Cobbe SM. Effects of cyclic adenosine monophosphate (cAMP) on sarcoplasmic reticulum Ca(2+)-loading in failing rabbit and human cardiac trabeculae. Basic Res Cardiol 1998; 93(5):396-404.

(78) Jones SM, Kirby MS, Harding SE, Vescova G, Wanless RB, Dalla Libera LD et al. Adriamycin cardiomyopathy in the rabbit: alterations in contractile proteins and myocyte function. Cardiovascular Research 24(10):834-42, 1990.

(79) Currie SC, Duncan AM, Cobbe SM, Smith GL. Characteristics of beta-adrenergic downregulation in a rabbit myocardial infarction model of heart failure. J Physiol 1999; 513P: 281.

(80) Pinto JM, Boyden PA. Electrical remodeling in ischemia and infarction. Cardiovasc Res 1999; 42(2):284-297.

(81) Walker NL. Optical mapping of cardiac electrophysiology in transmural myocardial infarction and global acidosis. PhD thesis, University of Glasgow 2004.

(82) Burton FL, McPhaden AR, Cobbe SM. Ventricular fibrillation threshold and local dispersion of refractoriness in isolated rabbit hearts with left ventricular dysfunction. Basic Research in Cardiology 2000; 95(5):359-367.

(83) Litwin SE, Bridge JHB. Enhanced Na+-Ca2+ Exchange in the Infarcted Heart : Implications for Excitation-Contraction Coupling. Circ Res 1997; 81(6):1083-1093.

(84) Mahaffey KW, Raya TE, Pennock GD, Morkin E, Goldman S. Left Ventricular Performance and Remodeling in Rabbits After Myocardial Infarction : Effects of a Thyroid Hormone Analogue. Circulation 1995; 91(3):794-801.

(85) McIntosh MA, Cobbe SM, Smith GL. Heterogeneous changes in action potential and intracellular Ca2+ in left ventricular myocyte sub-types from rabbits with heart failure. Cardiovascular Research 2000; 45(2):397-409.

(86) Ng GA, Cobbe SM, Smith GL. Non-uniform prolongation of intracellular Ca2+ transients recorded from the epicardial surface of isolated hearts from rabbits with heart failure. Cardiovascular Research 1998; 37(2):489-502.

(87) Pye MP, Cobbe SM. Arrhythmogenesis in experimental models of heart failure: the role of increased load. Cardiovasc Res 1996; 32(2):248-257.

(88) Pye MP, Black M, Cobbe SM. Comparison of in vivo and in vitro haemodynamic function in experimental heart failure: use of echocardiography. Cardiovascular Research 1996; 31(6):873-881.

(89) Burton FL, McPhaden AR, Cobbe SM. Ventricular fibrillation threshold and local dispersion of refractoriness in isolated rabbit hearts with left ventricular dysfunction. Basic Res Cardiol 2000; 95:359-367.

(90) Ng GA. Mechanical performance, intracellular calcium handling and ventriuclar repolarisation in isolated hearts from rabbits with heart failure. University of Glasgow, 1998.

(91) Ng GA, Cobbe SM, Smith GL. Non-uniform prolongation of intracellular Ca^{2+} transients recorded from the epicardial surface of isolated hearts from rabbits with heart failure. Cardiovasc Res 1998; 37:489-502.

(93) McIntosh MA, Cobbe SM, Smith GL. Heterogeneous changes in action potential and intracellular Ca^{2+} in left ventricular myocyte sub-types from rabbits with heart failure. Cardiovasc Res 2000; 45:397-409.

(94) Ng GA. Mechanical performance, intracellular calcium handling and ventriuclar repolarisation in isolated hearts from rabbits with heart failure.(PhD thesis). University of Glasgow, 1998.

(95) Choi BR, Salama G. Optical mapping of atrioventricular node reveals a conduction barrier between atrial and nodal cells. Am J Physiol 1998; 274(3 Pt 2):H829-H845.

(96) Efimov IR, Fahy GJ, Cheng Y, Van Wagoner DR, Tchou PJ, Mazgalev TN. High-resolution fluorescent imaging does not reveal a distinct atrioventricular nodal anterior input channel (fast pathway) in the rabbit heart during sinus rhythm. J Cardiovasc Electrophysiol 1997; 8(3):295-306.

(97) Efimov IR, Mazgalev TN. High-resolution, three-dimensional fluorescent imaging reveals multilayer conduction pattern in the atrioventricular node. Circulation 1998; 98(1):54-57.

(98) Efimov IR, Nikolski VP, Rothenberg F, Greener ID, Li J, Dobrzynski H et al. Structure-function relationship in the AV junction. Anat Rec A Discov Mol Cell Evol Biol 2004; 280(2):952-965.

(99) Hucker WJ, Nikolski VP, Efimov IR. Optical mapping of the atrioventricular junction. Journal of Electrocardiology 2005; 38(4, Supplement 1):121-125.

(100) Efimov IR, Nikolski VP, Salama G. Optical Imaging of the Heart. Circ Res 2004; 95(1):21-33.

(101) Rosenbaum D, Jalife J. Optical mapping of Cardiac Excitation and Arrhythmias. New York.: Futura Publishing Company inc., 2001.

(102) Knisley SB, Neuman MR. Simultaneous electrical and optical mapping in rabbit hearts. Ann Biomed Eng 2003; 31(1):32-41.

(103) Salama G. Optical Mapping: Background and Historical Perspective. In: Rosenbaum DS, Jalife J, editors. Optical Mapping of Cardiac Excitation and Arrhythmias. New York: Futura, 2001: 9-31.

(104) Hayashi H, Miyauchi Y, Chou CC, Karagueuzian HS, Chen PS, Lin SF. Effects of Cytochalasin D on Electrical Restitution and the Dynamics of Ventricular Fibrillation in Isolated Rabbit Heart. J Cardiovasc Electrophysiol 2003; 14(10):1077-1084.

(105) Qin H, Kay MW, Chattipakorn N, Redden DT, Ideker RE, Rogers JM. Effects of heart isolation, voltage-sensitive dye, and electromechanical uncoupling agents on ventricular fibrillation. American Journal of Physiology - Heart & Circulatory Physiology 2003; 284(5):H1818-H1826.

(106) Cheng Y, Li L, Nikolski V, Wallick DW, Efimov IR. Shock-induced arrhythmogenesis is enhanced by 2,3-butanedione monoxime compared with cytochalasin D. Am J Physiol Heart Circ Physiol 2004; 286(1):H310-H318.

(107) Kettlewell S, Walker NL, Cobbe SM, Burton FL, Smith GL. The electrophysiological and mechanical effects of 2,3-butane-dione monoxime and cytochalasin-D in the Langendorff perfused rabbit heart. Exp Physiol 2004; 89(2):163-172.

(108) Loew LM. Mechanisms and principles of voltage-sensitive fluorescence. In: Rosenbaum DS, Jalife J, editors. Optical mapping of cardiac excitation and arrhythmias. New York: Futura, 2001: 33-46.

(109) Muller W, Windisch H, Tritthart HA. Fluorescent styryl dyes applied as fast optical probes of cardiac action potential. Eur Biophys J 1986; 14(2):103-111.

(110) Motulsky H. Intuitive biostatistics. Oxford University Press, 1995.

(111) Bachman S, Sparrow D, Smith LK. Effect of aging on the electrocardiogram. The American Journal of Cardiology 1981; 48(3):513-516.

(112) Simonson E. The effect of age on the electrocardiogram. Am J Cardiol 1972; 29(1):64-73.

(113) Furberg CD, Manolio TA, Psaty BM, Bild DE, Borhani NO, Newman A et al. Major electrocardiographic abnormalities in persons aged 65 years and older (the Cardiovascular Health Study). The American Journal of Cardiology 1992; 69(16):1329-1335.

(114) Fleg JL, Das DN, Wright J, Lakatta EG. Age-associated changes in the components of atrioventricular conduction in apparently healthy volunteers. J Gerontol 1990; 45(3):M95-100.

(115) Schmidlin O, Bharati S, Lev M, Schwartz JB. Effects of physiological aging on cardiac electrophysiology in perfused Fischer 344 rat hearts. Am J Physiol Heart Circ Physiol 1992; 262(1):H97-105.

(116) Craft N, Schwartz JB. Effects of age on intrinsic heart rate, heart rate variability, and AV conduction in healthy humans. Am J Physiol Heart Circ Physiol 1995; 268(4):H1441-H1452.

(117) Opthof T, Coronel R, Rademaker HME, Vermeulen JT, Wilms-Schopman FJG, Janse MJ. Changes in Sinus Node Function in a Rabbit Model of Heart Failure With Ventricular Arrhythmias and Sudden Death. Circulation 2000; 101(25):2975-2980.

(118) Wallick DW, Martin PJ, Masuda Y, Levy MN. Effects of autonomic activity and changes in heart rate on atrioventricular conduction. Am J Physiol 1982; 243(4):H523-H527.

(119) Shryock JC, Belardinelli L. Adenosine and adenosine receptors in the cardiovascular system: biochemistry, physiology, and pharmacology. Am J Cardiol 1997; 79(12A):2-10.

(120) Belardinelli L, Isenberg G. Isolated atrial myocytes: adenosine and acetylcholine increase potassium conductance. Am J Physiol 1983; 244(5):H734-H737.

(121) Belardinelli L, Shryock J, West GA, Clemo HF, DiMarco JP, Berne RM. Effects of adenosine and adenine nucleotides on the atrioventricular node of isolated guinea pig hearts. Circulation 1984; 70(6):1083-1091.

(122) Belardinelli L, Shryock JC, Song Y, Wang D, Srinivas M. Ionic basis of the electrophysiological actions of adenosine on cardiomyocytes. FASEB J 1995; 9(5):359-365.

(123) Belardinelli L, Linden J, Berne RM. The cardiac effects of adenosine. Prog Cardiovasc Dis 1989; 32(1):73-97.

(124) Stangl V, Harms C, Frank T, Stangl K, Muss J, Buttke K et al. Cardiodepressant mediators are released after myocardial ischaemia: modulation by catecholamines and adenosine. Acta Physiol Scand 1999; 165(4):387-393.

(125) Beyer EC, Kistler J, Paul DL, Goodenough DA. Antisera directed against connexin43 peptides react with a 43-kD protein localized to gap junctions in myocardium and other tissues. J Cell Biol 1989; 108(2):595-605.

(126) Reaume AG, de Sousa PA, Kulkarni S, Langille BL, Zhu D, Davies TC et al. Cardiac malformation in neonatal mice lacking connexin43. Science 1995; 267(5205):1831-1834.

(127) Kirchhoff S, Nelles E, Hagendorff A, Kruger O, Traub O, Willecke K. Reduced cardiac conduction velocity and predisposition to arrhythmias in connexin40-deficient mice. Curr Biol 1998; 8(5):299-302.

(128) Kirchhoff S, Kim JS, Hagendorff A, Thonnissen E, Kruger O, Lamers WH et al. Abnormal cardiac conduction and morphogenesis in connexin40 and connexin43 double-deficient mice. Circ Res 2000; 87(5):399-405.

(129) van Rijen HV, van Veen TA, van Kempen MJ, Wilms-Schopman FJ, Potse M, Krueger O et al. Impaired conduction in the bundle branches of mouse hearts lacking the gap junction protein connexin40. Circulation 2001; 103(11):1591-1598.

(130) Boyett MR, Inada S, Yoo S, Li J, Liu J, Tellez J et al. Connexins in the sinoatrial and atrioventricular nodes. Cardiovascular Gap Junctions 2006; 42:175-197.

(131) Kuo CT, Wu JM, Lin KH, Young ML. The Effects of Aging on AV Nodal Recovery Properties. Pacing and Clinical Electrophysiology 2001; 24(2):194-198.

(132) Young ML, Tan RC, Ramza BM, Joyner RW. Effects of hypoxia on atrioventricular node of adult and neonatal rabbit hearts. Am J Physiol Heart Circ Physiol 1989; 256(5):H1337-H1343.

(133) Wu TJ, Chen SA, Chiang CE, Yang CJ, Cheng CC, Wang SP et al. Clinical features and electrophysiologic characteristics of accessory atrioventricular pathways and atrioventricular nodal reentrant tachycardia: comparative study between young and elderly patients. Am Heart J 1993; 126(6):1341-1348.

(134) Anselme F, Frederiks J, Papageorgiou P, Monahan KM, Epstein LM, Spach MS et al. Nonuniform anisotropy is responsible for age-related slowing of atrioventricular nodal reentrant tachycardia. J Cardiovasc Electrophysiol 1996; 7(12):1145-1153.

(135) Lenegre J, Moreau P. [chronic auriculo-ventricular block. Anatomical, clinical and histological study.]. Arch Mal Coeur Vaiss 1963; 56:867-888.

(136) Lev M. Anatomic basis for atrioventricular block. Am J Med 1964; 37:742-748.

(137) Royer A, van Veen TAB, Le Bouter S, Marionneau C, Griol-Charhbili V, Leoni AL et al. Mouse Model of SCN5A-Linked Hereditary Lenegre's Disease: Age-Related

Conduction Slowing and Myocardial Fibrosis. Circulation 2005; 111(14):1738-1746.

(138) Brodde OE, Zerkowski HR, Borst HG, Maier W, Michel MC. Drug- and disease-induced changes of human cardiac beta 1- and beta 2-adrenoceptors. Eur Heart J 1989; 10 Suppl B:38-44.

(139) Brodde OE, Zerkowski HR, Doetsch N, Motomura S, Khamssi M, Michel MC. Myocardial beta-adrenoceptor changes in heart failure: concomitant reduction in beta 1- and beta 2-adrenoceptor function related to the degree of heart failure in patients with mitral valve disease. J Am Coll Cardiol 1989; 14(2):323-331.

(140) Cohn JN, Levine TB, Olivari MT, Garberg V, Lura D, Francis GS et al. Plasma norepinephrine as a guide to prognosis in patients with chronic congestive heart failure. N Engl J Med 1984; 311(13):819-823.

(141) Fowler MB, Laser JA, Hopkins GL, Minobe W, Bristow MR. Assessment of the beta-adrenergic receptor pathway in the intact failing human heart: progressive receptor down-regulation and subsensitivity to agonist response. Circulation 1986; 74(6):1290-1302.

(142) Ginsburg R, Bristow MR, Billingham ME, Stinson EB, Schroeder JS, Harrison DC. Study of the normal and failing isolated human heart: Decreased response of failing heart to isoproterenol. American Heart Journal 1983; 106(3):535-540.

(143) Toda N, Shimamoto K. The influence of sympathetic stimulation on transmembrane potentials in the s-a node. J Pharmacol Exp Ther 1968; 159(2):298-305.

(144) Hewett KW, Rosen MR. Developmental changes in the rabbit sinus node action potential and its response to adrenergic agonists. J Pharmacol Exp Ther 1985; 235(2):308-312.

(145) Umemura K, Zierhut W, Quast U, Hof RP. Baroreflex and +¦-adrenoceptor function are diminished in rat cardiac hypertrophy due to volume overload. Basic Research in Cardiology 1992; 87(3):263-271.

(146) Motomura S, Hashimoto K. Beta 2-adrenoceptor-mediated positive dromotropic effects on atrioventricular node of dogs. Am J Physiol Heart Circ Physiol 1992; 262(1):H123-H129.

(147) Elnatan J, Molenaar P, Rosenfeldt FL, Summers RJ. Autoradiographic localization and quantitation of beta 1- and beta 2-adrenoceptors in the human atrioventricular conducting system: a comparison of patients with idiopathic dilated cardiomyopathy and ischemic heart disease. J Mol Cell Cardiol 1994; 26(3):313-323.

(148) Zhao J, Billette J. Characteristics and mechanisms of the effects of heart rate history on transient AV nodal responses. American Journal of Physiology 1996; 270(6 Pt 2):H2070-H2080.

(149) Dhingra RC, Winslow E, Pouget JM, Rahimtoola SH, Rosen KM. The effect of isoproterenol on atrioventricular and intraventricular conduction. Am J Cardiol 1973; 32(5):629-636.

(150) Elvan A, Rubart M, Zipes DP. NO modulates autonomic effects on sinus discharge rate and AV nodal conduction in open-chest dogs. Am J Physiol 1997; 272(1 Pt 2):H263-H271.

(151) Han X, Kobzik L, Balligand JL, Kelly RA, Smith TW. Nitric oxide synthase (NOS3)-mediated cholinergic modulation of Ca2+ current in adult rabbit atrioventricular nodal cells. Circ Res 1996; 78(6):998-1008.

(152) Dennis DM, Raatikainen MJP, Martens JR, Belardinelli L. Modulation of Atrioventricular Nodal Function by Metabolic and Allosteric Regulators of Endogenous Adenosine in Guinea Pig Heart. Circulation 1996; 94(10):2551-2559.

(153) Martynyuk AE, Kane KA, Cobbe SM, Rankin AC. Role of nitric oxide, cyclic GMP and superoxide in inhibition by adenosine of calcium current in rabbit atrioventricular nodal cells. Cardiovascular Research 1997; 34(2):360-367.

(154) Clemo HF, Belardinelli L. Effect of adenosine on atrioventricular conduction. I: Site and characterization of adenosine action in the guinea pig atrioventricular node. Circ Res 1986; 59(4):427-436.

(155) Wang D, Shryock JC, Belardinelli L. Cellular Basis for the Negative Dromotropic Effect of Adenosine on Rabbit Single Atrioventricular Nodal Cells. Circ Res 1996; 78(4):697-706.

(156) Brown AM, Birnbaumer L. Direct G protein gating of ion channels. Am J Physiol 1988; 254(3 Pt 2):H401-H410.

(157) Froldi G, Belardinelli L. Species-dependent effects of adenosine on heart rate and atrioventricular nodal conduction. Mechanism and physiological implications. Circ Res 1990; 67(4):960-978.

(158) Belardinelli L, Belloni FL, Rubio R, Berne RM. Atrioventricular conduction disturbances during hypoxia. Possible role of adenosine in rabbit and guinea pig heart. Circ Res 1980; 47(5):684-691.

(159) Isenberg G, Belardinelli L. Ionic basis for the antagonism between adenosine and isoproterenol on isolated mammalian ventricular myocytes. Circ Res 1984; 55(3):309-325.

(160) Linden J, Hollen CE, Patel A. The mechanism by which adenosine and cholinergic agents reduce contractility in rat myocardium. Correlation with cyclic adenosine monophosphate and receptor densities. Circ Res 1985; 56(5):728-735.

(161) Schrader J, Baumann G, Gerlach E. Adenosine as inhibitor of myocardial effects of catecholamines. Pflugers Arch 1977; 372(1):29-35.

(162) Baumann G, Schrader J, Gerlach E. Inhibitory action of adenosine on histamine- and dopamine-stimulated cardiac contractility and adenylate cyclase in guinea pigs. Circ Res 1981; 48(2):259-266.

(163) Kolassa N, Pfleger K, Tram M. Species differences in action and elimination of adenosine after dipyridamole and hexobendine. Eur J Pharmacol 1971; 13(3):320-325.

(164) Moser GH, Schrader J, Deussen A. Turnover of adenosine in plasma of human and dog blood. Am J Physiol 1989; 256(4 Pt 1):C799-C806.

(165) Drury AN, Szent-Gyorgyi A. The physiological activity of adenine compounds with especial reference to their action upon the mammalian heart. J Physiol 1929; 68(3):213-237.

(166) Schrader J, Haddy FJ, Gerlach E. Release of adenosine, inosine and hypoxanthine from the isolated guinea pig heart during hypoxia, flow-autoregulation and reactive hyperemia. Pflugers Arch 1977; 369(1):1-6.

(167) Jenkins JR, Belardinelli L. Atrioventricular nodal accommodation in isolated guinea pig hearts: physiological significance and role of adenosine. Circ Res 1988; 63(1):97-116.

(168) Wang D, Shryock JC, Belardinelli L. Cellular basis for the negative dromotropic effect of adenosine on rabbit single atrioventricular nodal cells. Circ Res 1996; 78(4):697-706.

(169) Gaskell WH. On the Tonicity of the Heart and Blood Vessels. J Physiol 1880; 3(1):48-92.

(170) Orchard CH, Kentish JC. Effects of changes of pH on the contractile function of cardiac muscle. Am J Physiol Cell Physiol 1990; 258(6):C967-C981.

(171) Orchard CH, Cingolani HE. Acidosis and arrhythmias in cardiac muscle. Cardiovasc Res 1994; 28(9):1312-1319.

(172) Fozzard HA, Makielski JC. The electrophysiology of acute myocardial ischemia. Annu Rev Med 1985; 36:275-284.

(173) Cascio WE. Myocardial ischemia: what factors determine arrhythmogenesis? J Cardiovasc Electrophysiol 2001; 12(6):726-729.

(174) Bing OH, Brooks WW, Messer JV. Heart muscle viability following hypoxia: protective effect of acidosis. Science 1973; 180(92):1297-1298.

(175) De Mello WC. Cell-to-cell communication in heart and other tissues. Progress in Biophysics and Molecular Biology 1983; 39:147-182.

(176) Turin L, Warner A. Carbon dioxide reversibly abolishes ionic communication between cells of early amphibian embryo. Nature 1977; 270(5632):56-57.

(177) Claydon TW, Boyett MR, Sivaprasadarao A, Ishii K, Owen JM, O'Beirne HA et al. Inhibition of the K+ channel kv1.4 by acidosis: protonation of an extracellular histidine slows the recovery from N-type inactivation. J Physiol 2000; 526 Pt 2:253-264.

(178) Komukai K, Brette F, Pascarel C, Orchard CH. Electrophysiological response of rat ventricular myocytes to acidosis. Am J Physiol Heart Circ Physiol 2002; 283(1):H412-H422.

(179) Komukai K, Brette F, Orchard CH. Electrophysiological response of rat atrial myocytes to acidosis. Am J Physiol Heart Circ Physiol 2002; 283(2):H715-H724.

(180) Choi HS, Trafford AW, Orchard CH, Eisner DA. The effect of acidosis on systolic Ca2+ and sarcoplasmic reticulum calcium content in isolated rat ventricular myocytes. J Physiol 2000; 529 Pt 3:661-668.

(181) Aberra A, Komukai K, Howarth FC, Orchard CH. The effect of acidosis on the ECG of the rat heart. Exp Physiol 2001; 86(1):27-31.

(182) Gryshchenko O, Qu J, Nathan RD. Ischemia alters the electrical activity of pacemaker cells isolated from the rabbit sinoatrial node. Am J Physiol Heart Circ Physiol 2002; 282(6):H2284-H2295.

(183) Garlick PB, Radda GK, Seeley PJ. Studies of acidosis in the ischaemic heart by phosphorus nuclear magnetic resonance. Biochem J 1979; 184(3):547-554.

(184) Komukai K, Pascarel C, Orchard CH. Compensatory role of CaMKII on ICa and SR function during acidosis in rat ventricular myocytes. Pflugers Arch 2001; 442(3):353-361.

(185) Gende OA, Camilion de Hurtado MC, Cingolani EH. Chronotropic response of isolated atria to acid base alterations. Archives Internationales de Physiologie et de Biochimie 86(5):997-1009, 1978.

(186) Hulme JT, Orchard CH. Effect of acidosis on transient outward potassium current in isolated rat ventricular myocytes. Am J Physiol Heart Circ Physiol 2000; 278(1):H50-H59.

(187) DiFrancesco D. Pacemaker Mechanisms in Cardiac Tissue. Annual Review of Physiology 1993; 55(1):455-472.

(188) Wahler GM. Cardiac Action Potentials. In: Nicholas Sperelakis, editor. Cell Physiology Source Book. California: Academic Press, 1994: 556-565.

(189) Brown HF, DiFrancesco D, Noble SJ. How does adrenaline accelerate the heart? Nature 1979; 280(5719):235-236.

(190) Baruscotti M, Bucchi A, DiFrancesco D. Physiology and pharmacology of the cardiac pacemaker ("funny") current. Pharmacology & Therapeutics 2005; 107(1):59-79.

(191) Effect of metoprolol CR/XL in chronic heart failure: Metoprolol CR/XL Randomised Intervention Trial in Congestive Heart Failure (MERIT-HF). Lancet 1999; 353(9169):2001-2007.

(192) Whorlow SL, Krum H. Meta-analysis of effect of beta-blocker therapy on mortality in patients with New York Heart Association class IV chronic congestive heart failure. Am J Cardiol 2000; 86(8):886-889.

(193) Leizorovicz A, Lechat P, Cucherat M, Bugnard F. Bisoprolol for the treatment of chronic heart failure: a meta-analysis on individual data of two placebo-controlled studies--CIBIS and CIBIS II. Cardiac Insufficiency Bisoprolol Study. Am Heart J 2002; 143(2):301-307.

(194) Tjeerdsma G, Szabo BM, van Wijk LM, Brouwer J, Tio RA, Crijns HJ et al. Autonomic dysfunction in patients with mild heart failure and coronary artery disease and the effects of add-on beta-blockade. Eur J Heart Fail 2001; 3(1):33-39.

(195) Daubert JC. Introduction to atrial fibrillation and heart failure: a mutually noxious association. Europace 2004; 5 Suppl 1:S1-S4.

(196) Maisel WH, Stevenson LW. Atrial fibrillation in heart failure: epidemiology, pathophysiology, and rationale for therapy. Am J Cardiol 2003; 91(6A):2D-8D.

(197) Coppen SR, Severs NJ. Diversity of connexin expression patterns in the atrioventricular node: vestigial consequence or functional specialization? J Cardiovasc Electrophysiol 2002; 13(6):625-626.

(198) Dobrzynski H, Nikolski VP, Sambelashvili AT, Greener ID, Yamamoto M, Boyett MR et al. Site of origin and molecular substrate of atrioventricular junctional rhythm in the rabbit heart. Circ Res 2003; 93(11):1102-1110.

(199) Simon AM, Goodenough DA, Paul DL. Mice lacking connexin40 have cardiac conduction abnormalities characteristic of atrioventricular block and bundle branch block. Curr Biol 1998; 8(5):295-298.

(200) Zhu W, Saba S, Link MS, Bak E, Homoud MK, Estes NA, III et al. Atrioventricular nodal reverse facilitation in connexin40-deficient mice. Heart Rhythm 2005; 2(11):1231-1237.